The University Of Sheffield.

Morphogenesis of the lateral semicircular canal in the zebrafish inner ear

By:

Davide Baldera

A thesis submitted in partial fulfilment of the requirements for the degree of Doctor of Philosophy

The University of Sheffield
Faculty of Science
Department of Biomedical Science

December, 2018

A Silvia e alla mia famiglia;

grazie per tutto il vostro sostegno.

To Silvia and my family;

thanks for all your support.

ACKNOWLEDGEMENTS

Firstly, I would like to thank Professor Tanya T. Whitfield for her patience, continuous support and for helping me overcome my limits throughout these last three years. She, and the rest of the laboratory, provided a friendly and stimulating environment, which I will always be grateful for.

My sincere thanks also go to my advisors Dr. Freek van Eeden and Dr. Mark Collins for providing me with continuous feedback, support and for the inspiring chats. This work would not have been possible without the help of the aquarium staff, who took really good care of the fish used during this PhD.

I would also like to thank my family in Sardinia; the long distance has not prevented them from supporting me in all possible ways. A big thanks also goes to my sister and family here in Sheffield, for making me feel not so far from home.

Last but not least, the most special thanks goes to my wife, Silvia. Words cannot explain the help she has given me throughout this whole adventure and how invaluable her support has been to me. I would not have come this far without her.

ABSTRACT

The study of the morphogenetic processes underlying organogenesis has always proved to be challenging, as many aspects need to be considered (e.g. cell movement and genetic interactions). This is particularly interesting in the case of very complex organs, such as the inner ear, which hosts both the auditory and vestibular apparatus, the latter being the organ of balance. This is composed by three semicircular canals, which detect angular acceleration of the head and send information to the brain to allow the maintenance of posture and stabilisation of gaze. A failure in the activity of these canals has been linked to various kinds of disease, such as the Branchio-Oto-Renal syndrome and Menière's disease.

This project is focused on the development of the lateral (horizontal) canal, as it has been proposed to be the last to have evolved and to be the most affected by inner ear malformations. In the zebrafish, the lateral canal development requires the formation of an epithelial pillar, between 48 and 72 hours post fertilisation (hpf), which is the hub of the canal. Previous studies have described the ventral pillar formation as an epithelial fusion between two cell populations

(ventral bulge and ventral projection), but the cell movements required to achieve that have never been described in detail.

By taking advantage of light-sheet microscopy, I have demonstrated that, upon fusion, other cell rearrangements need to take place to develop the ventral pillar. In particular, after the fusion event, the cells exhibit complex movements and a dynamism that is not characteristic of an epithelial state. In addition, I built on previous knowledge regarding the inner ear phenotype of the *otx1* and *eya1* mutants to analyse a possible genetic interaction between these two genes and how their mutation affects the ventral pillar development. Here, I show that these two mutants exhibit reciprocal phenotypes, with respect to the ventral pillar, and that this correlates with changes in the expression pattern of specific markers of the ventral otic epithelium. In conclusion, this study sheds light on the cell movements and genetics underlying the development of the ventral pillar and, more broadly, provides new ways of analysing the morphogenetic processes that take place during organogenesis.

TABLE OF CONTENTS

INDEX OF FIGURES AND TABLES

FIGURES

TABLES

LIST OF ABBREVIATIONS

AD primers – Arbitrary degenerate primers

adgrg6 – adhesion G-protein coupled receptor G6

ALL – Anterior lateral line

BCIP – 5-Bromo-4-Chloro-3-Indoyl-Phosphate

BLAST – Basic local alignment search tool

bmp4 – bone morphogenetic factor 4

BSA – Bovine Serum Albumin

bZIP – basic-region leucine zipper

CRISPR - Clustered regularly interspaced short palindromic repeats

Crx – Cone-rod homeobox-containing gene

DIC – Differential interference contrast

dlx/dll – distal-less transcription factors

dog – dog-eared mutants

dpf – Days post fertilisation

dpm3 – dolichyl-phosphate mannosyltransferase polypeptide 3

ECM – Extracellular matrix

EGFP – Enhanced green fluorescent protein

EMT – Epithelial-to-mesenchymal transition

ENU – *N*-ethyl-N-nitrosourea

EYA – Eyes absent gene family

eyaHR – eya homologous region

FGF – Fibroblast growth factor

GHOX7 – Gallus homeobox-containing gene

gpr126 – G-protein coupled receptor 126

gRNA – guide RNA

gsc – goosecoid

H2B – histone 2b

hpf – Hours post fertilisation

HR – Homologous recombination

lau – lauscher mutants

mir137 – miRNA137

MOotx2a – *otx2a* morpholino

Msx1 – msh homeobox 1

NBT – Nitro Blue Tetrazolium Chloride

neurod1 – neuronal differentiation 1

ngn1 – neurogenin 1

NHEJ – Non-homologous end joining

otd - orthodenticle

OTX – Orthodenticle homeobox gene family

PAM – Protospacer adjacent motif

PBS – Phosphate-buffered saline

PLL – Posterior lateral line

PPR – Pre-placodal region

Prd-like – Paired-like

RFP – Red fluorescent protein

s100a10a – s100 calcium binding protein A10a

SAG – Statoacoustic (VIII) ganglion

Six1 – sineoculis homeobox homolog 1

SOX2 – Sry-type HMG box gene

TAIL PCR – Thermal asymmetric interlaced polymerase chain reaction

tbx1 – T-box transcription factor 1

TUNEL – Terminal deoxynucleotidyl transferase dUTP nick end labelling

ugdh – uridine 5'-diphosphate (UDP)-glucose dehydrogenase

vcana/b – versican a and *b*

vgo – van gogh mutants

VN – Vestibular nerves

WISH – Whole mount *in situ* hybridisation

xEF1a – Xenopus elongation factor 1a

1. INTRODUCTION

1.1. Development and morphogenesis

The concept of morphogenesis, from the Greek μορφη (morphe = shape) and γενεσις (genesis = creation), encompasses all the physical and biological mechanisms aimed at the development of a system. These processes have been extensively described over the years using both animal and mathematical models. One of the first attempts to provide a model for morphogenesis was made by Alan Turing in 1952. He describes the whole morphogenetic process as a combination of genetic stimuli (for the first time called "morphogens") and mechanical forces that need to be finely regulated to give rise to an organism (Turing, 1952). This set the stage for scientific research over the following decades. We now know that there are many similarities but also important differences between the morphogenetic processes that take place during embryonic stages and later in development.

1.1.1. Morphogenesis during early development

The initial phases of embryonic development are characterised by specific morphogenetic events focused on establishing the body plan. This is achieved through gastrulation, during which cells are redistributed throughout the embryo to establish a domain for each of the three germ layers (ectoderm, mesoderm and endoderm). This takes place differently in amniotes and anamniote vertebrates. In particular, gastrulation requires the development of a primitive streak in mammals and avians, whilst, in anamniotes (such as fish and amphibians), gastrulation is initiated by the formation of the blastopore lip (Stower and Bertocchini, 2017).

These processes have many common features with respect to the activation of morphogens and the subsequent rearrangement of cells. In chicks and mammals, cells constituting the most external layer of the embryo (epiblast) are internalised through the primitive streak and undergo epithelial-mesenchymal transition (EMT) to give rise to the endodermal and mesodermal layers. This is characterised by cellular modifications that affect their interaction with extracellular matrix (ECM) components and with other cells (Keller, Davidson and Shook, 2003; Kantarci *et al.*, 2005; Stower and Bertocchini, 2017). In particular, the epithelial state defines cells with a clear apico-basal polarity and that express specific adhesion proteins that allow for

each cell composing the epithelium to maintain contact with the other cells of the same population, resulting in a very defined and regular tissue structure and collective migration. On the other hand, mesenchymal cells are characterised by a lack of apico-basal polarity and express less or no adhesion protein, resulting in cells showing high motility and individual migration (Campbell and Casanova, 2016). Nevertheless, it is important to consider that there are many shades of grey when it comes to define the epithelial and mesenchymal state and that many morphogenetic processes are driven by "partial mesenchymal" cells, such as dorsal closure, in *Drosophila*, lateral line development, in zebrafish, and palatal fusion, in vertebrates.

The process of dorsal closure involves the fusion of two sheets of epithelium stretching from the ventral to the dorsal side of the developing embryo. The movement of these sheets of epithelium has been proposed to be driven by a specific set of "leading edge" cells, showing an incomplete apico-basal polarity. This is due to the fact that, on one side, these cells maintain their contact with the rest of the epithelial cells, while showing a loose end on the other side (Bahri *et al.*, 2010; Campbell and Casanova, 2016) . This implies an uneven presence of cell adhesion proteins (such as E-cadherins) on the surface of the cells, which led to define these cells as

showing a partial mesenchymal behaviour (Bahri *et al.*, 2010; Campbell and Casanova, 2016).

Similarly, in zebrafish, the development of the lateral line is a process that requires the presence of leading cells in a partial-mesenchymal state driving the epithelial followers. In this case, different leading cells have been proposed to undergo different levels of EMT, which result in cells showing reduced or absent apico-basal polarity, loss of tight junctions and reduced presence of adhesion proteins, such as E-cadherin (Revenu and Gilmour, 2009).

Finally, in vertebrates, palate morphogenesis is an example of a process relying on the fusion of two sheets of epithelium (palatal shelves), which arise from the sides of the maxillary process (Schutte and Murray, 1999; Li *et al.*, 2018). The cells composing the palatal shelves migrate towards each other and meet to form a medial edge epithelium. The pathways leading to the clearance of the medial edge epithelium are subject to many studies and, so far, it has been proposed that this process is regulated by apoptosis triggered by high levels of hedgehog (Hh) signalling (Li *et al.*, 2018). This signalling pathway has, in fact, been suggested to interfere with the production of integrins, which allow the epithelial cells to maintain contact with the ECM (Reginato *et al.*,

2003; Li *et al.*, 2018). When epithelial cells lose contact with the ECM, cell death is triggered by apoptosis or anoikis (Reginato *et al.*, 2003).

The interaction between cells and ECM components is the basis of many processes that occur at later developmental stages. Otic development is a good example of the involvement of ECM components in organogenesis and will be analysed in greater detail in section 1.4.3. However, while the genetics underpinning the development of many organs have been extensively studied over the past decades, finding the right tools to obtain time-lapse recordings to study the behaviour of the cells involved in these processes has proven to be a great challenge.

1.2. The inner ear: anatomy and function

1.2.1. The auditory system

The ear is a remarkably complex organ responsible for detecting and transducing sound to the brain and detecting movement and gravity to provide spatial orientation and balance. The mammalian ear is made up by three distinct sections: outer ear, middle ear and inner ear. The first two merely retain an auditory purpose, with the sound being collected by the outer ear and sent to the middle ear. The vibration of the tympanic membrane propagates the sound waves to the cochlea, in the inner ear, which transduces it into electrical stimuli that are sent to the brain.

1.2.2. The vestibular system

The inner ear is also responsible for the detection of linear and angular acceleration through the vestibular system, which is the organ of balance. This is composed by the otoconia and the semicircular canal system. The otoconia are calcium carbonate deposits located on top of a dense layer of extracellular matrix (cupula), which separates them from a sensory patch (macula) composed of ciliated (hair) cells activated by the inertia of the otoconia to acceleration caused by sound, gravity or movement (Figure 1.1 A).

The hair cells exhibit a highly specialised set of stereocilia arranged according to their height, which makes them mechanosensitive. When the stereocilia bend towards the tallest or the shortest cilium, the transduction channels located on the tip respectively open or close and therefore regulating the current of calcium ions that is required to transform the mechanical into electrical stimuli to be sent to the brain (Gillespie and Müller, 2009; Qiu and Müller, 2018) (Figure 1.1 A). Another particularly interesting feature of the hair cells is that they are adaptive, so the tension of the transduction channels is tuned so that, even in the event of large movements, the cilia are still sensitive to smaller displacements (Gillespie and Müller, 2009; Qiu and Müller, 2018). Recently, a novel transduction channel has been described to be located on the surface of the cell body of the hair cells and to be activated by the bending of the cilia towards the shortest cilium, though its precise modus operandi is still being investigated (Qiu and Müller, 2018). The electrical stimuli elicited by the activation of the hair cells are sent to the brain to detect horizontal (utricular macula) or vertical (saccular macula) acceleration.

In teleost fish, in addition to the utricle and the saccule, the otoliths equivalent to the human otoconia, a third otolith (the lagena) has been

described. The otoliths overlie respectively the utricular, saccular and lagenar maculae (Whitfield *et al.*, 2002; Khorevin, 2008).

Information regarding angular acceleration is sent to the brain by the semicircular canal system.

1.2.2.1 The semicircular canal system

The semicircular canals are fluid-filled organs responsible for detecting angular acceleration of the head. There are three semicircular canals (anterior or superior, posterior and lateral or horizontal), each responsible for identifying a specific movement. The anterior canal is responsible for detecting rotational movement around the sagittal plane; the posterior canal detects rotations around the left-right axes and the lateral canal detects rotations around the vertical axes (Figure 1.1 B). The detection is achieved thanks to the endolymph that fills the canals, which has an inertia that, upon rotation of the canals, activates the ciliated cells contained in the cristae. These are sensory patches enclosed in an enlargement located at the base of each canal (ampulla) (Figure 1.1 A).

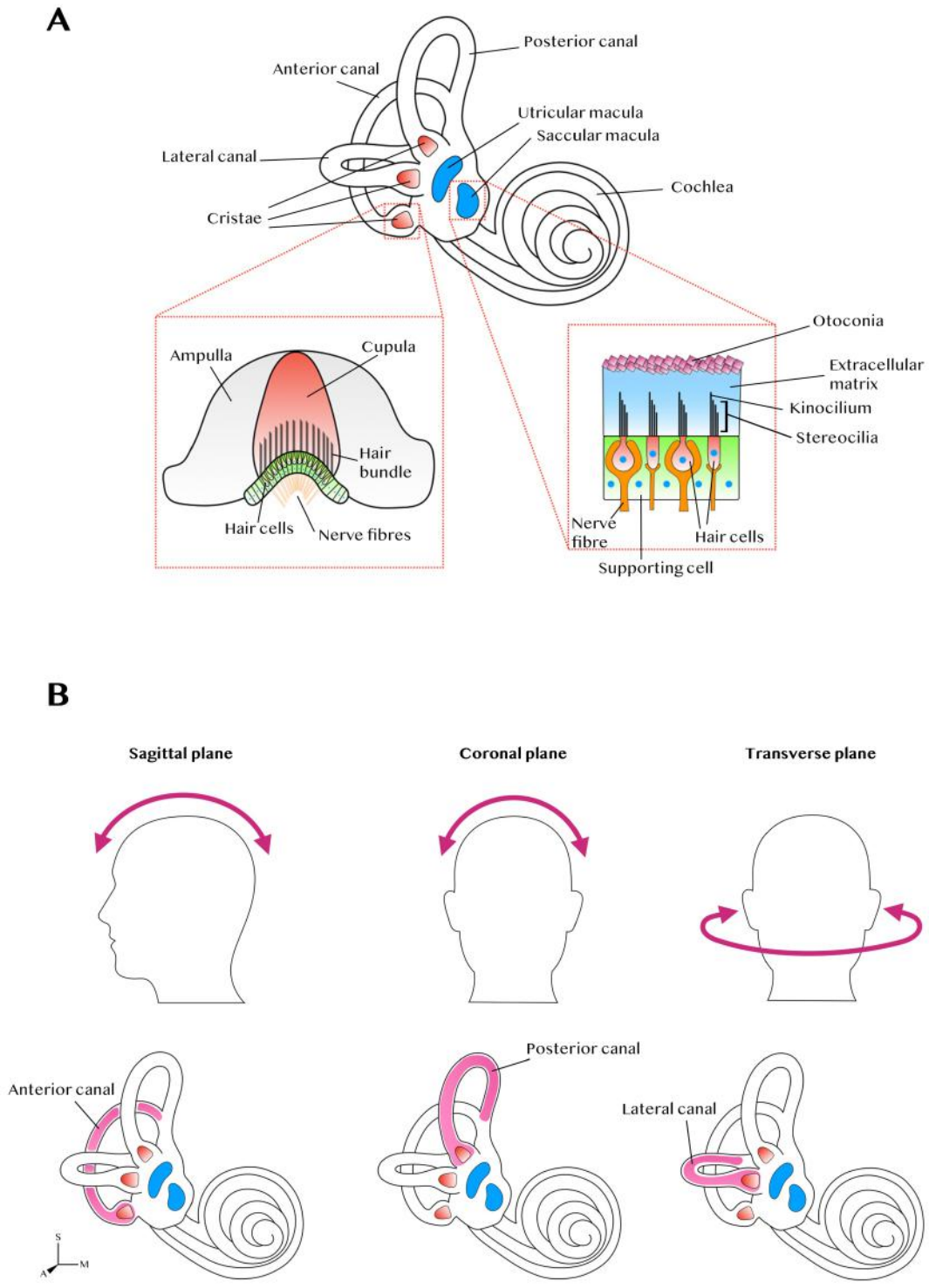

Figure 1.1. (A) Schematic representation of human inner ear with focus on the structures composing the cristae and the maculae. (B) Rotational movements of the head detected by each semicircular canal. Human inner ear diagram was adapted from John Wiley and Sons. Schematics of the cristae and maculae were adapted form Encyclopaedia Britannica.

1.3. The zebrafish as a model for inner ear development

Zebrafish are teleost fish that have proved to be a powerful vertebrate model organism and have been extensively used over the past decades for both biomedical and developmental research. This is possible thanks to the fact that zebrafish embryos are transparent, which allows for a better visualisation of organogenesis, and that many major structures develop within the first five days of development. Another advantage of this model is the ease with which specific genes can be mutated and fluorescent tags can be inserted in the genome to create transgenic lines. Adult zebrafish are cheap to be maintained and can spawn over 200 embryos from a single cross, allowing for higher numbers of samples tested during a single experiment compared with other models. Furthermore, genome-sequencing data has revealed that the human and zebrafish genome share many similarities, with at least one zebrafish orthologue for 71.4% human genes (Howe *et al.*, 2013).

However, it is important to notice that the fish genome exhibits duplications in many regions due to the whole-genome duplication, which is thought to have occurred during the evolution form a common teleostei ancestor (Amores *et al.*, 2011). This resulted in the presence of two or more homologous genes, which might share similar functions or both be required

to fulfil the activity of their mammalian orthologue (Amores *et al.*, 2011). The direct consequence of this process is that mutations of zebrafish genes often give rise to less severe phenotypes than those in their mammalian counterparts.

The zebrafish has been used as a model for studying the development of various organs, ranging from the heart to the eyes and the inner ear. The zebrafish and human inner ear share many similarities when it comes to anatomy of the vestibular organ. Both are characterised by the presence of the anterior, posterior and lateral semicircular canals, each exhibiting an enlargement at the base (ampulla) containing a sensory patch (crista). In zebrafish, the utricle and saccule can also be found but, unlike humans, fish ears contain a third otolithic macula (lagena). The otolith or asteriscus that lies on top of the lagenar macula is thought to have both auditory and vestibular functions (Khorevin, 2008). Another important difference in the anatomy of the fish and human inner ear is that, in humans, the vestibular organ is attached to the cochlea, while the zebrafish does not have a cochlea (Figure 1.2).

In the following sections, the mechanisms of zebrafish inner ear development will be analysed in greater detail.

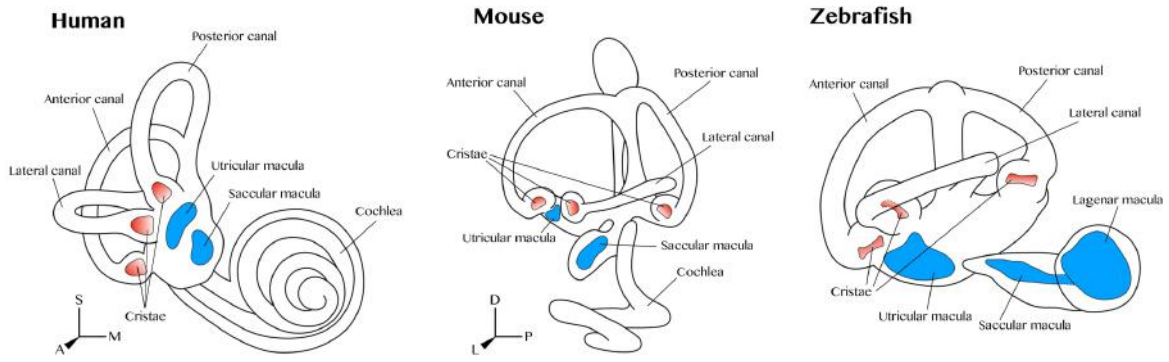

Figure 1.2. Schematic representation of the human, mouse and zebrafish inner ear. In all three organisms three semicircular canals (with their respective cristae) and the utricular and saccular maculae are present. The main difference resides in the absence of a cochlear duct in the zebrafish inner ear. Human inner ear was modified from a diagram of John Wiley and Sons. The mouse and zebrafish inner ear schematics are based on the diagrams published by Whitfield and Hammond, 2007.

1.4. Stages of inner ear development

To achieve the correct development of the zebrafish inner ear, a plethora of morphogens are activated to provide specific cells with information regarding their fate (e.g. neural or non-sensory). The lateral semicircular canal is thought to be the last to have evolved and to be genetically different from the other two (Mazan *et al.*, 2000). This section will analyse development of the semicircular canals during embryogenesis with particular emphasis on the lateral canal and the morphogens that have, so far, been associated with its formation.

1.4.1. Placode induction

The first step for vertebrate inner ear formation is the induction of the otic placode, a thickening derived from the ectoderm, located on both sides of the neural plate (Torres and Giráldez, 1998; Streit, 2002; Alsina and Whitfield, 2017). This structure arises from the pre-placodal region (PPR), which is also the cradle of all cranial placodes (reviewed in Alsina & Whitfield 2017). Time-lapse imaging of placode formation contributed to establish that, in chick embryos, a small proportion of cells forming the otic placode is derived from non-neural tissue expressing both *GHOX7*, orthologue to Drosophila *msx1*, and *SOX2*. The rest of the otic precursors are derived from an ectodermal region located laterally to the Hensen's node, the starting point of gastrulation (Torres and Giráldez, 1998; Streit, 2002). In both chick and zebrafish embryos, the PPR is already present at the 1-somite stage and, by the 10-somite stage, gives rise to the otic placode (Haddon and Lewis, 1996; Torres and Giráldez, 1998; Streit, 2002; Alsina and Whitfield, 2017). A number of transcription factors have been described to play a crucial role during placode induction and to establish the anterior-posterior and dorsal-ventral symmetry of the otic placode. Many of these are homeobox genes such as *dlx3*/*Dlx3*, *dll2* and *otx1*/*Otx1*, which are conserved among zebrafish, mice, *Xenopus laevis* and the chick (Torres and Giráldez, 1998). In addition to these factors, it has also been demonstrated that

FGF signalling is paramount for placode induction by regulating *pax2a*. In particular, in mice, chick and zebrafish, FGF is required during early phases of placode formation to induce the expression of *Pax2a* and *Pax8*, which serve as cues for the cells to become part of the otic placode (M. McCarroll *et al.*, 2012). Interestingly, upon induction of the placode, Fgf3 and Fgf8 signalling from rhombomere 4 has been suggested to be required for maintenance of several transcription factors, such as *eya1*, *dlx3* and *pax2a* (Léger and Brand, 2002).

Upon formation, the zebrafish otic placode appears already as a three-dimensional structure, which undergoes a cavitation process to form the otic vesicle.

1.4.2. Formation of the otic vesicle

The process of cavitation of the otic placode leads to the formation of a hollow organ: the otic vesicle. In recent years, confocal imaging of otic vesicle development has helped to understand that the cavitation of the placode is not a result of apoptotic events, but that it starts, around 16.5 hpf, with the formation of two small openings at the anterior and posterior poles of the placode. From these, the epithelium opens up towards the middle of what is, by 17 hpf, the otic vesicle (Hoijman *et al.*, 2015). The vesicle is an elliptic hollow organ exhibiting a longer antero-posterior axis, which is already established at

placodal stage by epithelialisation, and medio-lateral and dorso-ventral axes of equal size (Hoijman *et al.*, 2015). While the cavitation process is ongoing, the otoliths start to form, at the anterior and posterior poles of the vesicle, by the nucleation of otolith precursor particles (Riley *et al.*, 1997). Once the vesicle has formed, a compartmentation process needs to happen to develop the three semicircular canals and their respective cristae.

1.4.3. Semicircular canal morphogenesis

The morphogenesis of the three semicircular canals is a process that requires a complex set of cellular movements that have not been described in detail. Nonetheless, many genetic aspects of canal formation have been studied and understood. It is important to note that, in amniotes, the semicircular canals develop from three pouches that undergo a thinning to form a fusion plate, from which cells are either removed via apoptosis or reabsorbed into the duct (Martin and Swanson, 1993; Fekete *et al.*, 1997) (Figure 1.3). In the zebrafish and *Xenopus*, this is slightly different in that the process required to make the canals semicircular involves the formation of two epithelial finger-like projections protruding from the walls of the otic vesicle. The projections will meet and fuse at the fusion plate to create a single column of tissue and that has been termed a “pillar”, defining the semicircular

form of the canal (Waterman and Bell, 1984; Haddon and Lewis, 1996; Geng *et al.*, 2013) (Figure 1.3). During pillar formation, ECM components have been shown to play a crucial role in promoting the outgrowth of the projections. Both in *Xenopus* and zebrafish, it has been shown that the injection of hyaluronidase into a projection results in its collapse. Therefore, it has been proposed that the cells of the otic epithelium release ECM component where the projection needs to grow and this promotes the outgrowth into the lumen of the vesicle (Haddon and Lewis, 1991, 1996). This is in accordance with a more recent study showing that in the projections two genes coding for the core proteins for chondroitin sulphate proteoglycans (*versican a* (*vcana*) and *versican b* (*vcanb*)) can be found (Geng *et al.*, 2013). The expression of these genes is finely tuned: it is stronger during the outpocketing, extension and fusion of the projections and then it is downregulated once the fusion is complete and the pillar has formed. Interestingly, if the fusion does not occur, as in the case in *adgrg6* (formerly *gpr126*; *lauscher* (*lau*)) mutants, *vcana* and *vcanb* remain upregulated (Geng *et al.*, 2013). The transient expression of *vcana* and *vcanb* is a common feature of all three canals; however, they also exhibit genetic differences. Particularly interesting is the case of the lateral canal, which has been proposed to be the last one to have evolved and to

exhibit many genetic differences compared to the other two (Mazan *et al.*, 2000; Geng *et al.*, 2013).

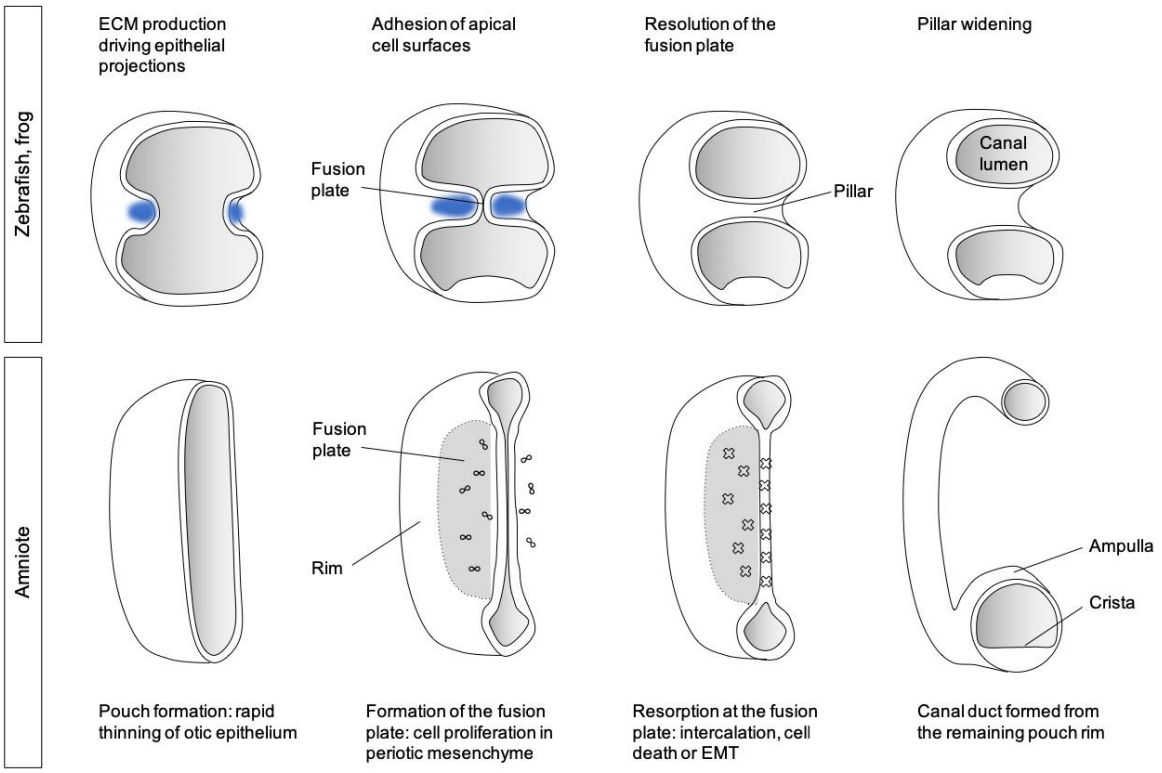

Figure 1.3. Diagram comparing the semicircular canal formation in anamniotes (zebrafish and frog) and amniotes. In the zebrafish and frog, two finger-shaped structures (highlighted in blue) meet and fuse to create a space (pillar) in the middle of the canal, therefore making it semicircular. In amniotes, the fusion plate is derived by the thinning of a pouch, from which cells are removed by apoptosis or EMT. This figure was reproduced with permission from Tanya T. Whitfield (Alsina & Whitfield 2017).

The abovementioned studies mainly focused on the genetic aspects underlying pillar formation. An attempt to provide a time-lapse imaging of pillar formation was made by Robert E. Waterman and Danny H. Bell, in 1984, and by Catherine Haddon and Julian Lewis, in 1996. These studies defined the role and activity of the bulge and projection and showed that a single layer of cells composes the walls of these structures. Before fusion, the cells surrounding the fusion plate produce junctional complexes that connect the bulge and projection, while the cells at the fusion plate do not. Instead, the cells at the fusion plate are integrated into the wall to allow for the formation of the pillar (Waterman and Bell, 1984; Haddon and Lewis, 1996). This is interesting because cell death has been proposed not to play a crucial role in this process, which implies that cells need to rearrange to form a gap in the middle of the pillar (Waterman and Bell, 1984; Haddon and Lewis, 1996; Geng *et al.*, 2013).

While these studies provide some basic information with respect to pillar development, many questions still remain unanswered:

- Are the cells at the fusion plate showing a different behaviour compared to the rest of the cells populating the projection and bulge?
- Upon fusion, do cells stop rearranging?
- Is the pillar composed by a mix of bulge and projection cells?

The following chapters will be focused on addressing these questions by taking advantage of the light-sheet microscope to visualise the ventral pillar development in living sample. Particular emphasis will be placed on the fusion event to provide more details on the cell movement required to accomplish this process. This will provide a new perspective on the pillar development, since previous analyses were carried out using fixed samples (Waterman and Bell, 1984), or differential interference contrast (DIC) microscopy (Haddon and Lewis, 1996).

In addition to that, this project will be focused on testing whether a specific gene network is required for the ventral pillar development. Previous work has, in fact, shown that many genes play a crucial role in pillar development, such as *eya1*, *otx1*, *tbx1* and genes coding for ECM components (Piotrowski *et al.*, 2003; Kozlowski *et al.*, 2005; Hammond and Whitfield, 2006; Geng *et al.*, 2013). For the purpose of this project, I focused specifically on the activity of *eya1* and *otx1* and on how they interact with other otic markers to give rise to the ventral pillar. The following sections will analyse in greater detail previous work on these two genes with respect to the inner ear development.

1.5. *EYA1* is crucial for otic development among vertebrates

1.5.1. Structure and function of EYA family

EYA1 plays a pivotal role in the process of inner ear development. The *EYA1* gene is conserved among humans, mice and zebrafish (Abdelhak *et al.*, 1997; Xu *et al.*, 1999; Kozlowski *et al.*, 2005). *EYA1* is the orthologue of the *Drosophila eyes absent* (*eya*) transcription factor, which has been described to regulate the development of anterior structures, such as the eyes. This gene encodes a protein that contains an homologous region (called eyaHR) at its C-terminus and a basic-region leucine zipper (bZIP) domain that accounts for the DNA binding (Abdelhak *et al.*, 1997). Human EYA1 is part of a family consisting of four members (EYA1, EYA2 and EYA3 and EYA4) exhibiting very similar amino acid sequences (Abdelhak *et al.*, 1997; Borsani *et al.*, 1999). For the purpose of the present work, the following sections will only focus on the activity of *EYA1*, but not the other members of the same family.

1.5.2. *Eya1* is required for multiple organ development

In *Drosophila* and mouse models, *eya/Eya* has been shown to control the survival of progenitor cells at early stages of eye and kidney development by indirectly repressing activation of the cell death route (Bonini, Leiserson and Senzer, 1993; Xu and Xu, 2015). Its loss, indeed, results in an increased death rate in the eye progenitor population and in the intermediate mesoderm giving rise to the nephric duct, which can be rescued by heat-shock overexpressing *eya* in the mutant *Drosophila* larvae (Bonini, Leiserson and Senzer, 1993; Xu and Xu, 2015). In humans, mutations in *EYA1* have been demonstrated to be causative for Branchio-Oto-Renal syndrome, an autosomal dominant disease characterised by branchial, otic and renal defects (Abdelhak *et al.*, 1997). Patients exhibit cervical cysts and fistulae, abnormalities in the outer, middle and inner ear that lead to hearing loss and vestibular defects and abnormalities in the kidneys, which fail to develop or show severe morphological defects (Fraser, Sproule and Halal, 1980). In contrast with the human condition, in other vertebrate models, such as mice and zebrafish, haploinsufficiency does not result in a similar phenotype (Xu *et al.*, 1999; Kozlowski *et al.*, 2005). In some cases, *Eya1*$^{+/-}$ mice show unilateral or bilateral hearing loss, due to abnormal development of the ossicles of the middle ear and a small percentage exhibit vestibular defect. *Eya1*$^{-/-}$ mutants die

at birth due to underdeveloped anterior structures, lack of kidneys, vestibular organs and acoustic ganglion. Moreover, TUNEL analysis showed that these morphological defects are accompanied by enhanced apoptosis (Xu *et al.*, 1999; Xu and Xu, 2015). These phenotypical observations have been corroborated by the analysis of the expression pattern of murine *Eya1*, which, at early developmental stages, can be found in all four branchial arches, except for the domains giving rise to the middle and outer ear structures, the metanephric mesenchyme, the ventromedial epithelium of the otic vesicle and the prospective statoacoustic ganglion. At later stages, *Eya1* is also expressed in mesenchymal region encompassing the prospective middle ear ossicles, which explains the previously described middle ear phenotype (Kalatzis *et al.*, 1998).

Further studies aimed at analysing the molecular foundations of these phenotypes highlighted the possibility that these can be linked to the inability of Eya1 to interact with Six1 (Ohto *et al.*, 1999; Buller *et al.*, 2001). The *Six1* gene is homologous to the *Drosophila* gene *sine oculis* and has been shown to act as a transcription factor and as a transcriptional co-factor in combination with *Eya1* (Xu *et al.*, 2003; Zheng *et al.*, 2003; Musharraf *et al.*, 2014). Specifically, it has been proposed that this interaction protects Eya1 from proteasome-mediated degradation. Its mutation is thought to prevent the interaction

between Eya1 and Six1 and, consequently, lead to the degradation of Eya1 (Musharraf *et al.*, 2014).

1.5.3. Role of *eya1* in zebrafish ear development

Studies on the zebrafish have shown similar results to those obtained on mice. The *dog-eared* (*dog*) mutation was first isolated in 1996, using the *N*-ethyl-*N*-nitrosourea (ENU) mutagenesis method, and was found to be caused by mutation in *eya1* in 2005 (Haffter *et al.*, 1996; Whitfield *et al.*, 1996; Kozlowski *et al.*, 2005). As in mice, a phenotype is only visible when both alleles are mutated and the homozygous mutants do not survive to adulthood (Whitfield *et al.*, 1996; Kozlowski *et al.*, 2005). However, zebrafish mutants for *eya1* live up to larval stage, which allows development of the semicircular canals to be followed (Whitfield *et al.*, 1996). Three *eya1* mutated alleles have been described: $eya1^{tm90b}$, $eya1^{to15b}$ and $eya1^{tp85b}$, with the first two sharing a similar 4 bp insertion, while the $eya1^{tp85b}$ mutation carries a C>T transition. Of these three, the $eya1^{tm90b}$ mutation has been shown to create a novel *MnlI* restriction site, which can be used for genotyping purposes (Kozlowski *et al.*, 2005).

With respect to the phenotype, it has been shown that these mutations have very similar effects on the embryos: the overall otic vesicle is smaller, and all three semicircular canals exhibit abnormalities comprising the lack of hair

cells in the cristae and dysmorphic pillars (Figure 1.5). There is enhanced apoptosis in the otic vesicle and posterior lateral line of mutants (Whitfield *et al.*, 1996; Kozlowski *et al.*, 2005) (Figure 1.4). This is interesting because, in zebrafish, it has been described that cell death is a very rare event during otic development (Bever and Fekete, 1999; Cole and Ross, 2001). This project is intended to provide more insights with about *eya1* mutant phenotype with particular interest in development of the ventral pillar. Apart from the brief descriptions of abnormal morphology and lack of cristae described above, no studies have examined development of the ventral pillar in these embryos. Finally, recent unpublished data from our laboratory suggest a genetic relationship between *eya1* and *otx1*, which could be required for the correct development of the ventral pillar and will be further investigated in chapter 5 (Blanco-Sánchez, B. and Giuliani, G., unpublished data).

With respect to the *eya1* and *otx1* expression in the otic vesicle, they are both expressed in the ventral otic epithelium at 24 hpf. The main difference between *eya1* and *otx1* expression is that, at 24 hpf, *eya1* is detectable in a larger domain of the ventral otic epithelium compared to *otx1* (Figure 1.7). To this day, there are no indications regarding *eya1* expression in the otic vesicle, at 72 hpf, with respect to the ventral pillar.

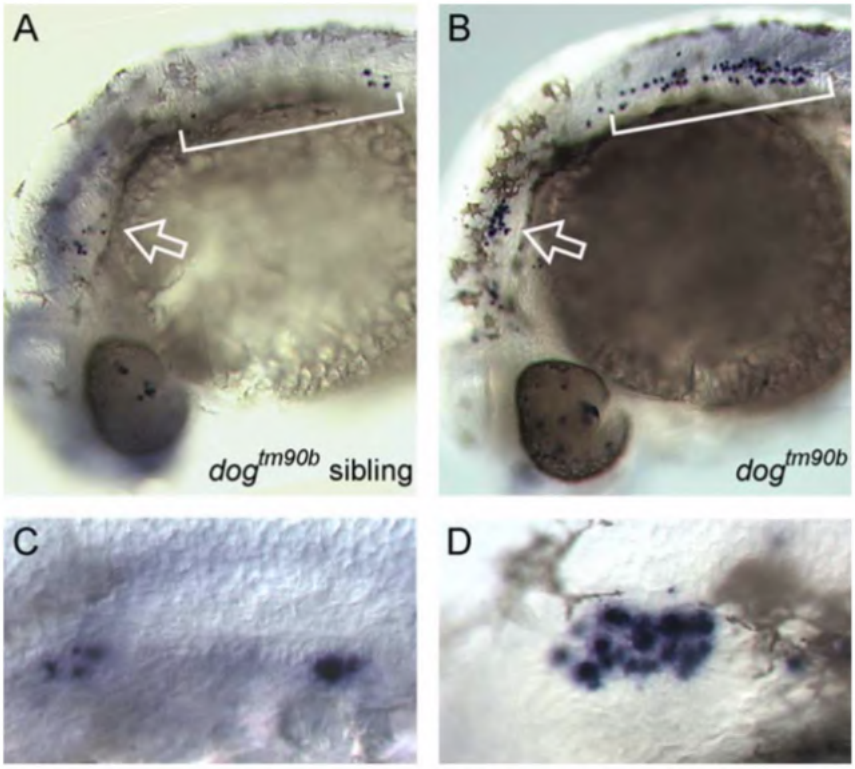

Figure 1.4. TUNEL staining showing enhanced apoptosis in the *eya1* mutant (B), compared to the siblings (A). The image was adapted from Kozlowski et al., 2005. White arrows indicate the increased number of apoptotic events in the mutant ear at 28 hpf (magnified in C and D). The square brackets highlight the increased apoptosis in the posterior lateral line.

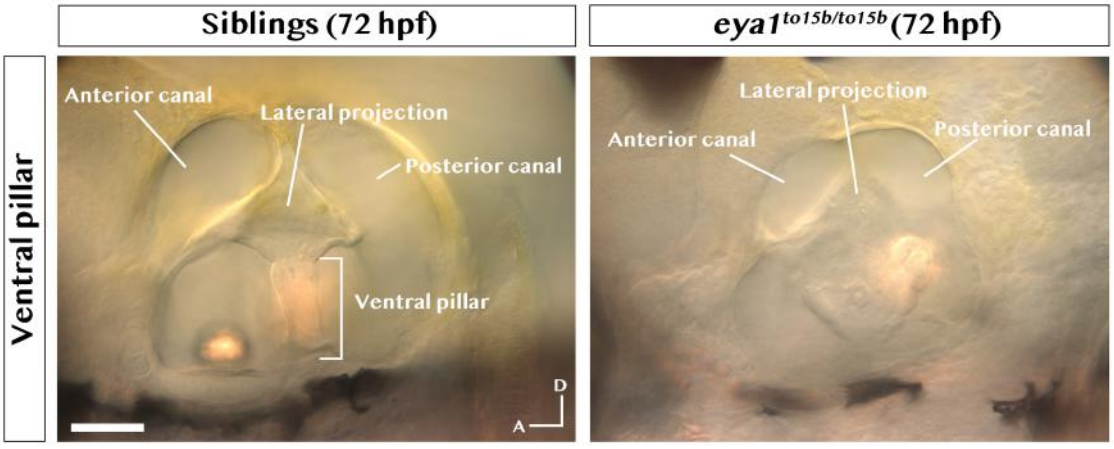

Figure 1.5. Panel showing the *eya1* mutant phenotype at 72 hpf. The overall otic vesicle is affected by the mutation and appears smaller. The ventral pillar phenotype is not clear from DIC imaging. This phenotype was firstly described by Whitfield and colleagues in 1996 and analysed by Kozlowski and colleagues in 2005. Scale bar, 50 μm.

1.6. Role of *otx1* during otic development

1.6.1. Structure and conservation of the OTX superfamily

In section 1.4.1, the importance of homeobox genes during otic placode induction has been discussed. This section is intended to provide more detailed information about the activity of *otx1* during embryonic development, with a particular focus on otic development.

Zebrafish *otx1* is a homeobox gene that belongs to the OTX superfamily of transcription factor genes. These are homologous to *orthodenticle* (*otd*) in *Drosophila melanogaster* and are part of the paired-like (Prd-like) class of transcription factor genes previously described to be involved in the development of anterior structures during embryonic development (Simeone *et al.*, 1993; Finkelstein and Boncinelli, 1994; Chen *et al.*, 1997; Simeone, 1998). The sequence of these genes shows several peculiarities: a lysine at position 50 (K_{50}), the homeodomain (a DNA-binding domain) at the N-terminus and an OTX-tail at the C-terminus (Furukawa, Morrow and Cepko, 1997; Galliot, De Vargas and Miller, 1999). The K_{50} residue is a characteristic of the Prd-like class that, among others, includes *Otx* and *Goosecoid* and differentiates this class from the Q_{50} Prd-like class and the Pax-type genes, which share the presence of the homeodomain (Galliot, De Vargas and Miller,

1999). The homeodomain is a sequence of ~ 180 base pairs (bp) (~ 60 amino acids) that allows the binding of homeoproteins to specific DNA target sequences. It is constituted by three α-helices, with the second and the third forming a helix-turn-helix architecture that provides the actual recognition and binding to the DNA (Gehring *et al.*, 1990). Finally, a study aimed at characterising the murine *Crx* (*cone-rod homeobox-containing*) gene helped to identify another common feature of the OTX superfamily: the OTX-tail. This is an amino acid sequence located to the C-terminus of the CRX, OTX1 and OTX2 proteins and has been found to be conserved among zebrafish, mouse, chick and *Xenopus laevis*, but not in *Drosophila* Otd (Mori *et al.*, 1994; Bally-Cuif *et al.*, 1995; Pannese *et al.*, 1995; Furukawa, Morrow and Cepko, 1997). The function of the OTX-tail has yet to be fully described.

1.6.2. *Otx* genes are fundamental for brain and sense organ development

During the first steps of embryogenesis, *Otx1* and *Otx2* have been found to be expressed in the developing diencephalon, mesencephalon and sense organs, such as the olfactory bulb, eye and inner ear (Cecchi, Mallamaci and Boncinelli, 2000). Mutation of both copies of *Otx2* is lethal due to the complete loss of the most anterior structures derived from the neural plate (forebrain, midbrain and anterior hindbrain), as well as severe impairments in their body

plan (Acampora and Simeone, 1999). *Otx1* homozygous mutants are viable but show severe brain abnormalities and epileptic seizures (Acampora *et al.*, 1996; Acampora and Simeone, 1999). With respect to sense organs, the mutation of murine *Otx1* has been shown to result in the loss of only the lateral semicircular canal of the inner ear (Acampora and Simeone, 1999). This effect is restricted to *Otx1*, which is mainly expressed in the prospective lateral canal (including the ampulla) and the pars inferior, which includes the saccular and lagenar macula; *Otx2* expression is, instead, restricted to the prospective pars inferior (Simeone *et al.*, 1993; Morsli *et al.*, 1999). The expression domain of *Otx1* becomes, then, confined to the posteroventral epithelium of the otic vesicle (presumptive lateral (horizontal) canal), but not in the presumptive crista, which arises from a more anterior domain characterised by the expression of *Bmp4* (Morsli *et al.*, 1998, 1999). Proof of the specificity of action of *Otx1* in lateral canal development is also provided by the fact that replacing murine *Otx1* with human *OTX2* does not rescue the lateral canal phenotype, but the epileptic and brain phenotypes are rescued (Acampora and Simeone, 1999). Interestingly, the activity on the inner ear development has been found to be a feature specific to *Otx1*, but not *Drosophila otd*, which can only rescue the head and brain phenotypes in *Otx1* mutant mice (Acampora *et al.*, 1998).

1.6.3. Zebrafish *otx1* in inner ear development

In zebrafish, five *otx* genes have been described: *otx1* (formerly *otx1b*), *otx2a* (formerly *otx3*, *otx1-like* and *otx1a*), *otx2b* (formerly *otx2*), *otx5* and *crx* (Li *et al.*, 1994; Mercier *et al.*, 1995; Germot *et al.*, 2001; Liu *et al.*, 2001). These genes have extensively been shown to play a role in the development of the forebrain and sense organs, such as eyes and inner ear (Mercier *et al.*, 1995; Mazan *et al.*, 2000; Liu *et al.*, 2001; Lane and Lister, 2012). This chapter will mainly focus on the activity of zebrafish *otx1* with respect to inner ear formation, due to it being one of the subjects of this project.

As previously described in section 1.4.3, the main difference in the development of semicircular canals between zebrafish and other vertebrates lies in the formation of three pillars in the fish, which become the hubs of the canals by 72 hpf (Waterman and Bell, 1984; Haddon and Lewis, 1996; Geng *et al.*, 2013). With respect to the ventral pillar (the hub of the lateral canal, see section 1.4.3), its development has been described to depend on the activity of *otx1* (Mazan *et al.*, 2000; Hammond and Whitfield, 2006). Morpholino-mediated knockdown of zebrafish *otx1* has, indeed, been described to result in the selective loss of the ventral pillar and lateral crista (Figure 1.6), in accordance to what has been previously described in murine models (Acampora and Simeone, 1999; Hammond and Whitfield, 2006). It is important to notice that, in

the zebrafish otic vesicle at 24 hpf, *otx1* is detectable in a very restricted region of the ventral otic epithelium (Figure 1.7) and, at 72 hpf, it stays expressed in the ventral floor of the vesicle surrounding the pillar, but it is never found in the actual pillar. How the expression of *otx1* relates with the region of outgrowth of the ventral projection will be discussed in the following chapters.

A recent study highlighted that the Otx1 protein sequence contains a histidine-rich region, which cannot be found in Otx2b (Bellipanni, Murakami and Weinberg, 2010). However, it is still unclear if this histidine stretch could provide Otx1 with a specificity of action when it comes to lateral canal development. So far, there are no indications in the literature as to whether the mutation of *otx1* would replicate the phenotype observed in the morpholino-injected embryos (hereinafter referred to as "morphants") (Figure 1.6). In the next chapters, the outcomes of *otx1* mutation will be analysed to provide further insights about the genetics underlying ventral pillar development.

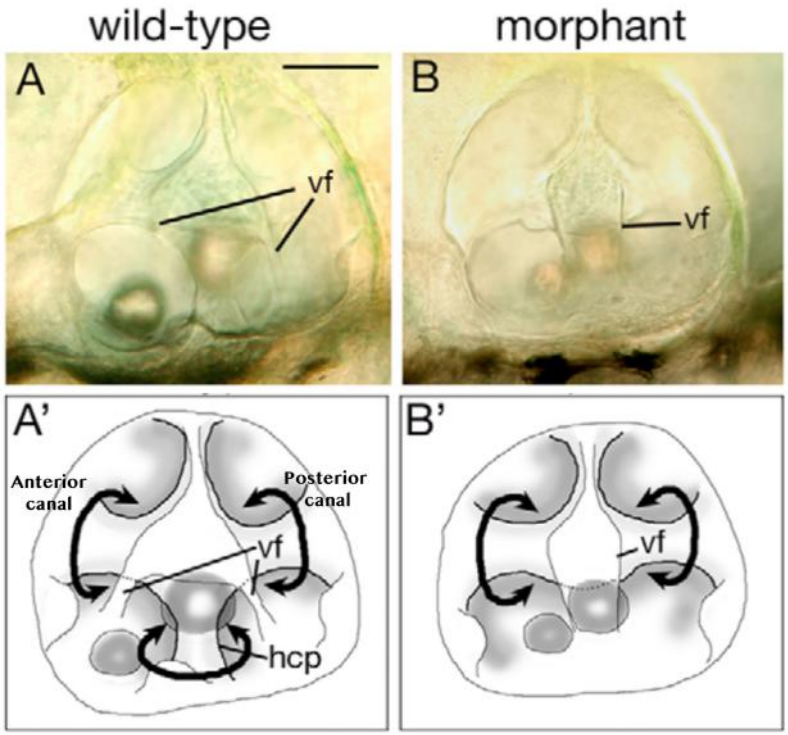

Figure 1.6. Panel showing the *otx1* morphant phenotype. The image was adapted from Hammond & Whitfield, 2006. Compared to wild-types (A and A'), the morphants (B and B') exhibit a complete loss of the ventral pillar, the two ventral folds (vf) are fused together and the otoliths lie closer. Scale bar, 50 μm.

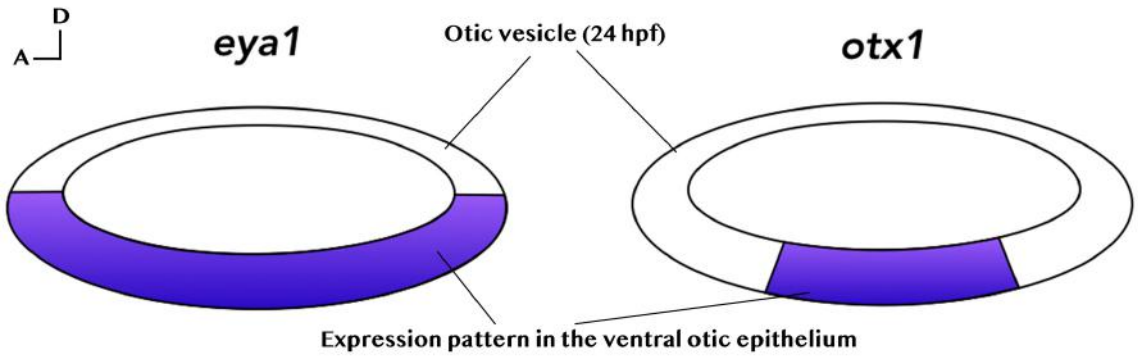

Figure 1.7. Diagram showing the expression patterns of *eya1* and *otx1* in the otic vesicle at 24 hpf, which overlap in a restricted region of the ventral otic epithelium.

1.7. The significance of light-sheet microscopy in the study of cell behaviour

In recent years, light-sheet imaging has established itself as a benchmark for live imaging over long time periods, allowing the study of the behaviour of cells in their native three-dimensional environment (Santi, 2011; Heddleston and Chew, 2016; Zagato *et al.*, 2018). The advantages of light-sheet microscopy and its design will be discussed in chapter 2, section 2.7.2. This helped to elucidate many aspects of organ development such as neurogenesis in the inner ear. It has recently been described that otic neurogenesis starts outside of the inner ear with a single *neurogenin1* (*ngn1*) positive cell that enters this structure from its antero-ventral pole and instructs other neighbouring cells to undertake neural fate. These cells become, therefore, committed to undergo epithelial-to-mesenchymal transition and initiate neurogenesis (Hoijman *et al.*, 2017). In addition, it has been observed that blocking FGF signalling inhibits the expression of *ngn1* and prevents the "pioneer" cell from entering the developing inner ear and initiating neurogenesis (Hoijman *et al.*, 2017). Light-sheet imaging also enabled tracking of the movement of these cells during delamination from the inner ear to form the statoacoustic ganglion (SAG). It has been shown that this starts around 18 hours post fertilisation (hpf) and that

the side of the inner ear from which the cells delaminate reflects their position into the SAG (Dyballa *et al.*, 2017).

These studies highlight the number of opportunities that are emerging in the biological field thanks to the advent of light-sheet microscopy. For this reason, I took advantage of this technology to study the behaviour of cells involved in lateral semicircular canal development and provide new insights to previous genetic analyses.

1.8. Aims

The aim of this project is to define and link the genetic and kinetic requirements leading to the development of the lateral semicircular canal using the zebrafish as a model. The pillar formation has always been considered as a process involving the fusion of two populations of epithelial cells. However, a number of questions still remain unanswered, such as what cells account for the ventral pillar structure after the fusion event and whether these cells effectively exhibit behaviours which are characteristic of an epithelial state. By taking advantage of live imaging, the three-dimensional cell tracking of the ventral bulge and ventral projection cells will be compared and contrasted to establish whether different cell populations exhibit different movements and behaviours.

In addition to the cell behaviour analysis, this project is also focused on testing whether a specific set of genes is involved in the cell specification during ventral pillar development. For this purpose, two mutant lines will be used: *otx1* and *eya1* mutants. *otx1* was chosen due to its previously described specificity of action on the lateral canal development (both in amniotes and anamniotes; see section 1.6.2 and 1.6.3). However, since our knowledge regarding *otx1* activity in the ventral pillar formation in zebrafish is derived

from morpholino-mediated knockdown experiments, these data will be further confirmed and strengthened by taking advantage of the mutant line. On the other hand, the effects of *eya1* mutation on the ventral pillar development will be analysed in more detail due to these being not fully described in the literature and to the fact that previous unpublished work linked the mutation of *eya1* with an expanded expression of *otx1* in the otic vesicle. This raised the question as to whether the *eya1* mutants could exhibit an opposite phenotype to that of the *otx1* mutant or if any structure of the otic vesicle is missing due to the enhanced apoptosis detected in this line (see section 1.5.3). The phenotypical and gene expression data obtained from the *otx1* and *eya1* mutants will then be used to hypothesise a gene network underlying cell specification events required for ventral pillar development.

Finally, this study contributes to establish new ways to extract data concerning cell behaviour from live imaging and link them with gene expression analysis in order to achieve a more comprehensive overview of the mechanisms underlying inner ear development.

2. MATERIALS AND METHODS

2.1. Zebrafish husbandry

All zebrafish lines used for the present work were raised and maintained at the temperature of 28.5°C in the Aquaria facilities of the University of Sheffield. They were provided with cycles of 14 hours of light and 10 hours of dark. All embryos used for experiments were raised in E3 medium at 28.5°C for up to 5.2 dpf in accordance with UK Home Office regulations.

2.1.1. Wild-type lines

Wild-type (WT) embryos used for this project were obtained from an AB line (ZDB-GENO-960809-7) and raised under the same conditions described above.

2.1.2. *eya1* mutant lines

Two different *eya1* mutations were used for this project: *eya1*^{tp85b} (ZDB-GENO-980202-1547) and *eya1*^{tm90b} (ZDB-GENO-980202-1557) (Whitfield et al. 1996; Kozlowski et al. 2005). Homozygous mutants for each allele were

obtained by incrossing heterozygous fish and sorted according to the ear phenotype as previously described (Whitfield et al. 1996).

2.1.3. *otx1* mutant line

The *otx1* mutants used during this project, namely *otx1*^{sa96} (ZDB-GENO-150326-5), were obtained from the Wellcome Trust Sanger Institute. Homozygous mutants were obtained by incrossing heterozygous fish and sorted after 3 dpf according to their ear phenotype, previously described for morpholino-mediated knock down of *otx1* (Hammond and Whitfield, 2006).

2.1.4. Transgenic lines

For live fluorescent imaging, the above-mentioned mutant lines were crossed with an *mir137::EGFP;xEF1a::H2B-RFP* transgenic line. The *xEF1a::H2B-RFP* line was obtained from the laboratory of Angela Nieto (Instituto de Neurociencias, Alicante, Spain) and exhibits red fluorescence in all the nuclei (Rodríguez-Aznar, Barrallo-Gimeno and Nieto, 2013). The *miR137::EGFP* line was obtained from Thomas S. Becker's laboratory (University of Sydney, Australia). This was designed as an enhancer trap line constituted of a human

miR137 enhancer, a *GATA2* promoter and an *EGFP* sequence flanked by two *Tol2* sequences. This construct was randomly inserted in the zebrafish genome resulting in multiple insertions sites. The enhancers surrounding the insertion sites, instead of the *mir137* enhancer, induced the *EGFP* expression in various regions, including the ventral pillar in the ear. Therefore, I selected and raised only the fish showing green fluorescence in the ventral pillar to obtain a line with a consistent *EGFP* expression only in that region. As part of this project, I attempted to identify the insertion site of the enhancer trap construct (section 3.7).

The analysis of the *neurod1* (formerly *neurod*) expression in the *otx1* mutants and siblings was carried out using the Tg(*neurod1::EGFP*) line, obtained from Walter Marcotti's laboratory (University of Sheffield), and firstly described by Obholzer and colleagues (Obholzer *et al.*, 2008). This line was injected at one cell stage with a lyn-tdTomato mRNA, which allows for the visualisation of cell membranes (Zecca *et al.*, 2015).

2.2. Genotyping protocols

2.2.1. *otx1*^{sa96} genotyping

As the *otx1* heterozygous and WT embryos were morphologically indistinguishable, a genotyping protocol was designed to identify and raise only heterozygous adult fish. The mutation is a C>T transition, which introduces an early stop codon and a *BfaI* restriction site. Primers were designed to amplify a 398 bp region surrounding the mutation site. The PCR product was subsequently digested using *BfaI* (*FspBI*) by incubating the digestion mix at 37°C overnight as recommended by Thermo Fisher Scientific. The success of the reaction was evaluated through electrophoresis on a 3% agarose gel. By design, two bands for the homozygous mutants (283 and 115 bp), three bands for the heterozygous (398, 283, 115 bp) and one band for the WT (398 bp) were expected. Primers (Table 2.1) and PCR settings used for this protocol are listed below.

Primers	Sequence
otx1 Forward primer	5'-CACCAGGGAGAGCACAGG-3'
otx1 Reverse primer	5'-TGAGCTGATGAGGGTGGTG-3'
Stock	**Concentration**
Master stock	100 μM
Working stock	10 μM

Table 2.1. List of the primers used for *otx1* genotyping and relative concentrations.

PCR settings:

1) 94°C 2 minutes
2) 94°C 20 seconds
3) 57.5°C 30 seconds
4) 72°C 24 seconds
5) Go to step 2) 25 times
6) 72°C 5 minutes
7) 12°C infinite hold

2.2.2. *eya1*^{tm90b} genotyping

As previously described from Kozlowski et al., *eya1* heterozygous and WT embryos are morphologically indistinguishable. For this reason, I used a genotyping protocol to identify *eya1* heterozygous at adult (3 months) (Kozlowski *et al.*, 2005). The protocol takes advantage of the T>G transversion occurring in the *eya1*^{tm90b} mutation, which introduces a novel *MnlI* restriction site. A genomic fragment of 170 bp surrounding this novel restriction site was amplified and digested using *MnlI*. Upon digestion, the PCR product is cleaved into various fragments depending on the genotype:

- Wild-type: 3 fragments (116, 42 and 12 bp)
- *eya1*$^{tm90b/+}$: 5 fragments (116, 79, 42, 37 and 12 bp)
- *eya1*$^{tm90b/tm90b}$: 4 fragments (79, 42, 37 and 12 bp)

However, since the 37 and 12 bp fragments are too small and cannot be detected on a 3% agarose gel, the bands visualised are two for the wild-types (116 and 42 bp), thee for the heterozygous (116, 79 and 42 bp) and two for the mutants (79 and 42 bp). Primers (Table 2.2) and PCR settings used for this protocol are listed below.

Primers	Sequence
eya1^{tm90b} Forward primer	5'-CCAACGTCGGTGTCATTGGGAC-3'
eya1^{tm90b} Reverse primer	5'-CGGTGAGCTTTGTAGGGGTGAGG-3'
Stock	**Concentration**
Master stock	100 μM
Working stock	10 μM

Table 2.2. List of the primers used for *eya1*^{tm90b} genotyping and relative concentrations.

PCR settings:

5) 94°C 2 minutes
6) 94°C 20 seconds
7) 55°C 30 seconds
8) 72°C 11 seconds
5) Go to step 2) 34 times
6) 72°C 5 minutes
7) 12°C infinite hold

2.3. Morpholino injection

Two different *otx2a* (formerly *otx1a*) antisense morpholinos (MOotx2a) were obtained from Corinne Houart's laboratory (MRC Centre and Department of Developmental Neurobiology, King's College, London). One was a fluorescein-tagged fluorescent splice-blocking morpholino and the other was an untagged ATG-morpholino (Foucher *et al.*, 2006). Sequences and stock concentrations are listed in Table 2.3. The splice-blocking morpholino (Foucher *et al.*, 2006) was injected at the doses of 1.2 ng, 1.8 ng, 2.4 ng and 3.0 ng. Success of the injection was evaluated by looking at the fluorescence of the embryos. The ATG-morpholino was injected at the doses of 6.0 ng and 9.0 ng. Injection mix was prepared as described in Table 2.3. Both morpholinos were denatured at 65°C for 7 minutes before the injection.

MOotx2a final concentration	1.2 ng	1.8 ng	2.4 ng	3.0 ng	6.0 ng	9.0 ng
Volume of MOotx2a	0.7 µl	0.7 µl	0.7 µl	0.7 µl	3.5 µl	3.5 µl
Phenol Red dye	0.5 µl	0.5 µl	0.5 µl	0.5 µl	0.5 µl	0.5 µl
H_2O milliQ	3.8 µl	3.8 µl	3.8 µl	3.8 µl	1 µl	1 µl
Total volume	5 µl	5 µl	5 µl	5 µl	5 µl	5 µl
Volume injected	1 nl	1.5 nl	2 nl	2.5 nl	1 nl	1.5 nl

Table 2.3. Table listing the doses and final volumes of MOotx2a injected in each embryo at one cell stage.

2.4. CRISPR/Cas9 system injection

The CRISPR/Cas9 system is an efficient method to introduce mutations in a specific region of a gene of interest. It is based on the approach used by bacteria to cleave and silence exogenous DNA by recognising clustered, regularly interspaced, short palindromic repeats (CRISPR) and cutting them with a Cas9 nuclease. To achieve that, a guide-RNA (gRNA), designed to anneal to a target sequence, and the Cas9 mRNA or protein are co-injected in a one-cell stage embryo. Once the gRNA has annealed to the target sequence, the Cas9 nuclease is recruited to induce a double-strand break upstream to a –NGG (PAM) site. The non-homologous end joining (NHEJ) and homologous recombination (HR) systems are activated and mutations can be introduced in the process of trying to repair the break (Hruscha *et al.*, 2013).

This method was used to make an attempt at creating a stable *otx2a* mutant line. Three gRNA antisense oligonucleotide (guide-oligo) sequences were designed as described by Hruscha et al. 2013. Each sequence was designed to target a specific restriction site for MwoI, MslI or BslI (Figure 2.1). The target sequences were chosen based on their location in the first two exons or the beginning of the third exon, which is the sequence that encodes for the homeodomain, the DNA binding site. Indeed, a mutation in the DNA binding

site is more likely to produce a non-functional protein. It is also desirable to induce a mutation as close as possible to the beginning of the open reading frame to induce a frameshift that could also affect the downstream domains.

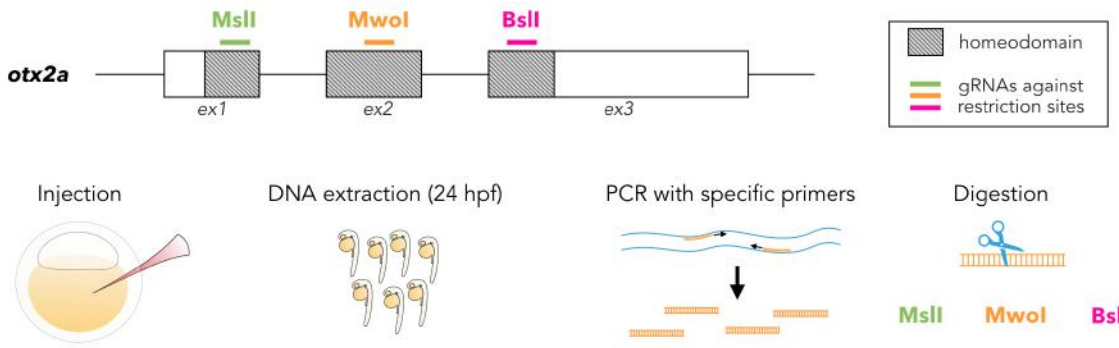

Figure 2.1. Schematic representation of the CRISPR/Cas9 mutagenesis method. In green, orange and magenta are shown the three gRNAs designed to target respectively MslI, MwoI and BslI restriction sites. Each gRNA was injected at one cell stage in combination with the Cas9 mRNA; the DNA was extracted at 24 hpf and amplified using specific primers for each restriction site. Upon amplification, the DNA was digested with the appropriate enzyme to assess the success of mutation.

To design each guide-oligo, a sequence of 18 nucleotides upstream to the chosen PAM site was inserted into a scaffold sequence containing a promoter for the T7 Polymerase (Table 2.5). Prior to transcription, the guide-oligo was amplified by PCR and purified from a gel to increase its purity (primers listed on Table 2.4). Details for amplification are listed below:

- Resuspend guide-oligo in TE buffer (Tris-HCl 10 mM, EDTA 0.1 mM) to make a 100 μM stock.
- Dilute the stock solution to 1 μM in milliQ H_2O.
- Prepare PCR mix as follows:
  - REDTaq Polymerase 50 μl
  - Guide-oligo primer F 1.25 μl
  - Guide-oligo primer R 1.25 μl
  - Guide-oligo DNA 2 μl
  - H_2O milliQ up to 100 μl of final volume

- PCR settings:

1) 95°C 1 minute
2) 95°C 15 seconds
3) 60°C 30 seconds
4) 72°C 20 seconds
5) Go to step 2) 40 times
6) 72°C 5 minutes
7) 12°C infinite hold

Primers	Sequences
Guide-oligo primer F	5'- GCGTAATACGACTCACTATAG -3'
Guide-oligo primer R	5'- AAAGCACCGACTCGGTGCCAC -3'
Stocks	**Concentrations**
Master stock	100 μM
Working stock	10 μM

Table 2.4. List of primers and relative concentrations used to amplify and increase purity of each guide-oligo.

The resulting PCR product was subsequently run on a 1% agarose gel, purified using the QIAquick gel extraction kit provided by Qiagen and transcribed using the MEGAshortscript T7 transcription kit. *In vitro* transcription was set up as follows:

- 10x Transcription buffer 2 μl
- ATP 2 μl
- CTP 2 μl
- GTP 2 μl
- UTP 2 μl
- T7 Enzyme mix 2 μl
- DNA 2 μl
- H_2O milliQ up to 20 μl of final volume

The transcription mix was incubated at 37°C for 2 hours and the following protocol was used:

- Add 1 µl of DNase and incubate for 30 mins at 37°C;
- Add H_2O milliQ to reach 100 µl in volume;
- Add 33 µl of 10 M ammonium acetate and 350 µl of absolute ethanol;
- Precipitate mix at -80°C for at least 2 hours;
- Centrifuge at max speed for 30 minutes at 4°C;
- Wash pellet with 70% Ethanol and air-dry;
- Dissolve pellet in 15 µl of milliQ H_2O.

Success of transcription was assessed by gel electrophoresis and concentration was measured using a NanoDrop spectrophotometer. The nCas9 mRNA was obtained by *in vitro* transcription using the Sp6 mMessage mMachine transcription kit. The transcription mix was set up as follows:

- 10x Transcription buffer 2 µl
- NTP/CAP 10 µl
- Sp6 Enzyme mix 3 µl
- DNA 1-2 µg
- H_2O milliQ up to 20 µl of final volume

The same protocol used for guide-oligo transcription was used. Finally, the gRNA was injected at the dose of 1024 ng/µl together with the nCas9 mRNA (500 ng/µl) (Hruscha *et al.*, 2013). Each embryo was injected with 1 nl of injection mix and grown for 24 hours at 28.5°C in E3 medium. The success of mutation was assessed by DNA extraction at 24 hpf from a fraction of injected embryos, PCR amplification and digestion with the appropriate restriction enzyme (MwoI, MslI or BslI).

Target sequence	**Restriction site**	**Restriction enzyme**
GCAGCAGCAGCAGAGCAG	GCNNNNN^NNGC	MwoI
GACATTTTCATGCGCGAG	CAYNN^NNRTG	MslI
GCATCCCTCTGTGGGATA	CCNN_NNN^NNGG	BslI
Scaffold sequence	5' – AAAGCACCGACTCGGTGCCACTTTTTCAA GTTGATAACGGACTAGCCTTATTTTAACTTGC TATTTCTAGCTCTAAAACNNNNNNNNNNNNNN NNNNNNCTATAGTGAGTCGTATTACGC - 3'	

Table 2.5. Table listing the target sequences inserted into the scaffold to produce a mutation in specific restriction sites.

2.5. Whole mount *in situ* hybridisation

2.5.1. *In situ* hybridisation protocol

The whole mount *in situ* hybridisation (WISH) protocol allows visualisation of a specific gene transcript through a colorimetric reaction. It is a multi-step protocol carried out over the course of three days. Embryos to be processed for WISH were fixed in 4% paraformaldehyde (PFA) and dehydrated by storing them in absolute methanol for at least 2 hours at -20°C. The protocol used was described by Thisse et al. 2008; all solutions are listed on Table 2.6:

- Day 1
    - Rehydrate the embryos by washing them with 75%, 50% and 25% methanol in PBS 1x for 5 minutes each at room temperature (RT);
    - Wash 4 times, 5 minutes each, with PBT at RT;
    - Permeabilise by incubating in Proteinase K (10 mg/ml stock, diluted 1:1000 in PBT) at 20°C for the appropriate amount of time depending on the stage:

– 1 cell to 1 somite	No Proteinase K needed
– 1 to 8 somites	1 minute
– 9 to 18 somites	3 minutes
– 18 somites (24 hpf)	10 minutes
– 36 hpf to 5 dpf	30 minutes

- Fix by incubating in 4% PFA for 20 minutes at RT;
- Wash 4 times, 5 minutes each, with PBT at RT;
- Incubate in hybridisation mix with tRNA and heparin (HM+) for at least 3 hours at 70°C;
- Incubate overnight at 70°C in HM+ containing digoxigenin (dig) labelled probe.

- Day 2
  - Wash with hybridisation mix without tRNA and heparin (HM-) for 10 minutes at 70°C;
  - Wash with 75%, 50% and 25% HM- in SSC 2x for 10 minutes each at 70°C;
  - Wash with SSC 2x for 10 minutes at 70°C;
  - Wash twice with SSC 0.2x for 30 minutes each at 70°C;

- Wash with 75%, 50% and 25% SSC 0.2x in PBT for 10 minutes each at RT;
- Wash with PBT for 10 minutes at RT;
- Incubate in blocking solution for at least 3 hours at RT;
- Incubate in blocking solution containing anti-dig antibody overnight at 4°C.

- Day 3
  - Wash 6 times with PBT for 15 minutes each at RT;
  - Wash 3 times with Alkaline Tris buffer for 5 minutes each at RT;
  - Incubate in staining mix at RT until embryos are stained;
  - Stop staining reaction by washing with PBT + EDTA 0.5M (diluted 1:500);
  - Fix the staining by incubating in 4% PFA for 20 minutes at RT;
  - Wash embryos with 25%, 50% and 75% glycerol in water and store at 4°C.

Solutions for *in situ* hybridisation			
PBT	**HM+**	**Blocking buffer**	**Alkaline Tris buffer**
Tween20 10% 500 µl	Formamide 25 ml	PBT 39.2 ml	$MgCl_2$ 1M 2.5 ml
PBS[1] 1x up to 50 ml	SSC 20x 12.5 ml	Sheep Serum 800 µl	Tris HCl pH 9.5 5 ml
Proteinase K 10mg/ml is diluted 1:1000	Tween20 10% 50 µl	BSA1[2] 8 mg	NaCl 5M 1 ml
	Citric acid 1M 460 µl	Antibody is diluted 1:2000	Triton 10% 500 µl
	Heparin 50 mg/ml 50 µl		H_2O milliQ up to 50 ml
	tRNA 50 mg/ml 500 µl		For staining mix add:
	H_2O milliQ up to 50 ml		NBT[3] 2.25 µl/ml
			BCIP[4] 3.5 µl/ml

Table 2.6. List of solutions used for WISH protocol. Phosphate-buffered saline; 2: Bovine Serum Albumin; 3: Nitro Blue Tetrazolium Chloride; 4: 5-Bromo-4-Chloro-3-Indoyl-Phosphate.

2.5.2. Antisense probe design and transcription

Digoxigenin labelled antisense mRNA probes for *in situ* hybridisation were obtained by *in vitro* transcription. Prior to the reaction, plasmids containing template DNA sequences were linearized with appropriate restriction enzymes. Afterwards, the transcription mix was prepared as follows:

- 10x Transcription buffer — 2 µl
- Dig-labelled nucleotides mix — 1 µl
- RNase inactivator — 1 µl
- RNA Polymerase — 2 µl
- Linearized DNA — 1-2 µg
- H_2O milliQ — up to 20 µl of final volume

The mix was incubated at 37°C for 2 hours and the following protocol has been followed:

- Add 1 µl of DNase and incubate for 20 minutes at 37°C;
- Add 10 µl of ammonium acetate and 75 µl of absolute ethanol;
- Spin at maximum speed for 20 minutes at 4°C;
- Wash with 70% ethanol;

- Dissolve in 25 μl of water;
- Add 23 μl of formamide and store at -20°C.

The success of the reaction was evaluated by electrophoresis on a 1% agarose gel.

2.6. Thermal asymmetric interlaced PCR

The thermal asymmetric interlaced (TAIL) PCR method was used to identify the insertion site of the enhancer trap construct providing the *EGFP* expression in the *mri137::EGFP* line. This method was described by Liu and Whittier in 1995 and relies on a series of three consecutive PCRs (primary, secondary and tertiary reaction) carried out using two sets of primes:

- Long specific primers (Tol2 primers): designed to anneal to the 5' and 3' ends of the Tol2 sites flanking the *EGFP* sequence. Each reaction is carried out using a Tol2 primer that is nested to the one used in the previous reaction and are, therefore, called Tol2-1, Tol2-2 and Tol2-3.
- Arbitrary degenerate (AD) primers: four different primers designed not to anneal to any specific sequence.

The primary reaction generates a product that contains various non-specific sequences derived from mixing one of the Tol2-1 primers (separate reactions are carried out for the 3' or the 5' primer) and one of the AD primers. This first product is then diluted 2:25 in milliQ water and 2 μl of this mix are used as template for the secondary reaction, where the same AD primer coupled with a Tol2-2 primer. The tertiary reaction is set up in the same way but using the product of the secondary reaction as template. This protocol is designed so that with every reaction a more specific product is amplified. Finally, the products from the secondary and tertiary reactions are visualised by electrophoresis on a 2% gel and selected candidate bands are excised, purified and sequenced. Results of the sequencing are, then, compared with the zebrafish genome using Basic Local Alignment Search Tool (BLAST) on the Ensembl database.

Further confirmation of the TAIL PCR result was obtained by designing two new primers, specific for the candidate insertion site, that would provide amplification when coupled with the Tol2-3 primers. Sequences of every primer (Table 2.7) and details on the settings of each reaction are listed below.

Long specific primers	
Tol2 5'-1	GGGAAAATAGAATGAAGTGATCTCC
Tol2 5'-2	GACTGTAAATAAAATTGTAAGGAG
Tol2 5'-3	CCCCAAAAATAATACTTAAGTACAG
Tol2 3'-1	CTCAAGTACAATTTTAATGGAGTAC
Tol2 3'-2	ACTCAAGTAAGATTCTAGCCAGA
Tol2 3'-3	CCTAAGTACTTGTACTTTCACTTG
Arbitrary degenerate primers	
AD-3	WGTGNAGNANCANAGA
AD-5	WCAGNTGWTNGTNCTG
AD-6	STTGNTASTNCTNTGC
AD-11	NCASGAWAGNCSWCAA
New specific primers	
Specific primer F	ATATTGCAGATACAGTATAT
Specific primer R	ATTAAAGCTAGCACGATTGC

Table 2.7. List of primers used for primary, secondary and tertiary TAIL PCR reaction. The 'new specific primers' were used for confirming the TAIL PCR results.

Below are listed the primer mixtures prepared ahead of reaction setup and containing one Tol2 primer (1.5 μM) and one AD primer (10 μM):

- **Primary reaction:** Tol2 5′-1/AD-3; Tol2 5′-1/AD-5; Tol2 5′-1/AD-6; Tol2 5′-1/AD-11; Tol2 3′-1/AD-3; Tol2 3′-1/AD-5; Tol2 3′-1/AD-6; Tol2 3′-1/AD-11
- **Secondary reaction:** Tol2 5′-2/AD-3; Tol2 5′-2/AD-5; Tol2 5′-2/AD-6; Tol2 5′-2/AD-11; Tol2 3′-2/AD-3; Tol2 3′-2/AD-5; Tol2 3′-2/AD-6; Tol2 3′-2/AD-11
- **Tertiary reaction:** Tol2 5′-3/AD-3; Tol2 5′-3/AD-5; Tol2 5′-3/AD-6; Tol2 5′-3/AD-11; Tol2 3′-3/AD-3; Tol2 3′-3/AD-5; Tol2 3′-3/AD-6; Tol2 3′-3/AD-11

Reaction mix:

- RedTaq Polymerase 10 μl
- Primer mix 4 μl
- DNA 2 μl
- H_2O milliQ up to 20 μl of final volume

Primary PCR settings:

1) 94°C 2 minute
2) 94°C 30 seconds
3) 62°C 1 minute
4) 72°C 2.5 minutes
5) Go to step 2) 4 times
6) 94°C 30 seconds
7) 25°C 3 minutes
8) Ramping 0.3°C/sec to 72°C
9) 72°C 2.5 minutes
10) 94°C 10 seconds
11) 61°C 1 minute
12) 72°C 2.5 minutes
13) 94°C 10 seconds
14) 61°C 1 minute
15) 72°C 2.5 minutes
16) 94°C 10 seconds
17) 44°C 1 minute
18) 72°C 2.5 minutes
19) Go to step 10) 14 times
20) 72°C 5 minutes

Secondary PCR settings:

1) 94°C 10 seconds

2) 61°C 1 minute

3) 72°C 2.5 minutes

4) 94°C 10 seconds

5) 61°C 1 minute

6) 72°C 2.5 minutes

7) 94°C 10 seconds

8) 44°C 1 minute

9) Ramping 1.5°C/sec to 72°C

10) 72°C 2.5 minutes

11) Go to step 1) 14 times

12) 72°C 5 minutes

Tertiary PCR settings:

1) 94°C 15 seconds

2) 44°C 1 minute

3) Ramping 1.5°C/sec to 72°C

4) 72°C 2.5 minutes

5) Go to step 1) 29 times

6) 72°C 5 minutes

To confirm the results of the TAIL PCR, a set of new specific primers listed above was used as follows:

Reaction mix:

- RedTaq Polymerase 10 µl
- Specific Primer 1 µl
- Tol2 primer 1µl
- DNA 3 µl
- H_2O milliQ up to 20 µl of final volume

PCR settings:

1) 94°C 2 minutes
2) 94°C 20 seconds
3) 44°C 30 seconds
4) 72°C 18 seconds
5) Go to step 2) 34 times
6) 72°C 5 minutes
7) 12°C infinite hold

2.7. Microscopy

2.7.1. Compound microscope

Pictures of live zebrafish embryos and *in situ* experiments were acquired using an Olympus BX51 compound microscope with a C3030 Zoom camera and Cell^{B} software.

2.7.1.1. Embryo mounting

Live embryos were anesthetised by incubating in Tricaine methansulfonate (MS-222), diluted 1:25 in the petri dish, and mounted on a glass slide with methyl cellulose. Samples processed by *in situ* hybridisation were mounted on glass slides using 75% glycerol.

2.7.2. Light-sheet microscope

A Zeiss Z1 light-sheet microscope and ZEN (Black edition) software were used to obtain time-lapse movies of the ventral pillar formation. The use of the light-sheet microscope, instead of a confocal, brings numerous advantages that result from the design and acquisition method. While in a normal confocal microscope the detection and illumination axes are the same, a light-sheet

microscope is built so that a laser beam is shaped into a thin sheet of light and illuminates the sample perpendicularly to the detection axis (Figure 2.2). This allows for better three-dimensional images because only the fluorescent particles that are in focus are excited, while those that are out of focus are not. In addition to that, the use of a thin sheet of light provides much less phototoxicity because only the focal plane of interest is illuminated. This results in the possibility to image living samples for long periods of time with almost no photo-bleaching and a high survival rate (Santi, 2011; Zagato *et al.*, 2018). Imaging was carried out in the Wolfson Light Microscopy Facility, supported by a BBSRC ALERT14 award for light-sheet microscopy (BB/M012522/1).

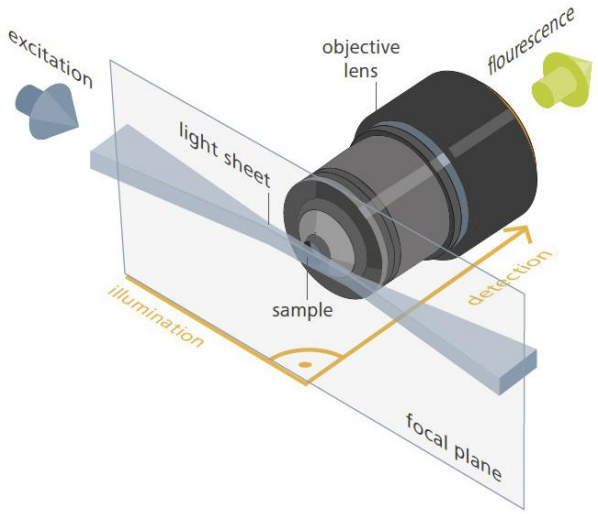

Figure 2.2. Schematic representation of the functioning of the light-sheet Z1 microscope provided by Zeiss. The image shows the detection axis being perpendicular to the illumination axis and the shape of the sheet of light that illuminates the sample, which is thicker at the sides and thinner in the centre. Image adapted from Zeiss website (https://blogs.zeiss.com).

2.7.2.1. Embryo mounting

Embryos were anaesthetised as described in paragraph 2.7.1.1 and mounted in 0.8% low melting point agarose using a glass capillary. The capillary was then inserted in the microscope using a magnetic adaptor and the embryo pushed out of the capillary and left to hang in a column of agarose. The chamber hosting the embryo was previously filled up with E3 medium and Tricaine (1:25 dilution).

2.7.2.2. Acquisition settings

Time-lapse movies were acquired using the following settings:

Pixel scaling	
Scaling X	0.225 μm
Scaling Y	0.225 μm
Scaling Z	1.000 μm
Detection settings	
Optics	W Plan-Apochromat 20x/1.0 UV-VIS_4909000084
Zoom	1.0x
Lasers	561 nm (5.0% power) 488 nm (5.0% power)
Laser plate	SBS LP 560
Laser block filter	LBF 405/488/561
Exposure time	99.9 ms
Light-sheet thickness	4.49 μm
Acquisition interval	5 minutes

2.7.3. Airyscan microscope

An Airyscan confocal microscope was used to obtain high resolution images of the *eya1* mutant inner ear. The reason for using an Airyscan, instead of a normal confocal microscope, is that normal fluorescence microscopes require the closing of a pinhole to eliminate out-of-focus emission light and obtain sharper images. This causes the resulting image being sharper, but dimmer, and having a low resolution. In the Airyscan microscope, the pinhole is never closed, resulting in more light illuminating the sample and brighter image, and the out-of-focus light is eliminated through an array of an additional array of 32 smaller pinholes, thus resulting in very high-resolution images (Huff, 2015). For Airyscan imaging, live embryos were anaesthetised and mounted on a glass slide using methyl cellulose as described in section 2.7.1.1.

2.8. Image analysis

2.8.1. Measurements of *in situ* staining

To measure the percentage of the otic vesicle occupied by the *otx1* and *gsc* staining in the *eya1*$^{tm90b/tm90b}$ mutants and siblings I used FIJI (Fiji Is Just ImageJ) (Schindelin *et al.*, 2012). By default, the software provides measurements using

the number of pixels as a unit. This was converted into micrometres by acquiring a picture of a microscope stage ruler with the same objective used for imaging the samples (40x water immersion objective). This allowed spatial calibration of the software by assigning a specific distance, in micrometres, to a specific number of pixels. Finally, the measure of the staining was divided by the total length of the otic vesicle and multiplied by a factor of 100 (Figure 2.3). Measurements were taken for both the left and right vesicle of each embryo. The means between left and right ear measurements for each mutant embryo were then compared with those of WT siblings.

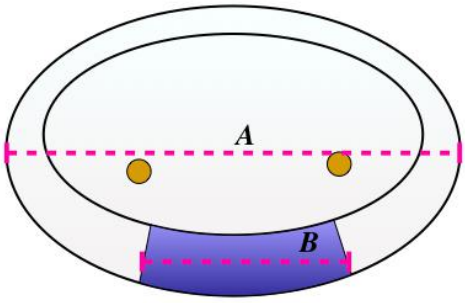

$$\text{Percentage of the otic vesicle occupied by the staining} = \left(\frac{B}{A}\right) \times 100$$

Figure 2.3. Diagram showing the method used to measure the percentage of the otic vesicle occupied by the staining. The measure of the staining (B) was divided by the total length of the otic vesicle (A) and multiplied by 100.

2.8.2. Manual cell tracking

Manual cell tracking was performed on the light-sheet movies to analyse various parameters related to cell movement (total length of the track, speed and directional persistence). This was achieved by using MTrackJ plugin for FIJI (Meijering, Dzyubachyk and Smal, 2012). The nuclei of the ventral projection and bulge cells were manually tracked over the course of 7.5 hours (90 time-points, divided into three short movies of 30 time-points each), between 64.5 and 72 hpf.

Upon manually tracking the cells of interest, two .csv file were exported: one containing a spreadsheet with general statistics for each track (e.g. total length, average speed) and the other containing the x, y and z coordinates, displacement, speed and other statistics calculated for each time-point of each track. These were used to compare and contrast the behaviour of cells belonging to different populations (ventral bulge and ventral projection around the fusion plate and at the base).

3D reconstruction of the tracks was achieved using MATLAB and Statistics Toolbox Release 2017a (The MathWorks Inc., Natick, Massachusetts, United States). The scripts were developed by Dr. Tania Mendonca (Department of Electrical Engineering, University of Sheffield).

2.9. Statistical analysis

Statistical analyses were performed using GraphPad Prism version 7.0 for MacOS (GraphPad Software, La Jolla California USA, www.graphpad.com). D'Agostino and Pearson's normality test was run on all datasets ahead of analysis. For normally distributed populations, an unpaired Student's *t* test (for the measurements of *in situ* stainings) or one-way ANOVA (for the kinetic features of cell tracking) was used. Populations that were not normally distributed were analysed using a non-parametric Kruskal-Wallis test. As post-correction tests, Sidak's correction for multiple comparisons was used on normally distributed populations and Dunn's correction was used for populations that were not normally distributed.

3. IMAGING VENTRAL PILLAR DEVELOPMENT USING LIGHT-SHEET MICROSCOPY

3.1. Introduction

The formation of the lateral canal is a complex process that, in zebrafish, requires the development of a ventral pillar (Waterman and Bell, 1984; Haddon and Lewis, 1996; Geng *et al.*, 2013). This has been previously described to result from the outgrowth and fusion of two populations of cells called the ventral bulge, derived from the lateral projection, and the ventral projection, derived from the ventral otic epithelium (Waterman and Bell, 1984; Haddon and Lewis, 1996; Geng *et al.*, 2013). However, what cells contribute to the final pillar structure, what type of behaviour they exhibit and whether the ventral projection and bulge equally contribute to the pillar formation in wild-types are questions that still remain unanswered.

In this chapter, the cell movements required to develop the ventral pillar will be analysed by comparing and contrasting the behaviour of ventral projection and ventral bulge cells. To tackle this, I took advantage of light-sheet imaging of the Tg(*mir137::EGFP;xEF1a::H2B-RFP*) line (see section 2.1.4),

which allowed me to track cell movement during the fusion and pillar extension phases and measure several parameters (e.g. speed of each cell, length of the tracks and directional persistence), which I used to identify differences in cell behaviour between different cell populations.

3.2. Characterisation of the *EGFP* expression pattern in the Tg(*mir137::EGFP;xEF1a::H2B-RFP*) line

The Tg(*mir137::EGFP;xEF1a::H2B-RFP*) line was obtained by crossing the Tg(*xEF1a::H2B-RFP*) and the Tg(*mir137::EGFP*) line, obtained respectively from the laboratories of Angela Nieto and Thomas S. Becker (see section 2.1.4). While the first line provides red fluorescence in all nuclei, the Tg(*mir137::EGFP*) was obtained with a random insertion of *EGFP* in the genome, which produced fish exhibiting green fluorescence in the cytoplasm of the cells composing many different organs: eyes, forebrain, midbrain, hindbrain, otic vesicle and heart (see section 2.1.4). Due to the expression in the otic vesicle being specific to the ventral pillar, we obtained this line to further characterise it. In several embryos, the *EGFP* expression in the heart was detectable also in absence of expression in the other organs, suggesting that this line had multiple insertion sites of the *EGFP* construct that accounted for its expression.

Interestingly, the expression pattern within the inner ear was very specific and, by 72 hpf, restricted to the ventral pillar and the three cristae. Therefore, I selected and raised only the embryos exhibiting a strong ventral pillar expression in an attempt to obtain a line showing a consistent *EGFP*

expression. Once they reached adulthood, these fish were able to spawn embryos showing, at 72 hpf, EGFP fluorescence consistently in the eye lens, brains and the ventral pillar of the otic vesicle (Figure 3.1). In some cases, very weak green fluorescence can be observed in few cells of the heart.

To achieve an overview of how the *EGFP* expression correlates and changes with the ventral pillar formation at early developmental stages, embryos obtained from GFP-positive adults were screened for the fluorescence at 24 and 48 hpf. At 24 hpf, the EGFP is visible, though weakly, in the eyes and brain, but not in the otic vesicle. The otic expression starts to be detectable as early as 48 hpf in a population of cells located in the ventral otic epithelium as well as in the anterior, posterior and lateral cristae. Finally, at 72 hpf, the otic EGFP signal is clearly visible in the ventral pillar and the three cristae, though the expression in the anterior and posterior cristae is weaker compared to the ventral pillar and lateral crista (Figure 3.1).

This highly specific expression pattern of the *EGFP* in the ear opened up many possibilities in terms of live imaging. In fact, even though the formation of the ventral pillar has been previously described as a process requiring the fusion of two finger-like protrusions, namely ventral projection and ventral bulge (see section 1.4.3), many questions still remain as to what behavioural

changes these cells exhibit during this process. The following sections will focus on analysing these cellular movements and behaviours.

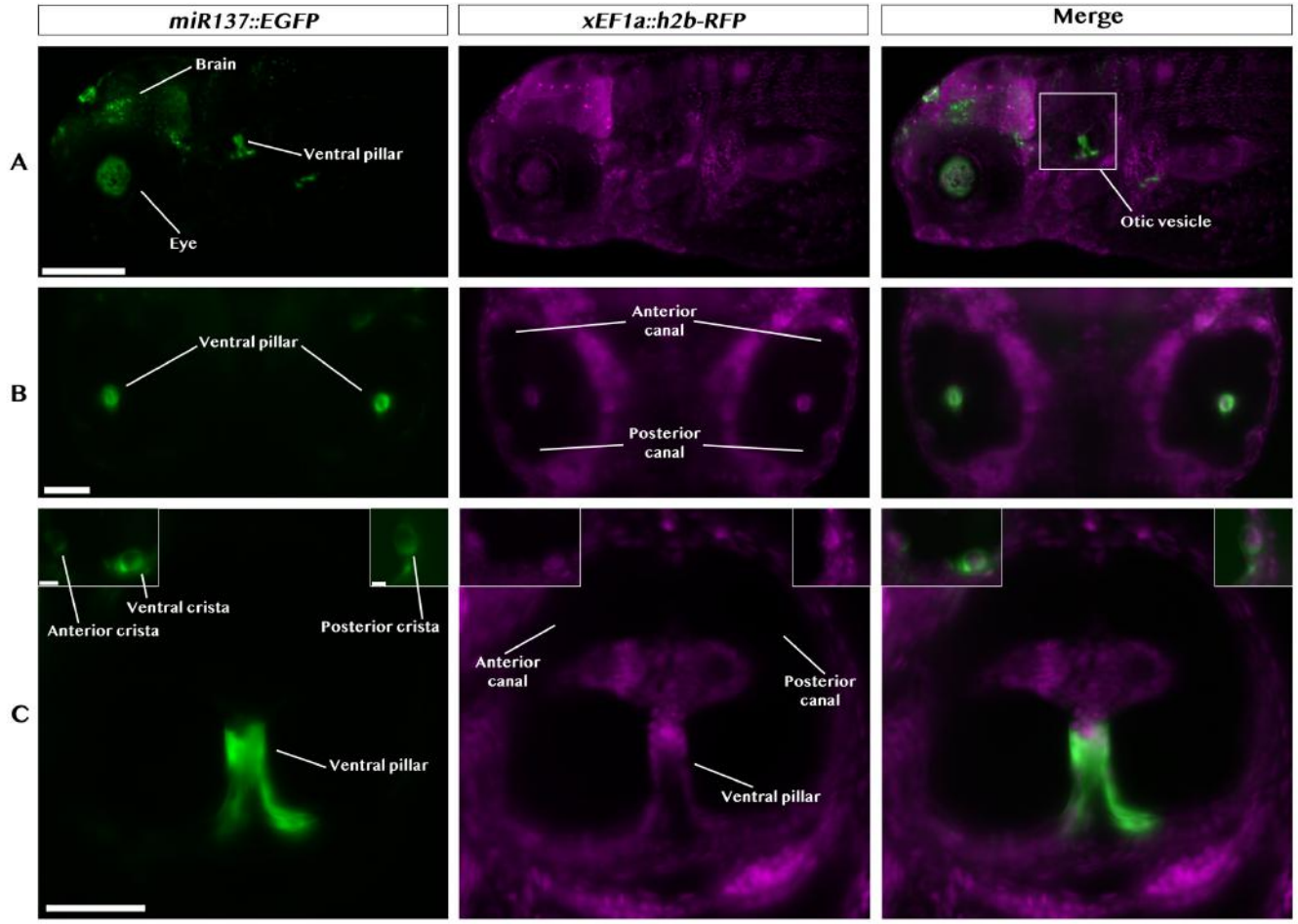

Figure 3.1. Light-sheet imaging of a wild-type embryo from the Tg(*mir137::EGFP;xEF1a::H2B::RFP*) line. (A) Side view of the head showing the strong *EGFP* expression in the forebrain, eye lens and ventral pillar of the inner ear. The *EGFP* is also present, though more weakly in the hindbrain. (B) Dorsal view of the *EGFP* expression in the ventral pillar. (C) Side view of the otic vesicle focused on the ventral pillar. Internal panels highlight the *EGFP* expression in the anterior and lateral (top left panel) and posterior cristae (top right panel) indicated by the arrowheads. The *EGFP* expression is weaker in the anterior and posterior cristae than in the ventral. For the posterior crista, brightness was enhanced to allow for better visualisation. Scale bar, (A) 200 μm; (B) 50 μm; (C) 50 μm; (cristae panels) 10 μm.

3.3. The ventral pillar is composed of cells derived from the ventral projection

The concept of pillar development as a process that requires the activity of two cell populations, one derived from the lateral projection (bulge) and the other derived from the otic epithelium (projection), has been tackled in other studies (Waterman & Bell 1984; Haddon & Lewis 1996). However, it has never been demonstrated whether the bulge and the projection equally account for the final pillar structure. To test this, 3 wild-type embryos were imaged for 24 hours between 48 and 72 hpf using light-sheet microscopy. This time window was chosen for two reasons: the first is that previous work had defined this as the time window during which the ventral pillar starts and completes its development (Waterman & Bell 1984; Haddon & Lewis 1996); the second is related to the timing of the expression of the *EGFP* in the Tg(*mir137::EGFP;xEF1a::H2B-RFP*) line, which has been described in the previous section.

The imaging of this line has revealed that the GFP-positive cells located in the ventral otic epithelium at 48 hpf account for the formation of the ventral projection (Figure 3.2 A-B and Figure S1-S2). The ventral bulge, on the other hand, is characterised by the presence of only GFP-negative cells derived from

the lateral projection (Figure 3.2 A-B and Figure S1-S2). These two populations meet and fuse, at 64 hpf, to form a pillar composed of GFP-negative cells in its top half and GFP-positive cells in its bottom half. At 72 hpf, no GFP-negative cells can be observed in the ventral pillar structure, indicating that the projection cells are the only ones accounting for the ventral pillar structure at this stage (Figure 3.2 A-B and Figure S1-S2).

To provide a better characterisation of the pillar development and to test whether the projection cells exhibit a specific behavioural pattern during ventral pillar formation I measured the variation in height of the projection over the course of 24 hours. This was performed on three time-lapses of the development of three otic vesicle, each belonging to a different wild-type embryo. All measurements are listed in Table 3.1.

This revealed that the pillar formation consists of three distinct phases, each characterised by a specific cell behaviour, defined as “extension phase”, “fusion phase” and “elongation phase”.

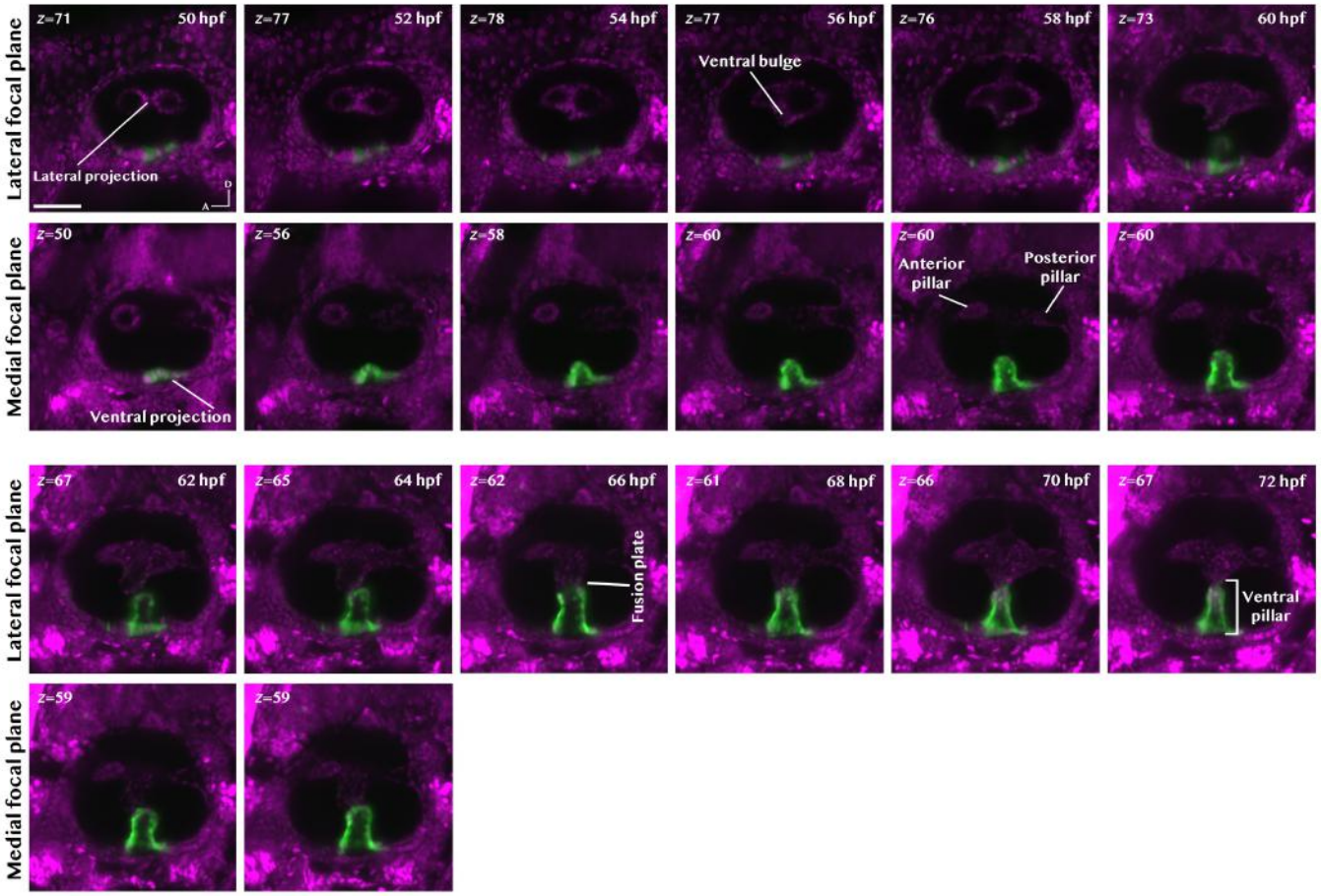

Figure 3.2 (A). Time-lapse of a wild-type embryo from the Tg(*mir137::EGFP;xEF1a::H2B::RFP*) line. All pictures are presented as maximum intensity projections of 2 to 5 *z*-stacks around the stack indicated in each picture. For time-points 50 to 64 hpf, two focal planes are shown: top row (ventral bulge) is focused on the formation of the ventral bulge and bottom row (ventral projection) is focused on the ventral projection development. The ventral projection can be distinguished thanks to the *EGFP* expression. Between 66 and 72 hpf, the focal plane of the bulge and projection coincide. "Extension phase" has been defined as the period of projection outgrowth from the ventral otic epithelium (between 50 and 64 hpf). The "fusion phase" comprises stages from 64 to about 70 hpf. Finally, the stages from 70 to 72 hpf have been defined "elongation phase". Scale bar, 50 μm.

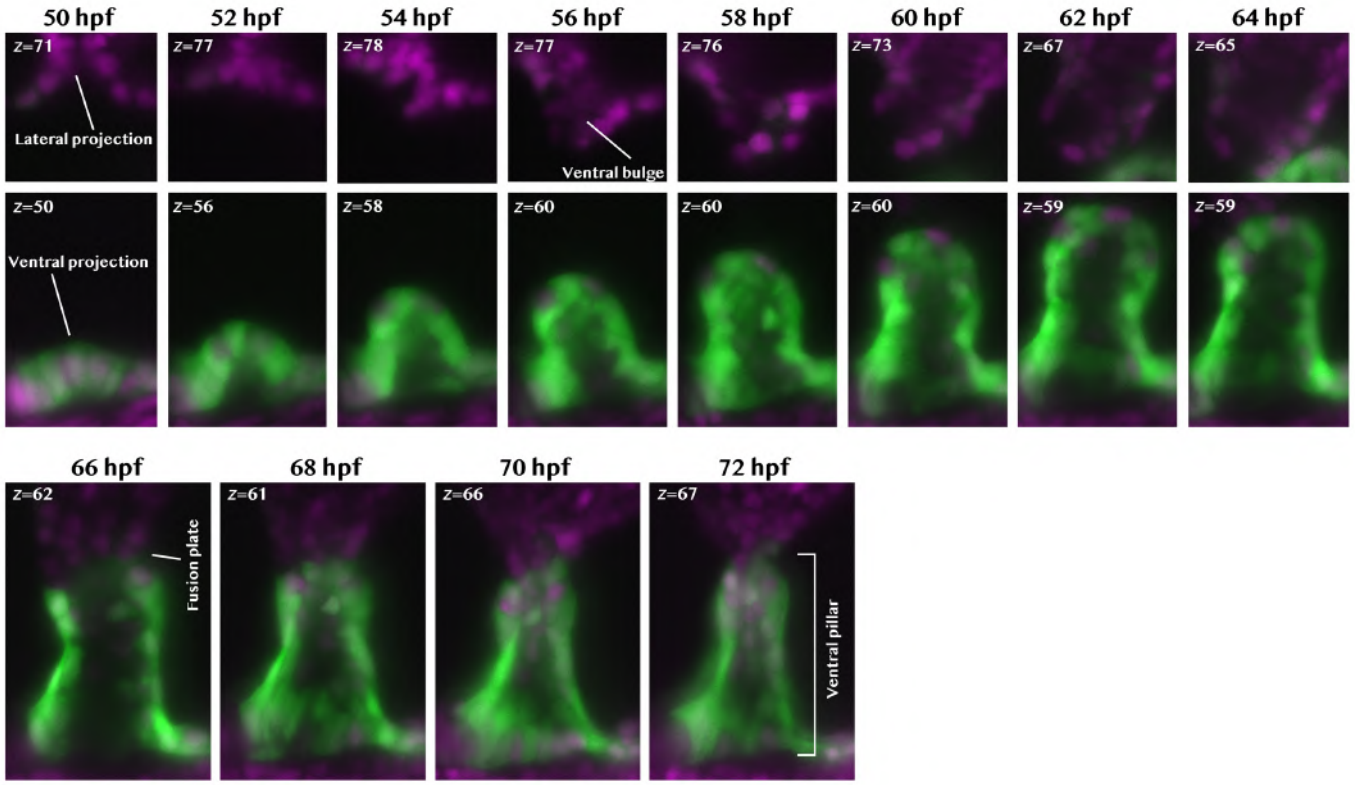

Figure 3.2 (B). Magnification of ventral pillar and bulge development from Figure 3.2 (A). The magnification focuses on the ventral bulge (top row) and projection (bottom row) development. The bulge sits on a more lateral domain (indicated by the higher *z*-stack) compared to the ventral projection, which is more medial (lower *z*-stack).

3.3.1. Extension phase

The extension phase is defined as the time window when the GFP-positive cells of the ventral otic epithelium start a process of folding to form the ventral projection, which grows steadily until 64 hpf (Figure 3.2 A-B and 3.3 A-B). At the same time, the GFP-negative cells of the lateral projection exhibit the same kind of behaviour, which allows for the formation and extension of the ventral bulge (Figure 3.2 A-B and 3.3 A-B). At these stages, when imaged from the side, the projection and bulge appear on two different focal planes, with the projection arising from a more medial domain and the bulge from a more lateral domain (Figure 3.2 A-B). In this case, the height of the projection is defined as the distance between the lowest limit of the ventral projection where the GFP is still detectable and the highest point of the same structure.

At 48.5 hpf, this measurement corresponds to the thickness of the ventral otic epithelium from which the projection arises, which appears flat (Table 3.1). Between 50 and 52 hpf, these cells start to fold and form a dome with an acellular core (the projection) that grows steadily until 64 hpf, when the projection and bulge start to make contact (Figure 3.2 A-B and 3.3 A-B).

3.3.2. Fusion phase

After the extension phase, follows the "fusion phase", during which the ventral projection and bulge fuse to form a pillar composed of both GFP-negative cells, in its top half, and GFP-positive cells, in its bottom half (Figure 3.2 A-B). During this phase the height of the projection is considered as the distance between the lowest limit of the ventral projection where the GFP is still detectable and the boundary between the GFP-positive and negative cells (fusion plate) (Figure 3.2 A-B).

This process takes place between 64.5 and 69 hpf and it characterised by a slower extension of the ventral projection (Figure 3.3 B and Table 3.1). In each of the three movies that were analysed, 3 to 4 bulge cells and 3 to 4 projection cells were observed contacting each other and, subsequently, move away to clear the fusion plate and allow for the formation of an acellular space defined by GFP-positive and negative cells at the sides (Figure 3.2 A-B). The details of the cell movements occurring at this stage will be analysed in section 3.4.

In addition, the movies show that the movement of the cells at the fusion plate causes a change in width; therefore, I decided to investigate in greater detail how the width of the projection changes over time. To test this, I measured the total width of the projection from 64.5 to 69 hpf (Figure 3.3 C and Table 3.2). These measurements were taken on the same abovementioned

three wild-type embryos (one otic vesicle for each embryo) imaged between 48 and 72 hpf. The measurements revealed that, between 64.5 and 68 hpf, the width of the projection, at the fusion plate, grows and, subsequently, reduces (Figure 3.3 C and Table 3.2).

This suggested that the cells at the fusion plate are very dynamic, which raised the question whether the base of the projection exhibits the same kind of behaviour. The base is defined as the ventral part of the projection located just above the ventral otic epithelium. Interestingly, the width of the base of the projection does not change significantly between 64.5 and 69 hpf (Figure 3.3 D and Table 3.3), suggesting that these cells could be less motile than the cells at the fusion plate and might merely have a structural purpose.

3.3.3. Elongation phase

The elongation phase takes place between 69 and 72 hpf and is the final step that allows for the formation of a ventral pillar composed only by GFP-positive cells (Figure 3.2 A-B). The measurements of the height of the GFP-positive domain indicate that, during this phase, it extends while the bulge cells retract back into the lateral projection (Figure 3.2 A-B and Table 3.1). At 72 hpf, this results in the fusion plate corresponding to the boundary between the ventral pillar and lateral projection (Figure 3.2 A-B).

To test whether the width of the pillar changes, the same measurements taken during the fusion phase were also applied to the elongation phase. This showed that, between 69 and 72 hpf, the width of the pillar at the fusion plate decreases (Figure 3.3 C and Table 3.2) while the width of the base of the projection remains mostly unchanged (Figure 3.3 D and Table 3.3), therefore strengthening the hypothesis that the cells at the fusion plate could be more dynamic than the cells at the base of the projection.

To test whether the cells involved in pillar formation exhibit specific behaviours, I tracked their movement between 64 and 72 hpf. In particular, I focused on testing the three-dimensional movement of the cells to understand whether GFP-positive and negative cells mix with each other, testing the possibility that cell death could be involved in this process and comparing kinetic features of cell movement (directional persistence, total displacement and speed). This will be the focus of the following sections.

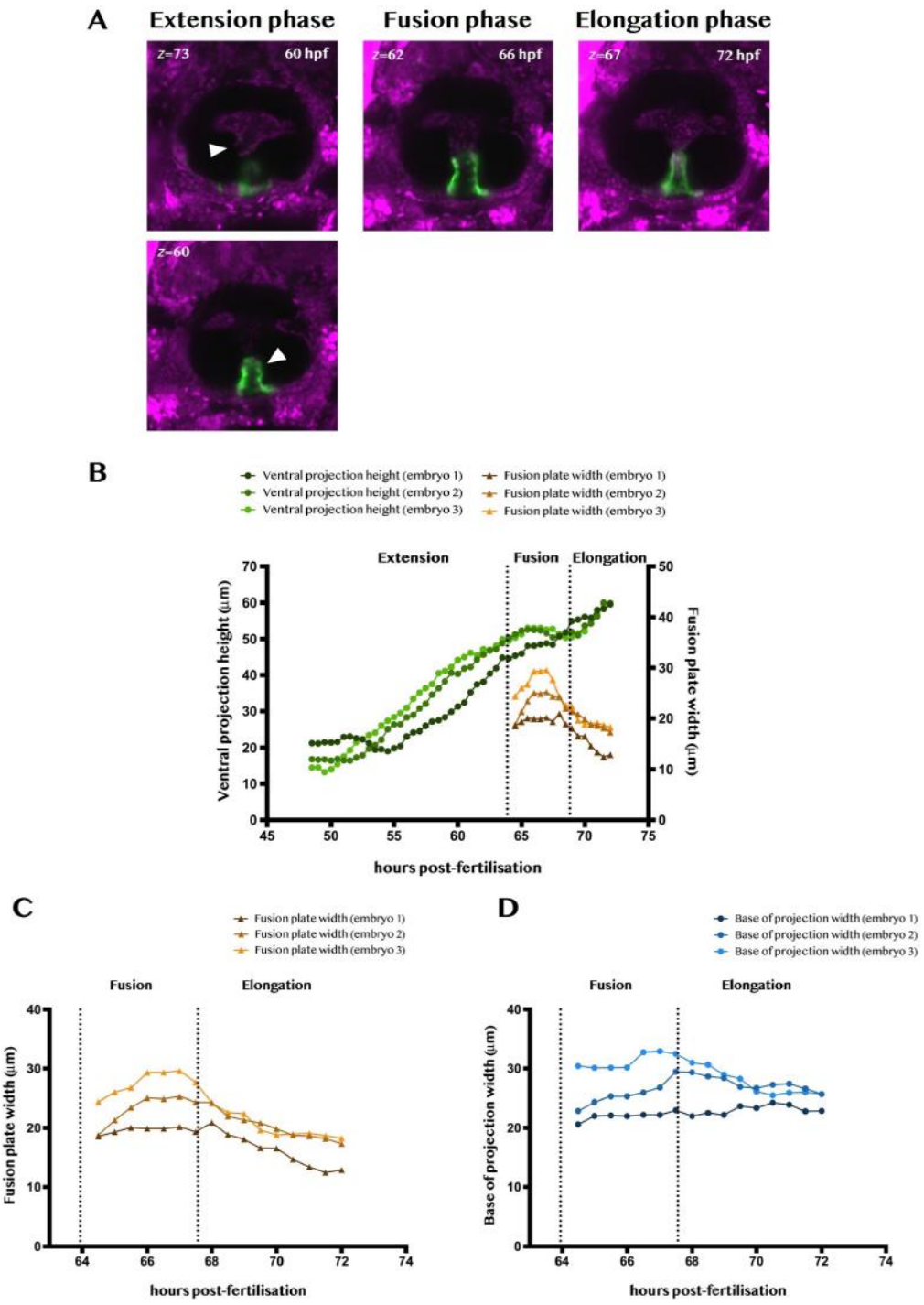

Figure 3.3. Panel showing the phases of pillar development. (A) Representative time-points showing the extension, fusion and elongation phases. For extension phase, two focal planes are presented: the top one is focused on the ventral bulge (arrowhead) and the bottom one is focused on the ventral projection (arrowhead). (B) Graph showing the development of the ventral projection over time compared with the width of the fusion plate. (C and D) Comparison between the change in the width of the projection at the fusion plate (C) and at the base (D). All measurements taken are listed in tables 3.1, 3.2 and 3.3.

Table 3.1. Measurements of ventral projection height (μm)			
hpf	**Embryo 1**	**Embryo 2**	**Embryo 3**
48:30	21.3	16.8	14.5
49:00	21.2	16.7	14.5
49:30	21.5	16.7	13.2
50:00	21.5	16.4	14
50:30	21.6	16.9	15.4
51:00	23	16.5	17.6
51:30	23	16.4	19.3
52:00	22.6	17.3	21.5
52:30	22.3	17.9	22.4
53:00	21.3	19.7	23.5
53:30	19.4	20.7	24
54:00	19.6	22.2	26
54:30	19	25	27.3
55:00	19.9	26.3	28.3
55:30	20.5	26.3	29.5
56:00	23	28.3	30.9
56:30	24.2	29	33.4
57:00	24.6	30.7	35
57:30	26	32	36.4
58:00	27	34.6	37.5
58:30	27.5	36.4	40.5
59:00	28.3	38.2	41
59:30	29.8	40.6	42.3
60:00	31.3	40.3	44.2
60:30	32.4	41.8	45
61:00	35.2	42.2	46.2
61:30	37.4	44.3	45.47
62:00	38	45.7	47.2
62:30	40.4	46.8	47
63:00	41.9	47.2	48.2
63:30	44.8	48.8	49.9
64:00	44.6	50.4	49.6
64:30	45.4	51.3	50.4
65:00	45.9	52.3	51.3
65:30	48	52.6	53
66:00	48	52.5	53
66:30	48.5	52.3	53
67:00	48.8	51.6	52.6
67:30	48.4	50.4	52.8
68:00	50.8	50.7	51.4
68:30	51.8	51.7	50.3
69:00	54.9	51.9	50.5
69:30	55.4	51	51.5
70:00	56	53.7	52
70:30	55.9	54.3	55
71:00	58	56.3	57.3
71:30	58.3	60	59.8
72:00	59.6	59.7	59.9

Table 3.2. Measurements of fusion plate width (μm)			
hpf	**Embryo 1**	**Embryo 2**	**Embryo 3**
64:30	18.6	18.8	24.4
65:00	19.3	21.3	26
65:30	20	23.4	26.7
66:00	19.9	25	29.3
66:30	19.9	24.9	29.3
67:00	20.2	25.3	29.6
67:30	19.3	24.3	27.7
68:00	20.9	24.3	24.2
68:30	18.9	22	22.6
69:00	18	21.3	22.4
69:30	16.6	20.8	19.6
70:00	16.5	19.8	18.8
70:30	14.7	18.7	19
71:00	13.4	18.6	19
71:30	12.4	18.2	18.7
72:00	12.9	17.3	18.2

Table 3.3. Measurements of the width at the base of the projection (μm)			
hpf	**Embryo 1**	**Embryo 2**	**Embryo 3**
64:30	20.6	22.9	30.4
65:00	22	24.3	30
65:30	22	25.3	30
66:00	22	25.3	30
66:30	22.2	25.9	32.7
67:00	22.2	26.8	32.9
67:30	23	29.4	32.5
68:00	22	29.3	31
68:30	22.5	28.7	30.6
69:00	22.2	28.4	28.9
69:30	23.7	26.9	28.3
70:00	23.4	26.7	26
70:30	24.3	27.2	25.4
71:00	23.9	27.4	25.9
71:30	22.8	26.6	26
72:00	22.9	25.6	25.7

3.4. Cell tracking reveals a number of rearrangements through the anteroposterior, dorsoventral and mediolateral axes

In sections 3.3.1 to 3.3.3, general rules underlying pillar formation have been presented and the measurements of ventral projection development, in terms of changes in its height and width suggested that the cells forming the ventral pillar are very dynamic. So far, it has been assumed that the pillars of the zebrafish inner ear are structures composed of epithelial cells (Waterman and Bell, 1984; Haddon and Lewis, 1991), which are not generally associated with complex migratory behaviours (Hay, 2005; Friedl and Gilmour, 2009; Campbell and Casanova, 2016). However, details about the cell movement contributing to the formation of this structures have never been provided. The following sections will be focused on providing evidences to answer the question as to whether these cells only exhibit epithelial behaviours or show other characteristics, which could be more specific to mesenchymal cells.

To test this, I analysed whether all the cells forming the ventral projection were showing a collective or individual migration due to this being one of the key features characterising the epithelial and mesenchymal state (Friedl and Gilmour, 2009; Campbell and Casanova, 2016). This was achieved by manually tracked a total of 12 cells in each of the three abovementioned time-lapses on

wild-type embryos (one otic vesicle for each embryo). Of the 12 cells tracked, 8 cells were located at the fusion plate (4 from the bulge and 4 from the projection) and 4 cells were located in the bottom half of the projection. Since the measurements of the height and width of the projection suggested that the fusion and elongation phases could be those when cells rearrange the most (see section 3.3.1 to 3.3.3), cells were tracked over a period of 7.5 hours between 64.5 and 72 hpf. To allow for better visualisation of the tracks, each time-lapses was divided into three short movies of around 2.5 hours each (31 frames, see section 2.7.2.2 for acquisition interval). The movies were edited and optimised for tracking as described in section 2.8.2.

3.4.1. The fusion between the bulge and projection (64.5 to 67 hpf)

In order to understand whether the cells forming the pillar could be considered epithelial or mesenchymal, based on the fact that they were showing a collective or individual migration, I analysed the cell movement during and after the fusion phase. Initially, modifications in the position of the ventral projection and bulge relatively to one another, and to the inner ear in general, were analysed to establish whether these two arise from a similar mediolateral domain.

The tracking shows that, at 64.5 hpf, the bulge and projection do not sit on the same focal plane (Figure 3.4); instead, the ventral projection arises from a more medial domain of the ventral floor of the otic vesicle, while the bulge outgrowth sits more laterally (Figure 3.4). The bulge and projection cells move towards each other but the two structures do not line up with each other prior to the fusion (Figure 3.4).

The fact that the bulge and projection are located respectively on a more lateral and medial focal plane results in these two structures fusing at an angle between 64.5 and 67 hpf (Figure 3.4). During fusion, the tracking confirmed that the cells located at the fusion plate move to the sides of the projection and bulge to create an acellular space (the pillar) (Figure 3.4) which has previously been described to be filled with ECM (Haddon and Lewis, 1991). This is in line with the measurements, presented in section 3.3, showing that the width of the fusion plate grows during this phase.

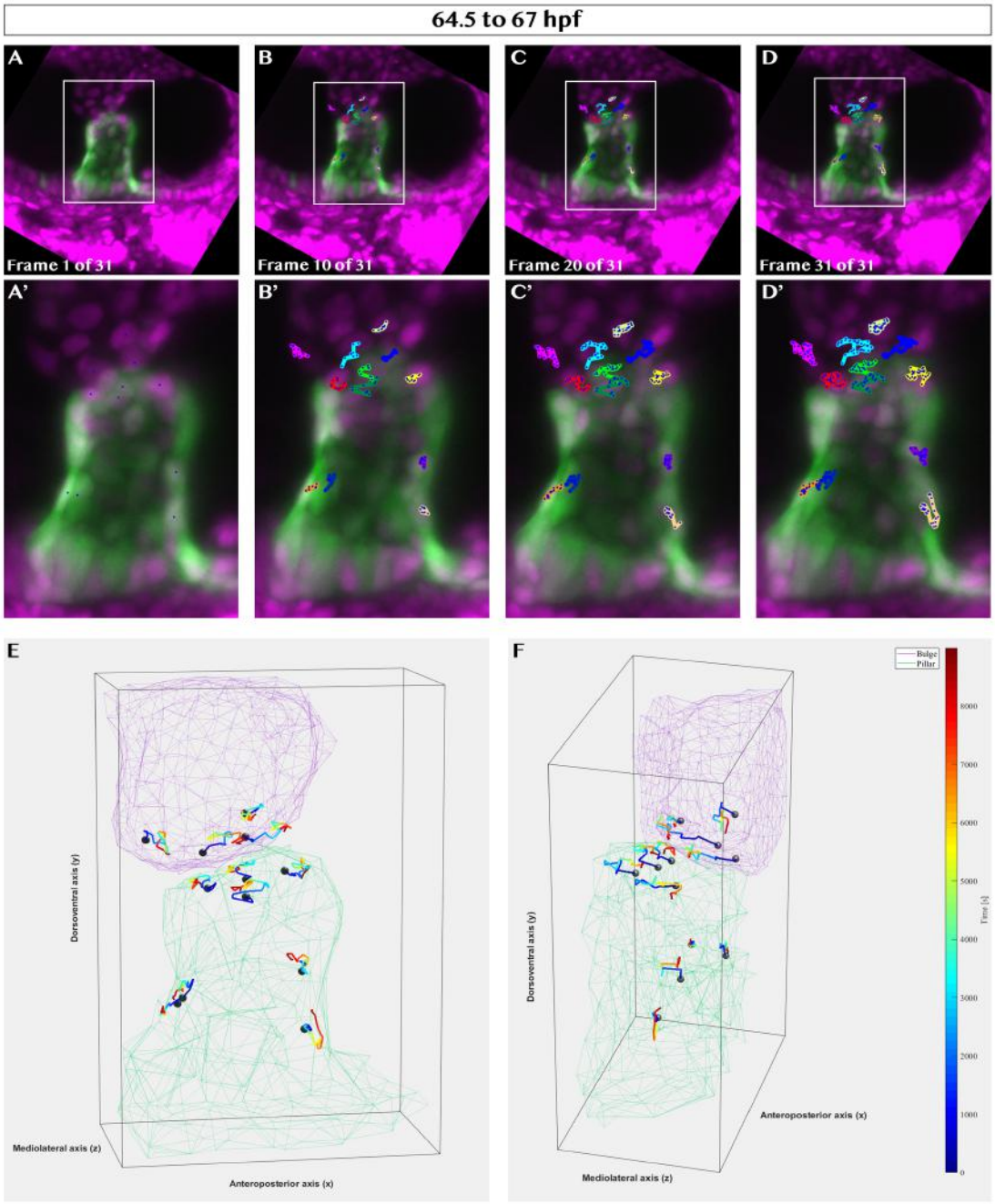

Figure 3.4. Cell tracking showing the movement of the cells in the anteroposterior (x), dorsoventral (y) and mediolateral (z) axes during the first part of fusion phase. The tracking is shown in 2D in panels A to D and, with a focus on the pillar, in panels A' to D'. In these panels, different colours identify different cells and was not possible to colour-code the tracks for the time elapsed. The same tracks are shown in 3D in E (anterior to the left) and F (medial to the left). The pillar and bulge were reconstructed using x, y and z coordinates obtained from the movies and superimposed on the tracks to make it easier to distinguish between bulge and projection cells. The x, y and z coordinates used to create these meshes are random points and do not represent the position of specific cells. The starting point for each track is indicated by a black sphere and the tracks were colour-coded for the time. The tracks show the bulge and projection cells moving towards each other (F) and clear the fusion plate by also moving on the anteroposterior axis (E). The 3D rendering of the cell tracking was obtained using MATLAB for Windows. The scripts for MATLAB were created by Dr. Tania Mendonca (Faculty of Engineering, University of Sheffield).

3.4.2. The ventral projection and bulge line up with the otic vesicle (67 to 69.5 hpf)

Upon fusion, the ventral projection and bulge cells, which are now forming the pillar, exhibit a movement towards a more lateral domain of the otic vesicle (Figure 3.5). This movement allows for the newly formed pillar to line up with the rest of the otic vesicle. At the same time, the cells at the sides of the pillar move in a way that allows for a "thinning" of this structure (Figure 3.5), therefore providing confirmation for the changes in width of the pillar described before (section 3.3.2 and figure 3.3).

3.4.3. The elongation of the projection (69.5 to 72 hpf)

By 69.5 hpf, the pillar is lined up with the rest of the otic vesicle (Figure 3.2 A-B). This is confirmed by the cell tracking, which shows that, during the elongation phase, the cells rather than moving on the mediolateral axis, move mainly on the dorsoventral axis (Figure 3.3), allowing for the retraction of the ventral bulge cells into the lateral projection and elongation of the GFP-positive domain. At this stage, the ventral bulge becomes a structure so compact that it is difficult to distinguish one cell from its neighbour, thus, causing them not to be trackable for the entire movie.

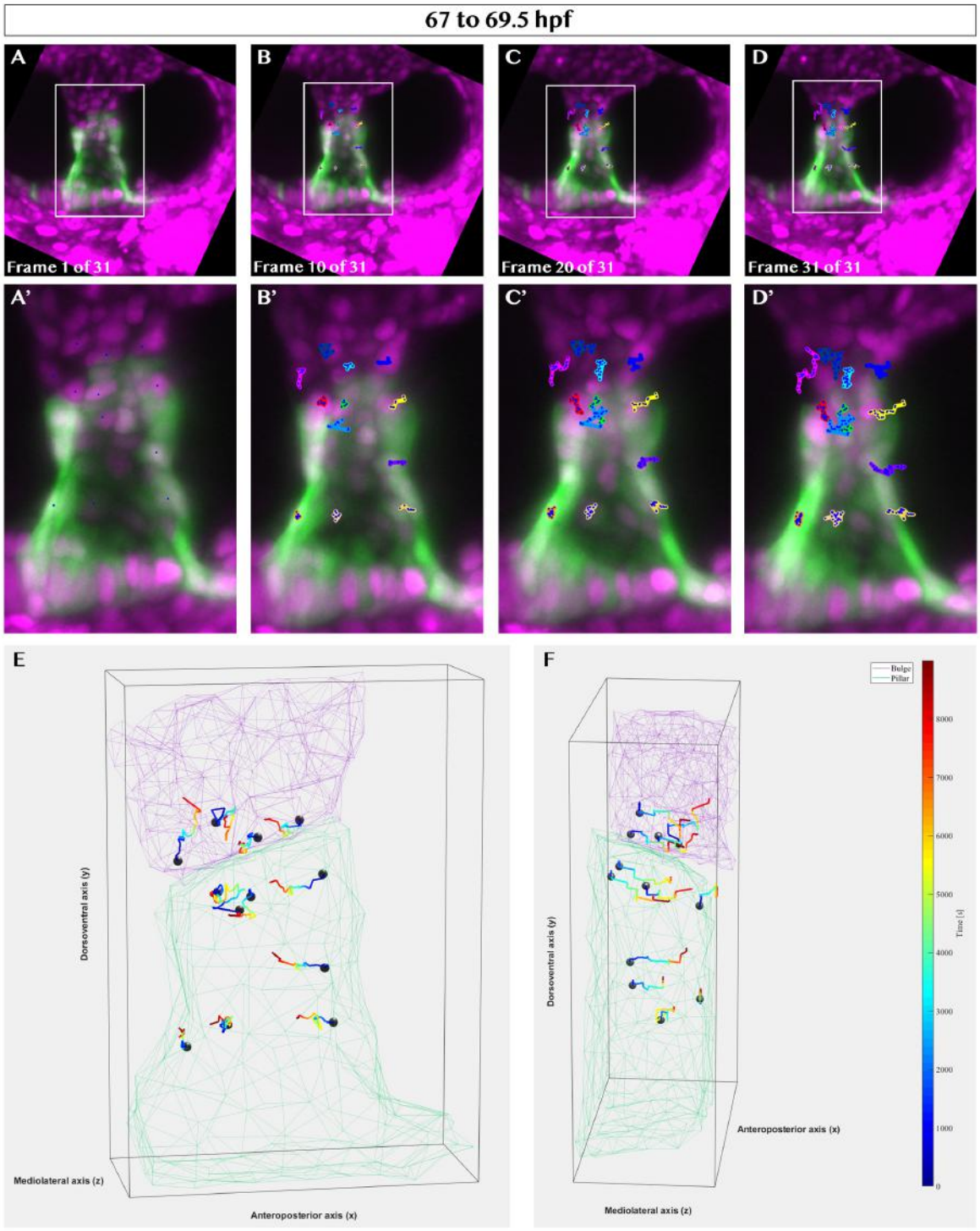

Figure 3.5. Cell tracking showing the movement of the cells in the anteroposterior (x), dorsoventral (y) and mediolateral (z) axes during the final part of the fusion phase. In E and F is shown the 3D rendering of the tracks shown in 2D in panels A to D and, with a focus on the pillar, in panels A' to D'. At these stages (67 to 69.5), the cells move back toward the acellular space located in the middle of the pillar and allow for a thinning of the same (E). At the same time the bulge and projection cells move more laterally to allow the newly formed pillar to line up with the rest of the otic vesicle (F).

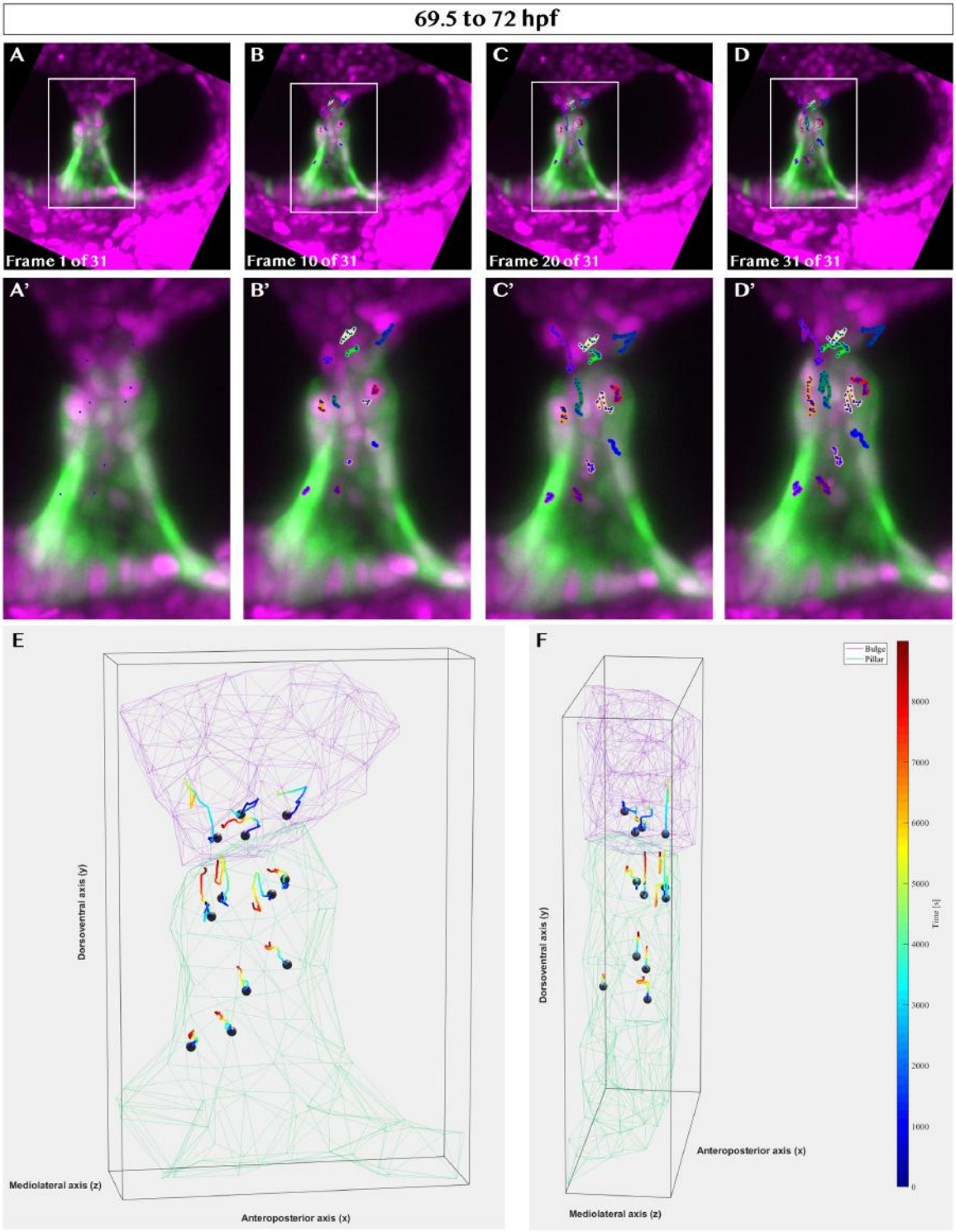

Figure 3.6. Cell tracking showing the movement of the cells in the anteroposterior (x), dorsoventral (y) and mediolateral (z) axes during the elongation phase. In E and F is shown the 3D rendering of the tracks shown in 2D in panels A to D and, with a focus on the pillar, in panels A' to D'. During the elongation phase, both the bulge and projection cells move towards the dorsal side of the otic vesicle, resulting in the bulge retracting back into the lateral projection and in the extension of the ventral projection (E). At these stages, no significant movement in the mediolateral axis was detected.

3.5. Kinetics of cell movement during fusion and elongation phases

3.5.1. Kinetics of the cells at the fusion plate

The information regarding the directional changes in the cell movement showed that the GFP-positive and negative cells show specific movements along the mediolateral and dorsoventral axis of the otic vesicle that are required for the ventral pillar development. To analyse this in greater detail, I analysed how several kinetic features of the cell tracks (directional persistence, total displacement and speed) change over time. Firstly, these were used to establish how the behaviour of each cell population tested changes over time and, secondly, to establish whether different cell populations were showing different behaviours. In particular, I divided the ventral projection cells into two classes (projection cells at the fusion plate and at the base of the projection) and hypothesised that if all projection cells were in an epithelial state, the directional persistence, length and speed of the tracks would be very similar as a result of collective migration.

With respect to the "directional persistence", it has been defined as the "straightness" of the tracks and it ranges from 0.05 (rounded track) to 1

(straight track) (Campbell and Casanova, 2015) (formula displayed in figures 3.7 and 3.8). By comparing the directional persistence of the cells located around the fusion plate, I observed that these cells do not move in straight lines, but reach a specific point in space through a series of complex movements in the *x*, *y* and *z* axes. This is common to both the bulge and projection cells, which show no significant difference in terms of directional persistence (Figure 3.7 A-B and 3.8 A).

A significant change was observed when analysing the total displacement of the cells. During the initial (64.5 to 67 hpf) and final (67 to 69.5 hpf) steps of the fusion event, both the bulge and projection cells travel a similar distance, which decreases during the elongation phase (Figure 3.7 D-E and 3.8 C). Particularly striking is the difference in the displacement of the bulge cells between the fusion and the elongation phase; however, this could be influenced by the fact that not all the bulge cells could be tracked for the same amount of time during the elongation phase, due to the problems described in section 3.4.3.

The speed of the cells undergoes the same decline, which means that the bulge and projection cells move faster during the fusion phase and, then, slow down during the elongation phase (Figure 3.7 G-H and 3.8 E).

Taken together, all these data show that, during the fusion event, even though they belong to different populations, the bulge and projection cells exhibit a similar kind of behaviour which comprises a high dynamism, which decreases during the final steps of pillar development.

3.5.2. Kinetics of the cells at the fusion plate and base of the projection

The measurements of the width of the projection at the fusion plate and at the base, presented in section 3.3, suggested a different dynamism between these cells. This led to the abovementioned idea that the cells belonging to the ventral projection might not be showing a collective behaviour, which could indicate that these cells are not in a completely epithelial state. To test whether the cells populating the ventral projection are showing different kinds of behaviour, I compared the kinetics of the cells located at the fusion plate with those of the cells located at the base of the projection.

Interestingly, these data suggest that, during the initial phase of the fusion event the cells at the fusion plate travel a longer distance and move significantly faster than the cells at the base of the projection (Figure 3.7 F-I and 3.8 D-F). Once the fusion event is completed, the cells at the fusion plate travel a shorter distance and are slower, resulting in the difference with the cells at the base of the projection to disappear (Figure 3.7 F-I and 3.8 D-F). No

difference was observed in terms of directional persistence (Figure 3.7 C and 3.8 B).

All these data support the idea that the cells at the fusion plate have a more dynamic behaviour compared to the base of the projection, which hardly exhibit any change in their kinetics over the course of pillar formation.

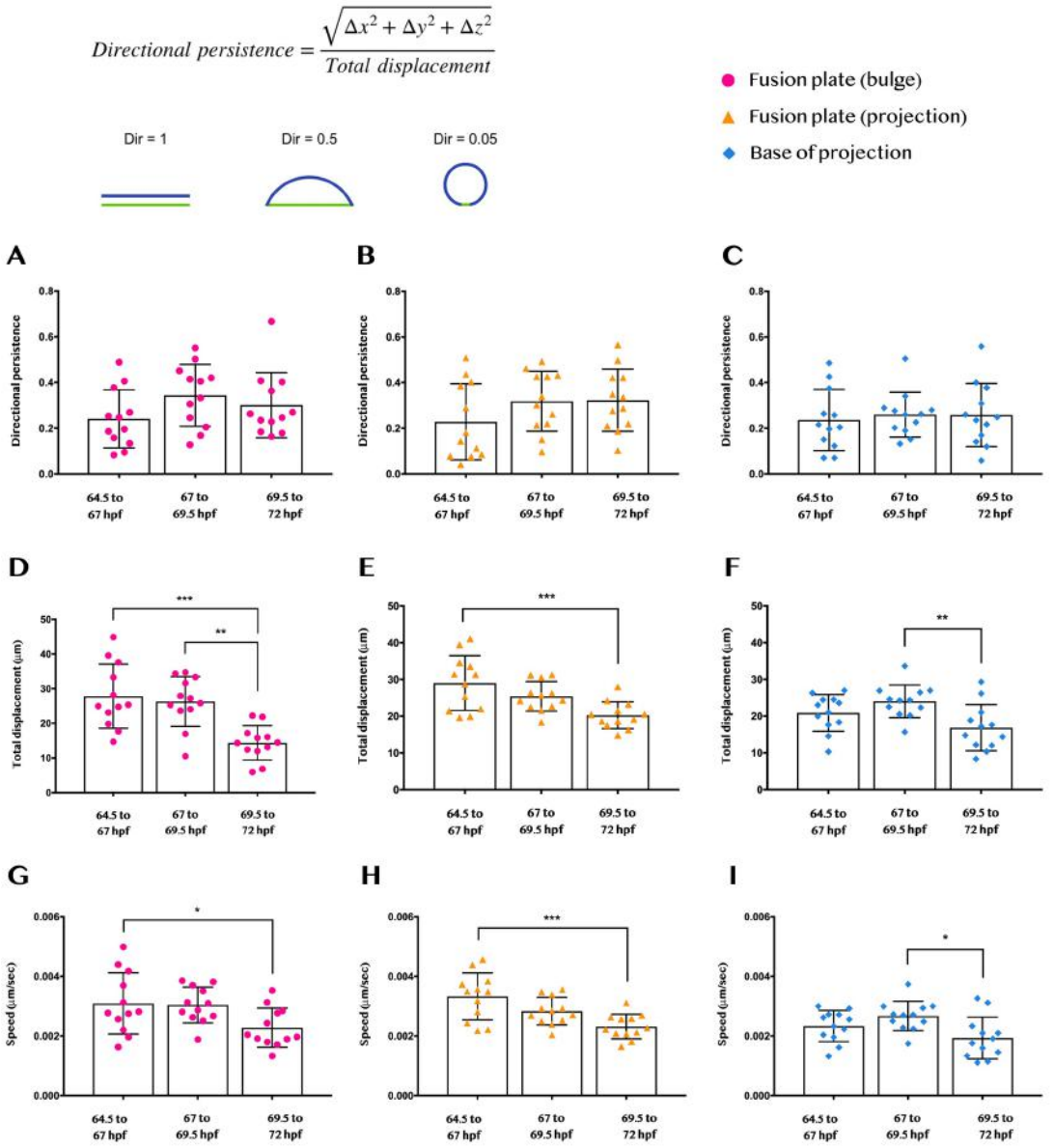

Figure 3.7. Panel showing the kinetic features of the three cell populations analysed (bulge and projection cells at fusion plate and cells at the base of the projection) obtained from the cell tracking. D'Agostino and Pearson normality test was used on all populations to establish whether they were normally distributed. For A and C, which are not normally distributed, the non-parametric Kruskal-Wallis test and Dunn's correction for multiple comparisons, were used. For all other populations that followed a normal distribution, one-way ANOVA, with Sidak's correction for multiple comparisons, was used to analyse changes in the directional persistence, total displacement and speed of the cells from the same populations over time. Error bars represent standard deviation (SD). Only significant differences are shown. (A, B and C) The directional persistence does not change over time, in any of the populations tested. (D and E) The total displacement of the cells of the projection and bulge at the fusion plate decreases over time. These cells travel a longer distance during the initial step of the fusion phase and slow down (G and H) during the elongation phase. (F and I) No difference was observed between the distance travelled by the cells at the base of the projection, and their speed, during the initial and final steps of the fusion event. However, during the elongation phase, the total displacement and speed significantly decrease. (D) $^{**}p = 0.0011$; $^{***}p = 0.0002$. (E) $^{***}p = 0.0009$. (F) $^{**}p = 0.0066$. (G) $^{*}p = 0.0478$. (H) $^{***}p = 0.0005$. (I) $^{*}p = 0.0114$.

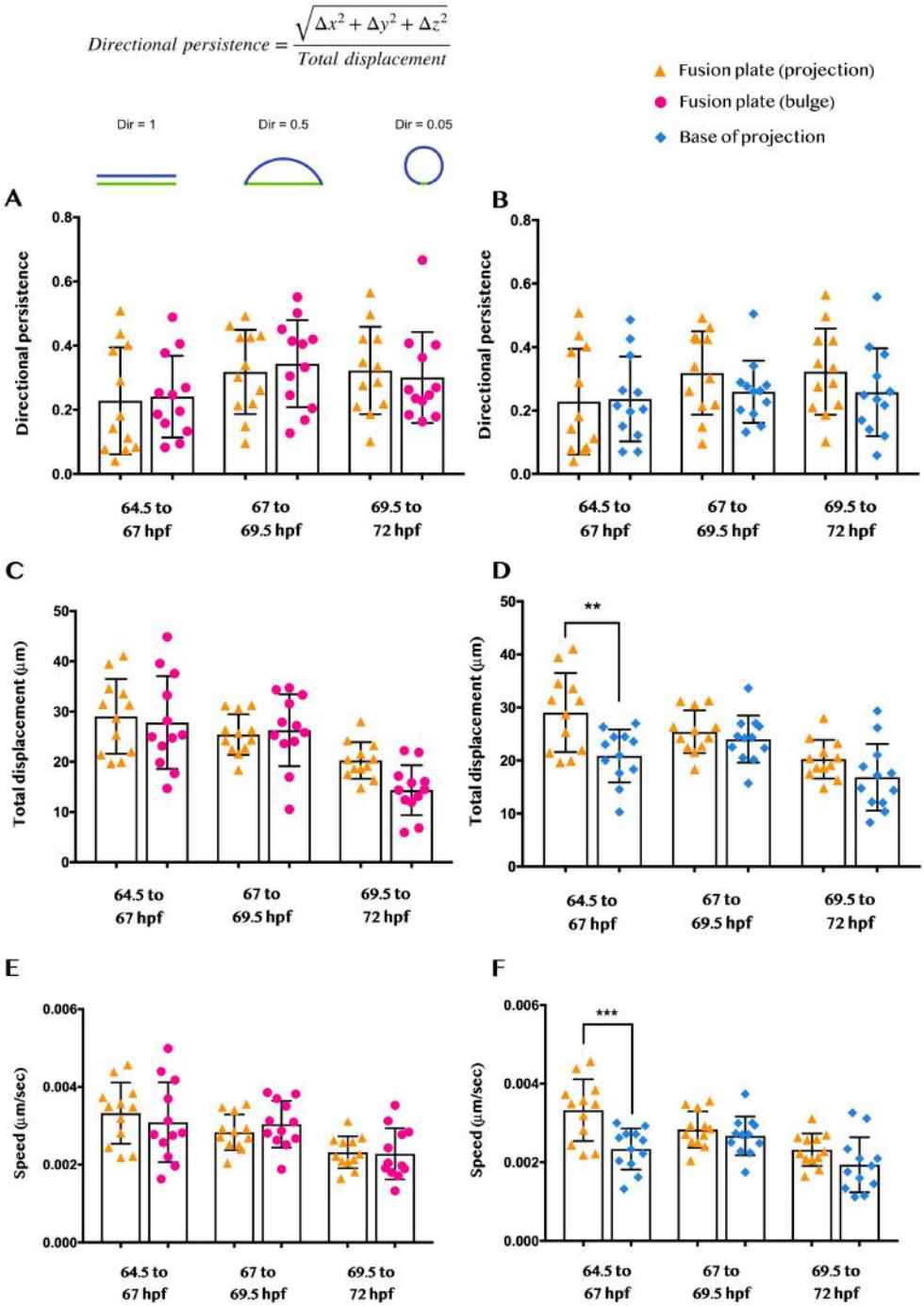

Figure 3.8. Comparison of the kinetic features between different populations of cells. Only significant differences are shown. For each kinetic feature, the data obtained from the tracking of the projection cells at the fusion plate were compared with those of the cells of the bulge and at the base of the projection. D'Agostino and Pearson normality test was used on all populations to establish whether they were normally distributed. For A and B, non-parametric Kruskal-Wallis test and Dunn's correction were used. For datasets C to F, one-way ANOVA, with Sidak's correction, was used. Error bars represent standard deviation (SD). (A and B) No difference was observed in terms of directional persistence between any of the cell populations analysed. There is no difference in the total displacement (C) and speed (E) of the projection and bulge cells at the fusion plate. The cells located at the base of the projection, though travel a shorter distance (D), during the first step of the fusion event, and move more slowly (F). (D) $^{**}p = 0.0011$. (F) $^{***}p = 0.0003$.

3.6. Cells of the bulge and projection exhibit exploratory movements

The cell tracking presented in the previous sections, provided more details regarding the movements exhibited by the cells during the fusion and elongation phase. In particular, it indicated that the cells at the fusion plate show a more migratory behaviour compared to the cells at the base of the projection. To test whether the cells at the fusion plate exhibit behaviours that could be linked to a mesenchymal state, I analysed the cell organisation at the fusion plate under the assumption that mesenchymal cells are prone to migrate individually and detach from their native population, due to modifications in the expression of genes coding for cell adhesion molecules, such as E-cadherin (Hay, 2005; Campbell and Casanova, 2016).

I observed that the bugle and pillar cells do not remain completely separated at the fusion plate, but exhibit "exploratory movements". These consist of a single cell moving away from its neighbours, mixing with cells of a different population and, finally, retracting back to its original population (Figure 3.2 A-B and 3.9). These mixing events were observed after the fusion event and, in particular, between 67 and 72 hpf. No specific pattern could be detected in how these cells mix and both bulge and projection cells are

involved. In the three abovementioned light-sheet movies used for tracking, I observed a total of 6 GFP-positive and 5 GFP-negative cells exhibiting these movements. Interestingly, these cells never lose contact completely from their original population (Figure 3.2 A-B and 3.9). These numbers are not presented as a proportion of the number of cells tracked for two reasons: a) some of the cells showing the exploratory behaviour were not easily trackable throughout the movie, because of the low resolution of the light-sheet, which, in some cases, makes it difficult to distinguish two cells that are close together; b) it was not possible to provide an accurate cell count of the cells in the region that was analysed due to the low resolution of light-sheet images. More details regarding the problems encountered with cell count will be discussed in section 5.3.1.

Taken together, all these data illustrate that during pillar formation, cells exhibit a number of complex behaviours, ranging from the organised migration to allow for the extension of the projection and bulge, to the complex rearrangements required for the fusion event, to the acquisition of the abovementioned exploratory movements, where cells of the projection and bulge exchange neighbours. This might suggest that, during and after the fusion phase, the cells located at the fusion plate could undergo transient EMT to allow for the correct formation of the pillar. However, while this idea is very

attractive, more experiments will be needed to provide further information regarding the expression of markers of EMT and the presence of cellular junctions in this structure.

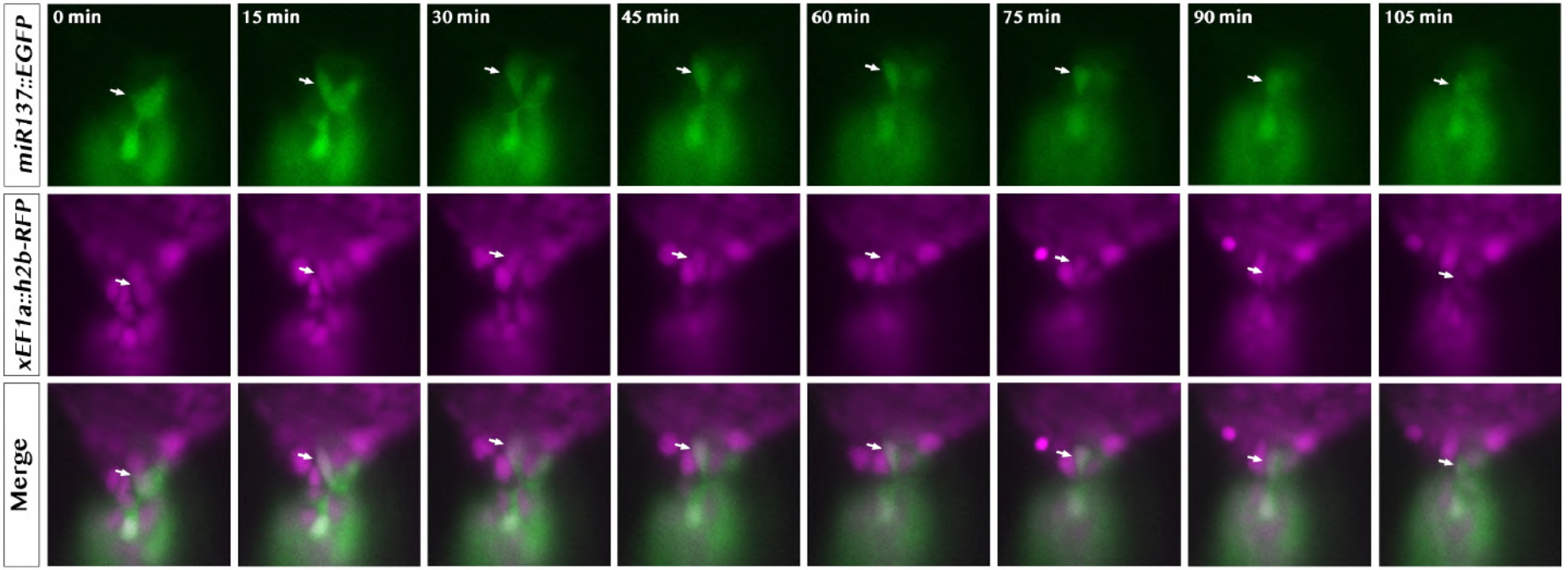

Figure 3.9. Time-lapse highlighting a GFP-positive cell (arrow) showing an exploratory movement. $T = 0$ minutes corresponds to ~ 70.5 hpf and $T = 105$ minutes corresponds to 72 hpf. It is interesting to notice how the cell elongates, overcomes the boundary between GFP-positive and negative cells (fusion plate) and retracts back into its native population without losing contact with the other GFP-positive cells.

3.7. Cell death does not play a major role during pillar development

The role of cell death during semicircular canal formation has been subject of debate over the years. It has been shown that, in the mouse and chick, cell death is fundamental to allow for the clearance of the fusion plate (Martin and Swanson, 1993; Fekete *et al.*, 1997). In zebrafish, this has been proposed not be the case as TUNEL staining revealed that there is no evidence of cell death during pillar formation (Waterman and Bell, 1984; Bever and Fekete, 1999).

Thanks to the fact that the light-sheet microscope allows us to follow the complete development of the pillar, it is also possible to visualise of cell death in real time (Figure 3.10). Thus, to confirm previous observations from previous work, I counted the number of cell death events that occurred both in the ventral projection and bulge in the three above mentioned movies used for cell tracking. As previously stated for the exploratory events, the numbers of apoptotic events are not presented as a proportion due to the problems encountered with cell count (see sections 3.6 and 5.3.1).

In all three otic vesicles tested, between 48 and 72 hpf, I observed a total of 6 cell death events (5 bulge cells and 1 projection cell). As far as the timing at which these events occur, only 1 cell out of these 6 died during the final steps

of the fusion phase, while all the others died during the elongation phase. No specific pattern could be observed in terms of timing or location of the cells at the time of their death, thus further strengthening the notion that cell death is not required for the clearance of the fusion plate and, in general, for pillar development in the zebrafish embryos. Though, it is important to notice that these results were obtained from three wild-type embryos; thus, more experiments are needed to further confirm this hypothesis on a higher number of embryos.

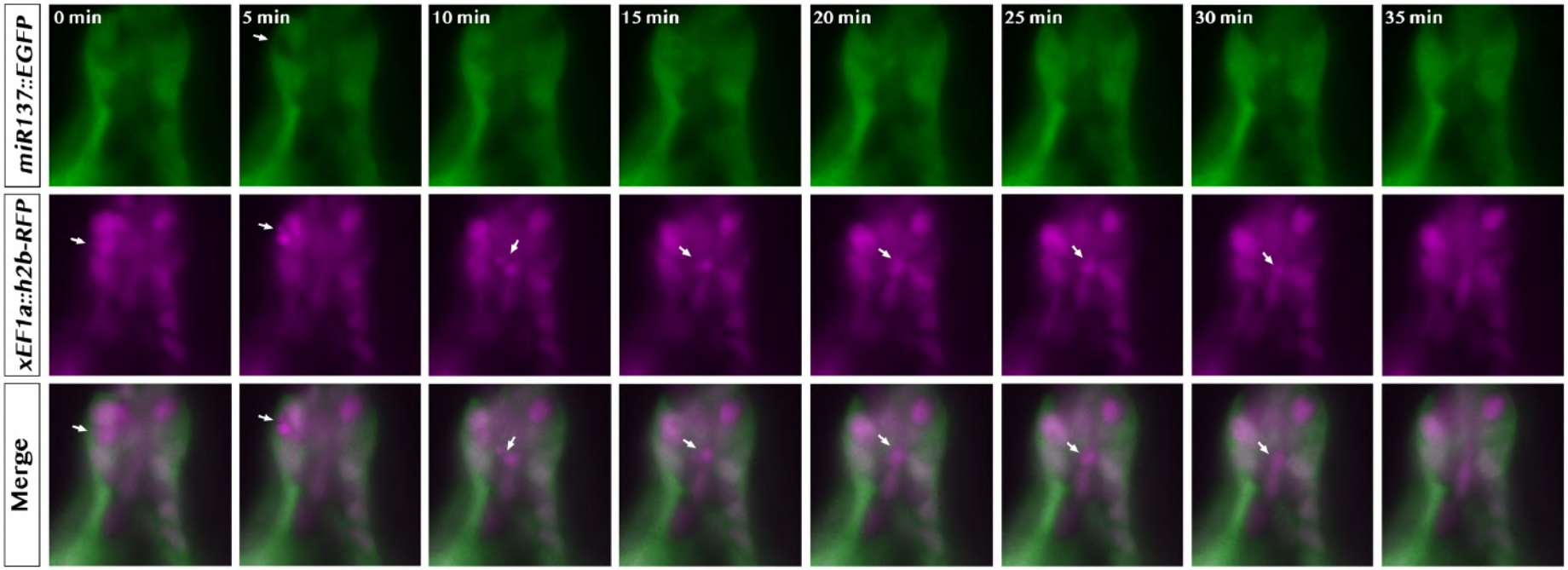

Figure 3.10. Time-lapse showing a cell death event. A GFP- positive cell located in the ventral pillar wall (arrow) dies causing the production of debris, which is cleared out within 35 minutes. *T*= 0 min corresponds to 70 hpf.

3.8. Identification of candidate sites for *EGFP* insertion in the Tg (*mir137::EGFP*) line

The Tg(*mir137::EGFP*) line that was used for the light-sheet imaging described in previous sections of this chapter, was obtained from Thomas Becker's laboratory. The line was generated by randomly inserting an enhancer trap construct into the zebrafish genome. The construct was designed as described in section 2.1.4. As part of this project, I attempted to identify the insertion site of this *EGFP* construct and understand what regulatory elements could be driving its expression in the ventral pillar. To achieve this, I took advantage of the TAIL PCR method, which is designed to amplify the region surrounding the insertion site through a series of three reactions, carried out using a mix of nested primers, specific to the Tol2 sites of the enhancer trap construct, and arbitrary degenerate primers (Liu and Whittier, 1995b) (see section 2.6).

The secondary and tertiary PCR products were run adjacent to one another on agarose gel and checked for the correct difference in bp length. The Tol2 5'-2 primer is designed to generate a product that is 100 bp longer than the Tol2 5'-3 primer and the Tol2 3'-2 primer generates a product that is 50 bp longer than the Tol2 3'-3 (Liu and Whittier, 1995b) (Figure 3.11). Upon electrophoresis

the selected bands were excised from the gel and the purified DNA was sent for sequencing. The sequencing of the bands resulting from amplification with the AD5 primer gave no hits. Instead, the sequences of the bands amplified with the other degenerate primers matched with the same regions, listed below. Here are shown the results obtained by sequencing the bands amplified with the Tol2 3'-3/AD11 and Tol2 5'-3/AD11 as a representative example:

- Tol2 3'-3/AD11 = 19:8536571 to 8536822; 85.43% match (E-value: 7^{-66}).
- Tol2 5'-3/AD11 = 19:8563340 to 8536562; 96.86% match (E-value = 9^{-105}).

These regions surround the predicted insertion site, which is located in a region that is within intron 1 of the longest predicted transcription unit for *s100 calcium binding protein A10a* (*s100a10a*) gene (Ensembl GRCz11), which is only expressed in the intestine primordium from 30 hpf to 5 dpf (Thisse and Thisse, 2004, ZFIN direct data submission) and is upstream of the coding region of the *dolichyl-phosphate mannosyltransferase polypeptide 3* (*dpm3*) gene, which is expressed in many regions of the body, including the telencephalon, cerebellum and hindbrain (Thisse and Thisse, 2004, ZFIN direct data submission; Marchese et al. 2016). With respect to *s100a10a*, its expression does not correlate with the *EGFP* expression in the Tg(*mir137::EGFP*) line, as no EGFP can be detected in the intestine primordium. On the other hand, since *dpm3* is expressed in the forebrain and hindbrain, I decided to analyse in more

detail this predicted insertion site to confirm the results of the TAIL PCR and test whether the expression of *dpm3* correlates with that of the *EGFP*.

To confirm the results of the TAIL PCR, I designed a set of primers specific to the predicted insertion site. These were designed to amplify a ~350 bp region around the predicted insertion site when used in combination with the Tol2 3'-3 and the Tol2 5'-3. If the TAIL PCR results were correct, the PCR amplification with the specific primers would give me the exact location of the predicted insertion site. The PCR products obtained using the Tol2 3'-3/Specific primer F and Tol2 5'-3/Specific primer R were subsequently sent for sequencing and aligned with the zebrafish genome. The alignment respectively gave a 93.33% (E-value = 2^{-53}) and 96.86% (E-value = 2^{-121}) match with the following regions:

- Tol2 3'-3/Specific primer F = 19:8536564 to 8536711.
- Tol2 5'-3/Specific primer R = 19:8536308 to 8536562.

These results indicated that the region located between these two (19:8536563) could be the *EGFP* insertion site (Figure 3.12). For all these reasons, I decided to analyse the expression pattern of *dpm3* to test whether it matched the *EGFP* expression. The cDNA obtained from 24 hpf wild-type embryos was used to amplify the *dpm3* sequence using a set of previously published primers (Marchese *et al.*, 2016). A 1089 bp PCR product sequence

was subsequently cloned into a pCRII vector and transformed into NEB 10β competent bacteria cells. Upon extraction using a MIDI prep kit (Qiagen), the plasmid was sequenced to check for the orientation of the inserted PCR product. Finally, the plasmid was digested using NotI and transcribed using Sp6 RNA polymerase to obtain the antisense probe. As a negative control the same plasmid was also digested with KpnI and the probe transcribed using the T7 RNA polymerase to obtain the sense probe (details of the transcription are listed in section 2.5.2). WISH was carried out as described in section 2.5.1 on embryos at 24, 48 and 72 hpf.

Unfortunately, no embryos showed any staining using either the sense or antisense probe, which led to hypothesise that there could be a problem in the sequence of the PCR product inserted in the plasmid. To overcome other problems with the sequence, I obtained the original plasmid that was used for the abovementioned study from Maria Marchese (Istituto di Ricovero e Cura a Carattere Scientifico, University of Pisa, Italy). The plasmid was sequenced to confirm the orientation of the insert, digested with EcoRV and transcribed with Sp6 RNA polymerase to obtain the antisense probe, which was tested on embryos at 24, 48 and 72 hpf. Upon WISH, no staining was detectable and, at present, I have not been able to replicate the published expression pattern or provide any information regarding the otic expression of *dpm3*. More

experiments will be needed to characterise in detail the expression of *dpm3* and compare it to the *EGFP* expression.

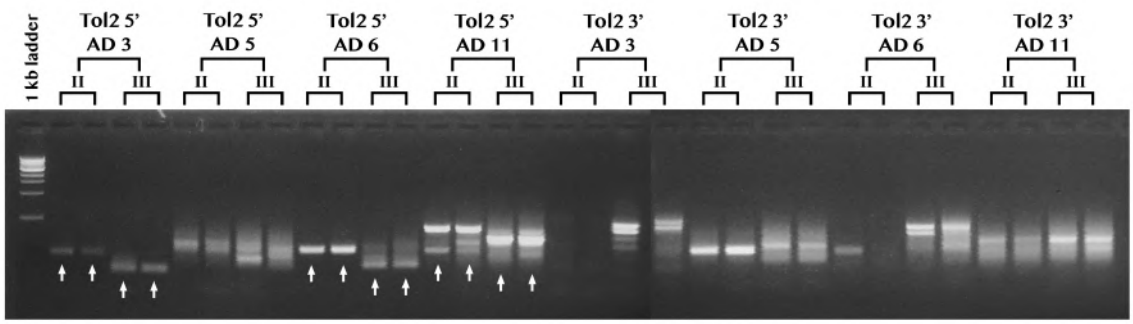

Figure 3.11. Picture showing a representative example of the bands obtained upon TAIL PCR amplification. Arrowheads indicate the bands that were excised from gel to be sequenced. Secondary and tertiary reactions are indicated respectively with II and III. Two reactions for each primer mix were prepared to increase the amount of DNA to be extracted from the gel.

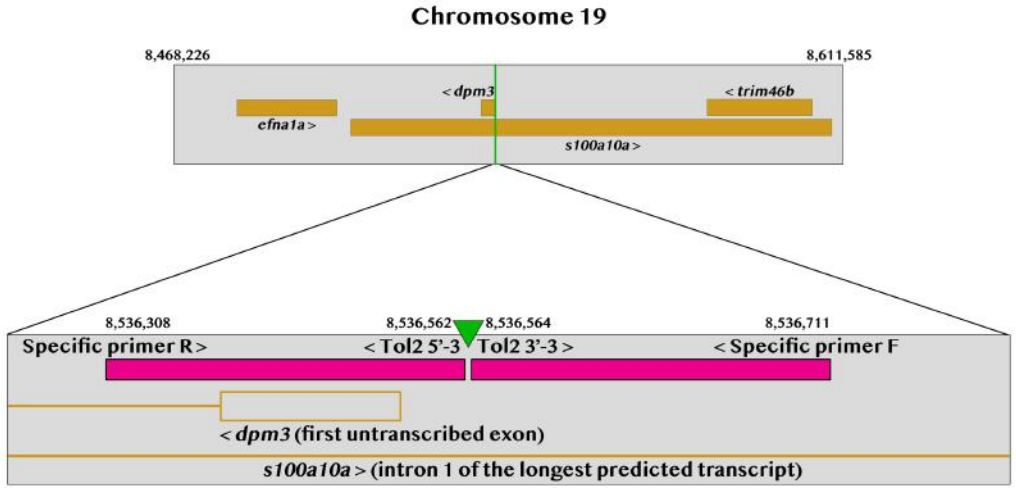

Figure 3.12. Diagram showing the predicted insertion site for the *EGFP* enhancer trap construct in the Tg(*mir137::EGFP;xEF1a::H2B-RFP*) line. Top panel shows an overview of the region surrounding the predicted insertion site (indicated with the green line) and the location and orientation of nearby genes: *efna1a* (*ephrin-A1a*); *s100a10a* (*s100 calcium binding protein A10a*); *dpm3* (dolichyl-phosphate mannosyltransferase polypeptide 3) and *trim46b* (*tripartite motif containing 46b*). Bottom panel shows a zoom around the predicted insertion site (indicated with the green arrowhead). In magenta are shown the sequences amplified using the newly designed specific primers in combination with the Tol2 5'-3 an Tol2 3'-3 primers. This region is located upstream to the first untranscribed exon of *dpm3* (yellow empty square) or within the intron 1 of the longest predicted transcript of *s100a10a* (yellow line). Information regarding the location and orientation of these sequences were obtained from Ensembl (GRCz11).

3.9. Discussion

The main focus of this chapter is the development of the ventral pillar in wild-type embryos. This is a subject that has not been tackled in many studies and, therefore, many questions regarding pillar formation remained unanswered, one of these being whether the bulge and projection cells account for the formation of the pillar at the same level. Previous work established that the formation of the pillars in the zebrafish inner ear is a process requiring the fusion between a bulge and a projection (Waterman and Bell, 1984); however, there are no indications as to what is the destiny of these cells after the fusion event.

With respect to the ventral pillar, the data shown in this chapter indicate that the projection cells are the only population forming the ventral pillar by 72 hpf. It is interesting to notice how the bulge cells emerge from the lateral projection to fuse with the projection, before retracting back and allow for the extension of the GFP-positive domain. This suggests that the purpose of these cells could be to ensure that the ventral projection anchors to the lateral projection and that the pillar forms in the correct position of the mediolateral domain of the otic vesicle. This is also confirmed by the cell tracking analysis that shows how the ventral projection emerges from a more medial domain of

the ventral otic floor and moves to a more lateral domain, upon fusion with the bulge, therefore allowing the newly-formed pillar to line up with the rest of the otic vesicle by 72 hpf.

Particularly interesting are the rearrangements that the cells at the fusion plate exhibit during the fusion and subsequent phases, as these rearrangements have, so far, been described only in the zebrafish. In amniotes, in fact, the clearance of the fusion plate has been shown to require cell death events (Martin and Swanson, 1993; Fekete *et al.*, 1997) or reabsorption of the cells in the duct through EMT (Salminen *et al.*, 2000; Kobayashi, Nakamura and Funahashi, 2008). Conversely, in the *Xenopus* and zebrafish, TUNEL staining demonstrated the lack of apoptotic cells during pillar formation (Waterman and Bell, 1984; Bever and Fekete, 1999). This is confirmed by our light-sheet imaging, where no apoptotic events can be detected during the fusion between the ventral projection and bulge.

However, the subject of the fusion between sheets of epithelial cells is more complicated. Recent studies have reported that, in many cases, the migration of an epithelium could be driven by a single cell or few cells that exhibit a "partial mesenchymal state" (Hava *et al.*, 2009; Revenu and Gilmour, 2009). An example is the development of the zebrafish lateral line, where the migration has been proposed to be driven by few "leader cells" which maintain their

contact with the rest of their cell population (Revenu *et al.*, 2014). The development of the pillar can be considered similar as our data show that the cells located at the fusion plate, exhibit an enhanced motility compared to the cells located nearer to the ventral otic epithelium and do not lose contact with their native population.

Once the fusion has completed, though, these cells exhibit a very peculiar behaviour consisting of a cell protruding out and then retracting back into its original population. This neighbour-exchanging process is very interesting as it could be an indication that, at this stage, these cells achieve a partial mesenchymal state. The reason for not considering it a complete mesenchymal behaviour lies in the fact that while the cells overcome this boundary between the GFP-positive and GFP-negative cells, I did not observe any cells completely losing contact with their population and migrate in the three wild-type embryos imaged between 48 and 72 hpf.

In support of this hypothesis, recent studies have reviewed the characteristics of epithelial and mesenchymal cells and illustrated that, instead of classifying a cell population as epithelial or mesenchymal, there are many nuances to be considered (Revenu and Gilmour, 2009; Campbell and Casanova, 2016). As described in section 3.5.1, one of the characteristics that have to be considered is the fact that epithelial cells show a collective type of

migration, which should result in a similar directional persistence, distance travelled and speed among cells belonging to the same population. However, the results shown in sections 3.5 and 3.6 show that the cells at the base of the projection travel a shorter distance and move more slowly compared to the cells at the fusion plate, which could be an indication that the cells at the fusion plate are showing a more mesenchymal behaviour. Nevertheless, it is important to consider that the epithelial or mesenchymal state also depends on other factors ranging from the cell shape to the expression of adhesion proteins and the presence of an apico-basal polarity (Revenu and Gilmour, 2009; Campbell and Casanova, 2016). Therefore, while the results shown in this chapter provide information about the motility of the cells involved in the development of the ventral pillar, it would be interesting to check for changes other characteristics, such as cell shape, polarity and distribution of junctions on the cell surface. The formation of cell-cell junctions between the projection and bulge cells, upon fusion, has been shown before (Waterman and Bell, 1984); however, a more in-depth analysis to test whether these junctions are redistributed during different phases of pillar formation will be needed.

This will help to understand whether the state of these cells changes during the formation of the pillar and to what extent they can be considered epithelial or mesenchymal.

Finally, the data showed in section 3.10 show that a region upstream to the 5'-UTR of *dpm3* is a candidate site for the insertion of the *EGFP* construct. The fact that *dpm3* codes for a sugar transferase is intriguing as it is established that polysaccharides play a pivotal role in inner ear development as part of the ECM (Haddon and Lewis, 1991). An example is provided by the mutation of *ugdh* (also known as *jekyll* mutation), which codes for a uridine 5'-diphosphate (UDP)-glucose dehydrogenase and results in the inner ear projections failing to grow, fuse and form the pillars (Neuhauss *et al.*, 1996; Walsh and Stainier, 2001). This further strengthens the idea that ECM components are key players in the zebrafish pillars development (Haddon and Lewis, 1991) and supports the fact that the region upstream to *dpm3* could be a good candidate site for the *EGFP* insertion in our transgenic line.

Nonetheless, further studies are necessary to analyse whether the expression pattern of *dpm3* is consistent with the expression of the *EGFP* and whether there are other insertion sites that have not been identified with the TAIL PCR. Moreover, since the *EGFP* expression is so specific, it would be important to know whether the sequence driving its expression belongs to a gene expressed only in the ventral pillar or also in the anterior and posterior. In the latter scenario, there could be other regulatory elements upstream or

downstream that might interact with the insertion site, resulting in the specific ventral pillar expression.

4. ROLE OF *otx1* IN VENTRAL PILLAR DEVELOPMENT

4.1. Introduction

Many studies have highlighted the importance of OTX family genes in various processes leading to the formation and development of sensory organs. Loss of *Otx1* has been shown to result in mice lacking the lateral semicircular canal (Acampora & Simeone, 1999; Fujimoto et al., 2010). In zebrafish, *otx1* starts to be expressed during epiboly stages in the prospective forebrain and midbrain. At 24 hpf, it is expressed in the most rostral regions of the embryo (olfactory epithelium, eyes, telencephalon and mid-hindbrain boundary) and in the otic vesicle, where it is restricted to the ventral-medial otic epithelium. The expression of *otx1* persists also at later stages and, at 72 hpf, it becomes expressed in the ventral floor of the otic vesicle surrounding the ventral pillar.

The morpholino-mediated knockdown of *otx1* has been described to result in the complete loss of the ventral pillar, but not the anterior and posterior (Hammond and Whitfield, 2006). However, whether the mutation of *otx1* is able

to fully replicate the outcomes of morpholino injection has not been fully described.

In addition, recent unpublished work from our laboratory has highlighted that the mutation of *otx1* has repercussions on *otx2a* expression (Giuliani, G. unpublished results). Since *otx2a* was previously known as *otx1a* and its expression in the otic vesicle overlaps with that of *otx1* (Thisse and Thisse, 2005), I decided to test whether the knockdown or mutation of *otx2a* alone could affect the development of the ventral pillar. Previous work showed that *otx2a* (formerly *otx3*, *otx1-like* and *otx1a*) morpholino injection produces no specific phenotype or other genetic defects when injected alone, but only in association with *otx1* and *otx2b* (formerly *otx2*) morpholino (Foucher et al., 2006; Lane & Lister 2012). However, there are no indications as far as the ventral pillar is concerned.

In this chapter, the morphological and genetic characteristics of *otx1* mutants are analysed using different techniques. An initial phenotypical analysis was carried out to further confirm previous data obtained using morpholino-mediated knockdown (Hammond and Whitfield, 2006) and preliminary analysis of the *otx1* mutant phenotype (Giuliani, G., PhD thesis). Subsequently, I took advantage of the *otx1*^{sa96}*;mir137::EGFP;xEF1a::H2B-RFP* line

to establish what is the destiny of the ventral pillar cells at 48 hpf (see section 3.3). Embryos were then tested for the expression of various genes through WISH. Finally, the *otx2a* morpholino was injected in WT embryos to look for any specific ear phenotype and several attempts have been made to create a new *otx2a* mutant line using the CRISPR/Cas9 mutagenesis method.

4.2. Phenotypical analysis of *otx1*^{sa96} mutants

Previous study from our laboratory described the *otx1* morphant phenotype, which is highly specific and consists in the selective loss of the ventral pillar by 72 hpf (Hammond and Whitfield, 2006). However, since there was no indication in the literature regarding the *otx1* mutant phenotype, I tested whether the mutant phenotype recapitulated the morphant phenotype. This is important because morpholino injection could give rise to side effects that might not be specific to the knockdown of a target gene.

The phenotypical analysis revealed that, at 24 hpf and 48 hpf, *otx1* mutants are morphologically indistinguishable from the wild-type siblings. At 72 hpf, the ventral pillar and ventral crista are completely missing, and the otic vesicle appears smaller compared to the siblings (Figure 4.1). These observations are in line with what was previously described in the morphants (Hammond and Whitfield, 2006). To further confirm that the effects of the *otx1* mutation are specific to the ventral pillar, I measured the total height and width of the otic vesicle in *otx1* siblings (n=10) and mutants (n=10) at 72 hpf.

These measurements revealed a statistical difference in the length of the dorsoventral axis, which is smaller in the mutants, but not in the anteroposterior axis (Figure 4.1), therefore strengthening the concept that the

anterior and posterior pillar are not affected by this mutation. A closer look also revealed that the space between the lateral projection and the ventral otic epithelium (occupied by the ventral pillar in the siblings) is significantly smaller in the mutants (Figure 4.1). As for the utricular and saccular otoliths, they sit closer to each other in the mutants compared to the siblings. (Figure 4.1). These data demonstrate that the mutant phenotype recapitulates the morphant phenotype and further confirm that the activity of *otx1* is highly specific to the lateral semicircular canal. This raised the question as to what is the destiny of the cells contributing to the ventral pillar formation in these mutants. The following sections will be focused on answering this question using light-sheet imaging and gene expression analyses.

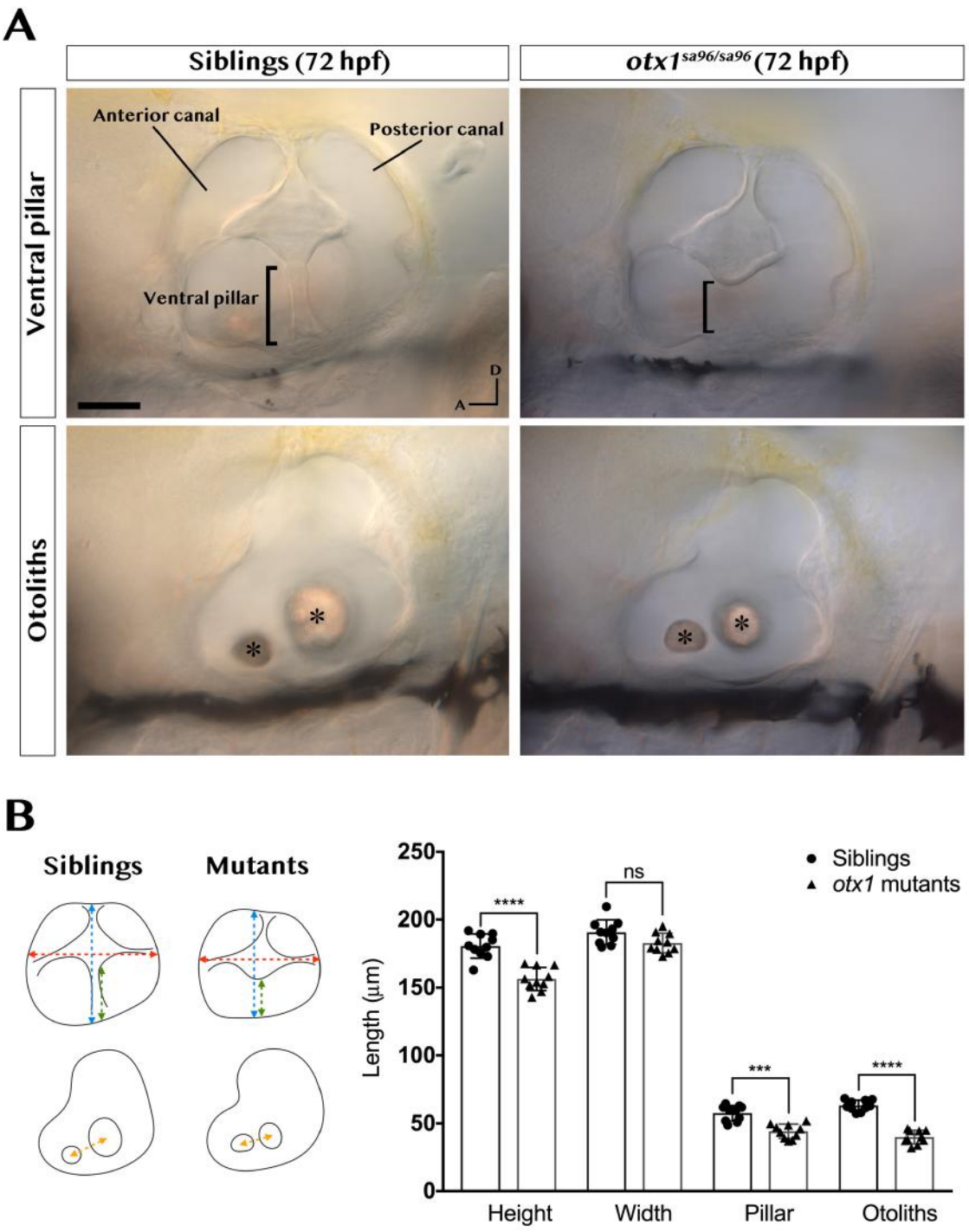

Figure 4.1. (A) Phenotype of *otx1* mutants and siblings at 72 hpf. The ventral pillar is completely missing in the mutants (square bracket) and the otoliths lie closer to each other (stars). Scale bar 50 µm. (B) Schematic showing the measurements taken of the height (blue) and width (red) of the otic vesicle, ventral pillar length (green) and distance between the otoliths (orange). Measurements were taken from n=10 siblings and n=10 mutants. Multiple comparisons were carried out using one-way ANOVA and Sidak's correction for multiple comparisons. Data are presented as mean ± standard deviation (SD). ns = not significant; ****$p < 0.0001$; ***$p = 0.0002$.

4.3. The *otx1*^{sa96} mutant otic phenotype arises before pillar development

The phenotypical analysis described in the previous section provides further confirmation regarding the specificity of action of *otx1* during otic development. However, this does not give any indication with respect to the destiny of the cells contributing to the pillar formation. In this respect, several possibilities were taken into consideration:

a) The cells are still present in the otic epithelium but do not evaginate to form the bulge or the projection;

b) The cells are still present in the otic vesicle but die due to apoptotic events occurring during pillar formation (between 48 and 72 hpf);

c) The cells are not present in the vesicle due to apoptotic events occurring ahead of ventral bulge and projection development (before 48 hpf);

To test these hypotheses, I crossed the *otx1*^{sa96} mutants with the Tg(*mir137::EGFP;xEF1a::H2B-RFP*) line. The expression of the *EGFP* in this line has been discussed in section 3.2. At 24 hpf, in the otic vesicle of wild-type embryos and *otx1* siblings, the EGFP is not yet detectable, while weak expression can be observed in the eyes. After 48 hpf, the EGFP is clearly

detectable also in the ventral otic vesicle and becomes stronger in the eyes and the brains. By 72 hpf, the EGFP-positive cells populating the ventral otic epithelium have formed the ventral pillar through a complex series of rearrangements described in sections 3.3 to 3.6. Finally, at this stage, weak EGFP expression can also be found in the three cristae. In particular, I focused on the cells of the ventral otic epithelium to test whether the EGFP expression was still detectable in the *otx1* mutants.

By taking advantage of this line, I was able to establish that the *otx1* mutant phenotype can be detected as early as 48 hpf, as a result of the complete loss of EGFP-positive cells in the ventral otic epithelium (Figure 4.2 A-B and Figure S1-S2). The expression in the eyes, brain and anterior and posterior cristae remain unaltered, while no ventral crista is observable (Figure 4.2 A-B and Figure S1-S2). Time-lapse imaging was carried out on two mutants (one otic vesicle for each embryo) to test whether the lack of EGFP-positive cells in the ventral otic epithelium was due to enhanced cell death occurring between 48 and 72 hpf. Over this period, I did not observe cell death events in the ventral otic epithelium. As a control for the mutant phenotype, three phenotypically wild-type siblings (one vesicle for each embryo) were imaged between 48 and 72 hpf. No differences were detectable between these embryos and morphologically wild-type siblings (Figure 4.3 A-B and Figure S1-S2).

The fact that cell death events were not detectable between 48 and 72 hpf did not allow to rule out the possibility that this occurs between 24 and 48 hpf. For this reason, I attempted to image the otic development of a sibling between 24 and 48 hpf with the aim to apply the same analysis on the mutants. However, at these stages, the embryo undergoes a straightening process that allows the head to line up with the trunk and this is impeded by the column of agarose in which the embryo is mounted inside the light-sheet microscope. After 24 hours of imaging, the embryo failed to straighten up correctly and all projections failed to fuse and form proper pillars. It is reasonable to believe that the failure in the straightening process causes the otic vesicle to be so compressed that the projections and bulges form but do not fuse as they are not in line with each other. Further imaging, between 24 and 48 hpf, carried out under different conditions (e.g. lower percentage of agarose or bigger capillary) is needed to establish with certainty whether cell death is part of the reason why *otx1* mutants do not exhibit any projection cell in the ventral otic epithelium.

To test whether the loss of *EGFP* expression observed in the *otx1* mutants was related with modifications in the expression of markers of the ventral otic epithelium, a gene expression analysis was carried out on these mutants and will be the main focus of the following sections.

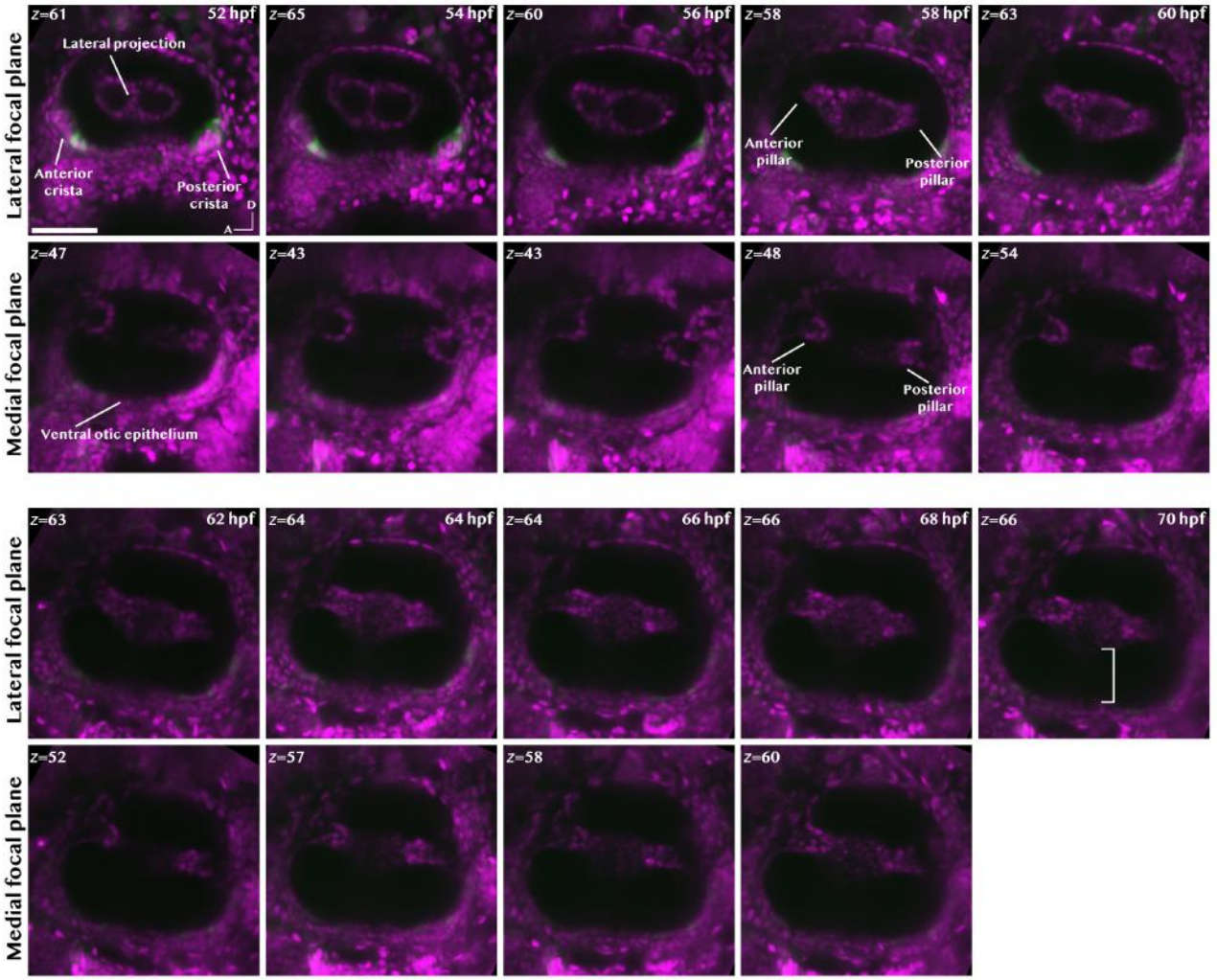

Figure 4.2 (A). Time-lapse showing the otic vesicle development in an *otx1* mutant. Each frame is presented as a maximum intensity projection of 2 to 5 *z*-stacks around the indicated stack. The brightness of the GFP was enhanced to provide further confirmation that, though these embryos do not exhibit any fluorescence in the ventral otic epithelium corresponding to the region of outgrowth of the projection, the GFP is still present in the anterior and posterior cristae. For all time-points, a more lateral and a more medial focal plane are shown to highlight the lateral projection, from where the bulge should develop (lateral), and the

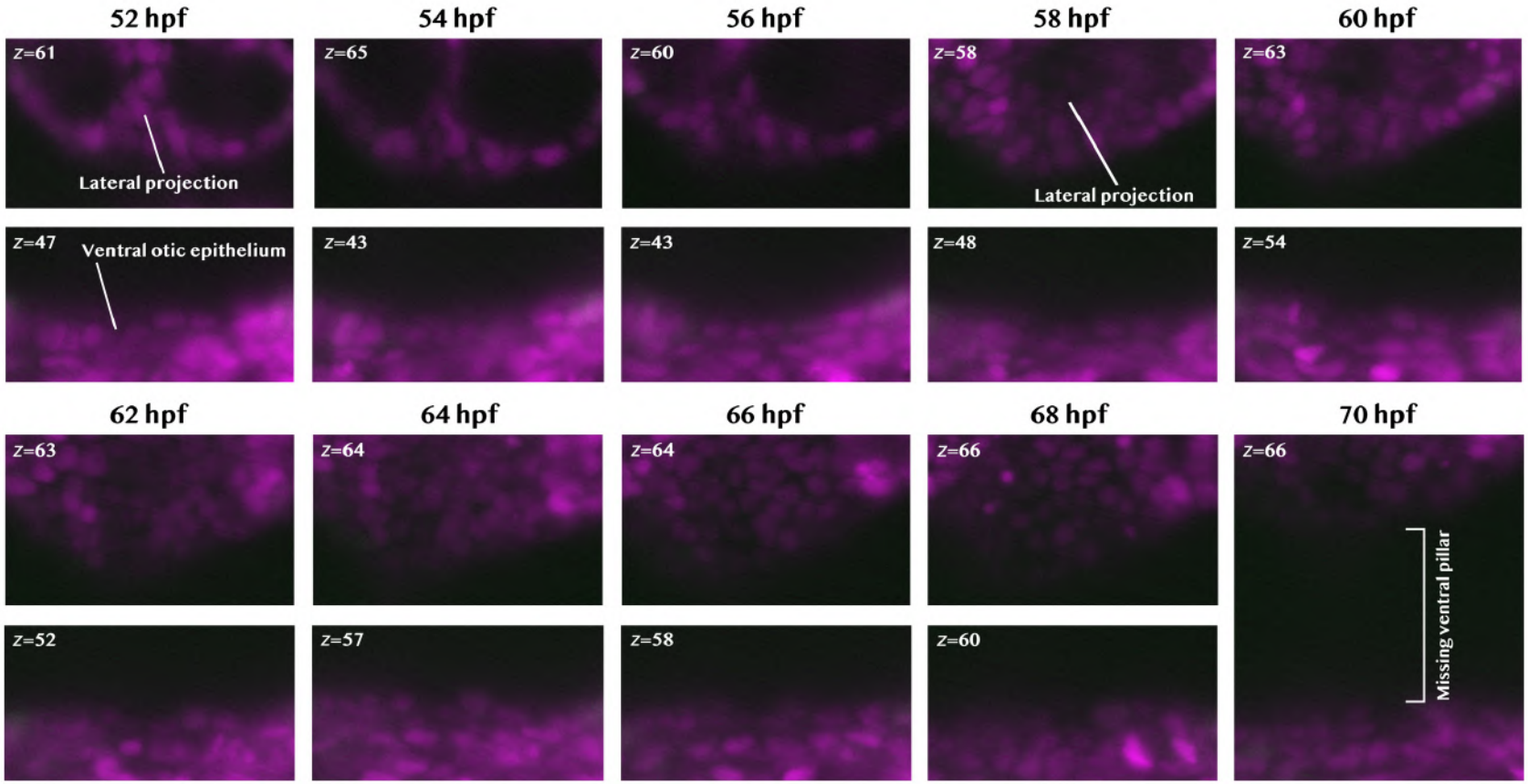

Figure 4.2 (B). Magnification of *otx1* mutant otic development from Figure 4.2 (A). The magnification focuses on the lateral projection (top row) and ventral otic epithelium (bottom row). The ventral bulge and projection are not distinguishable, resulting in the lack of ventral pillar by 70 hpf. Particularly important is the complete lack of GFP-positive cells in the ventral otic epithelium. Each time-point is shown as a maximum intensity projection of 2 to 5 *z*-stacks around the one indicated in the figure.

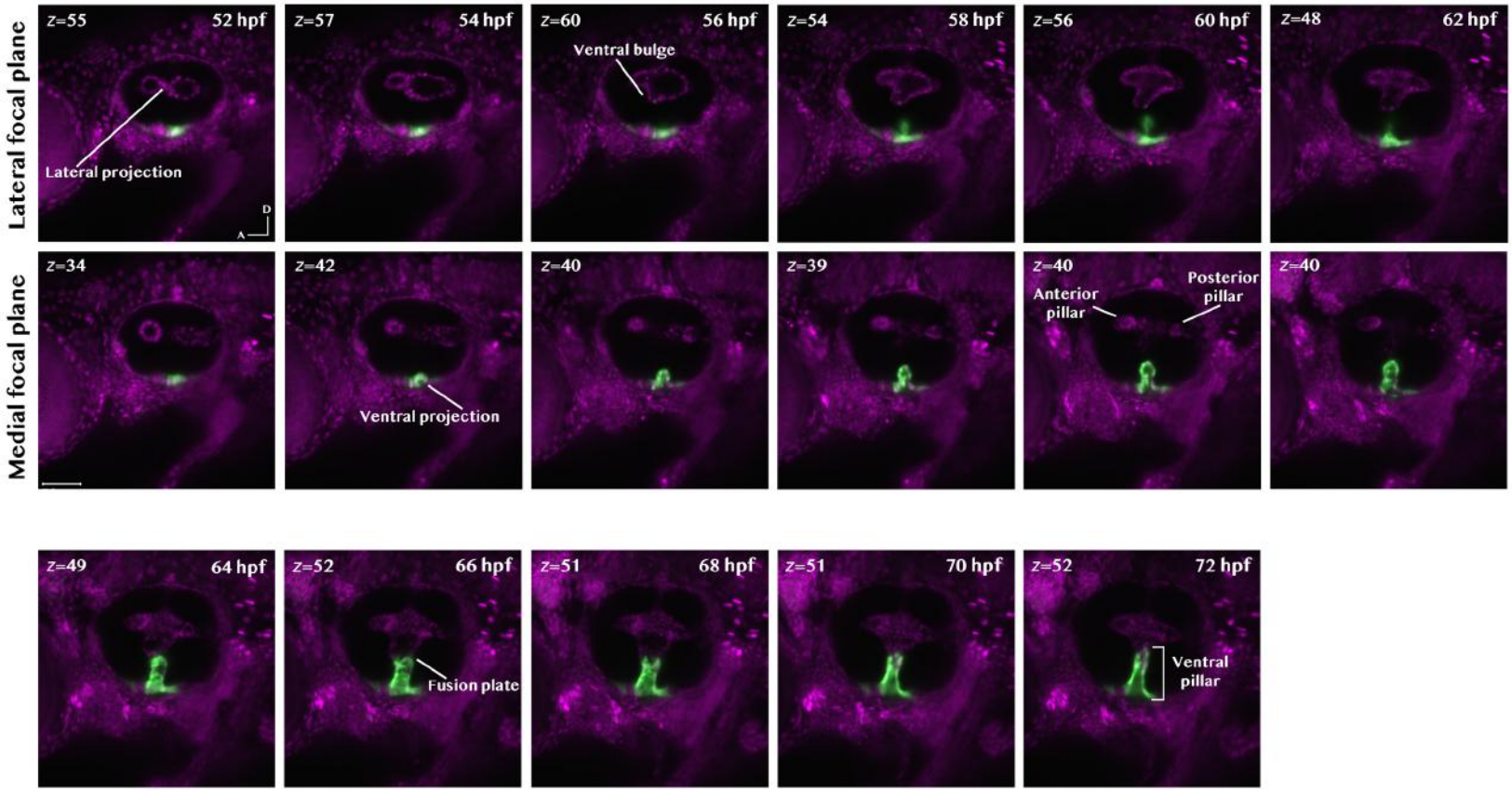

Figure 4.3 (A). Time-lapse of the ventral pillar development in an *otx1* sibling. Each time-point is presented as a maximum intensity projection of 2 to 5 *z*-stacks around the stack indicated in the figures. The ventral bulge and projection lie on two different focal planes: a more lateral plane (top row, ventral bulge) and a more medial plane (bottom row, ventral projection). Arrowheads highlight the focus of the figures. No difference was detected between the ventral pillar development in the *otx1* siblings and wild-types. Scale bar, 50 μm.

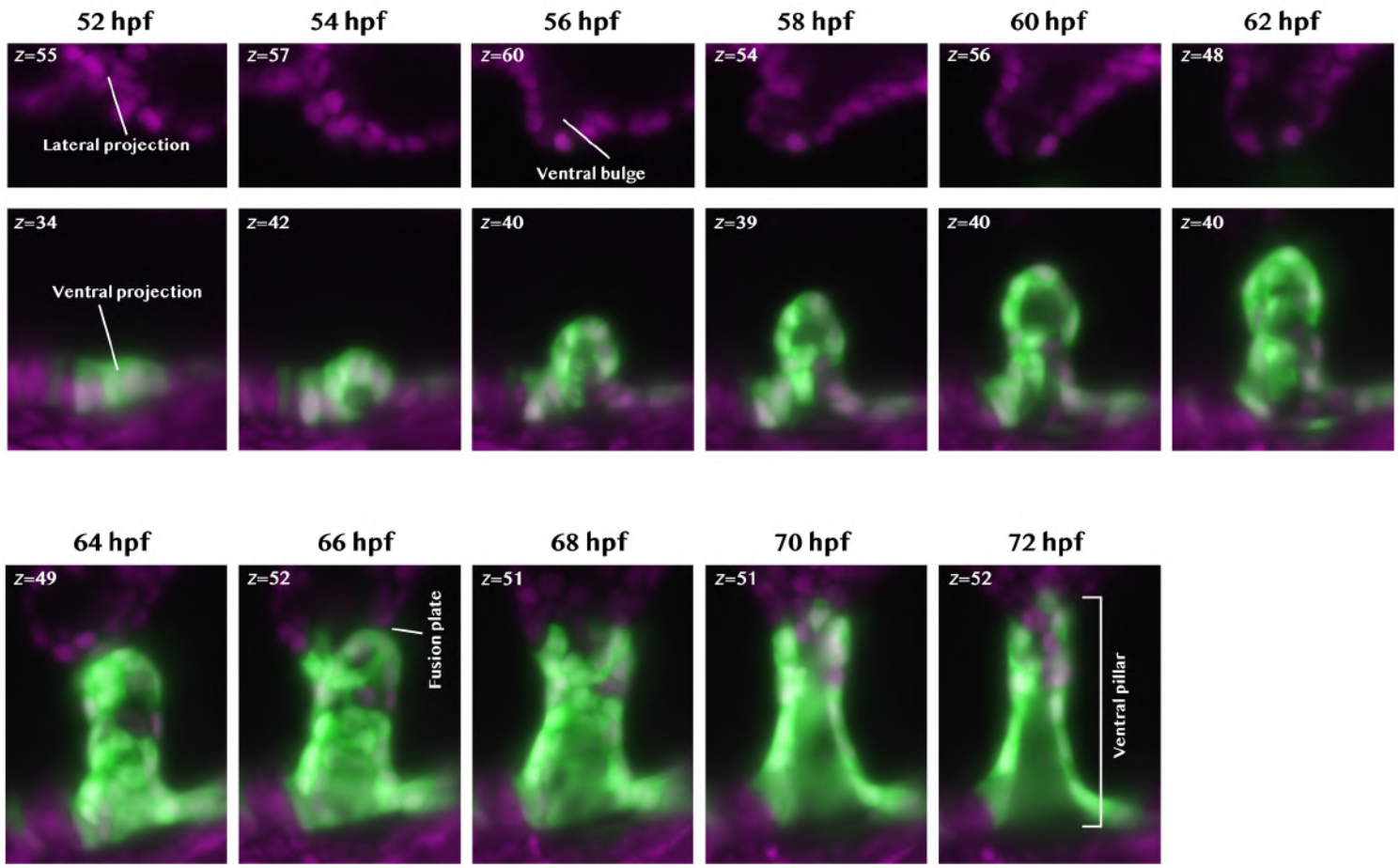

Figure 4.3 (B). Magnification of ventral pillar and bulge development from Figure 4.3 (A). The magnification focuses on the ventral bulge (top row) and projection (bottom row) development. The bulge and projection sit on different focal planes (bulge more lateral, projection more medial) until around 64 hpf, when they both become visible in the same *z*-stacks.

4.4. Gene expression analysis of *otx1*^{sa96} mutants

4.4.1. *otx1* mutation results in the loss of otic *gsc* and *otx2a* expression, but not on otic *eya1* and *tbx1* expression

The analysis of the transgenic line described in section 4.3 highlighted the loss of *EGFP* expression in the ventral otic epithelium and, in particular, in the region from which the ventral projection arises. Interestingly, many genes are expressed in this area of the ventral otic epithelium (*eya1*, *tbx1*, *gsc* and *otx2a*). At early developmental stages, the expression pattern of these markers, in the ventral otic epithelium, overlaps with that of *otx1* (Figure 1.7 and 6.1 B). Therefore, I decided to test whether, in the *otx1* mutants, the loss of *EGFP* expression correlated with a disruption in the expression of the abovementioned genes.

Previous work from our lab suggested that *otx1* morpholino knockdown had no effect on *eya1* and *tbx1* expression in the ear but resulted in the loss of otic *otx2a* and *gsc* expression (Giuliani, G. and Blanco-Sánchez, B. unpublished results). For further confirmation, I retested this in the *otx1*^{sa96} mutants around 26 hpf. This developmental stage was chosen because, at this stage, the expression pattern of these genes overlaps and it could give us indications

about a possible gene network required to specify the destiny of the cells at early stages.

At 26 hpf, the *otx1* mutants completely lose the expression of both *otx2a* and *gsc* in the ventral otic epithelium. Interestingly, their expression remains unaltered in the diencephalon, midbrain and branchial arch (*otx2a*) (Figure 4.4 A-B) and anteroventral prosencephalon nuclei and one branchial arch (*gsc*) (Figure 4.4 C-D). This was in accordance with previous knowledge gained from the morphants; however, since there is no indication in the literature as to where is *gsc* expressed at 72 hpf in the otic vesicle, I performed WISH also at this stage. At 72 hpf, the *otx1* mutants show a complete loss of *gsc* only in the ventral otic epithelium compared to the siblings, in a region that is very close to the ventral pillar (Figure 4.4 E-F). In the rest of the body, while strongly downregulated, *gsc* expression is still detectable, providing, once again, further confirmation about the specificity of action of *otx1* in the otic vesicle compared to the rest of the body.

With respect to *eya1* and *tbx1* expression both in the ear and the rest of the body, the *otx1* mutants (n=29 for *eya1* and n=51 for *tbx1*) were indistinguishable from the siblings, therefore confirming previous results obtained from the morphants.

4.4.2. *vcanb* is never expressed in the ventral otic vesicle of *otx1* mutants

The loss of both *gsc* and *otx2a* in the ventral otic epithelium of the *otx1* mutants, at early stages, led me to hypothesise that markers required at later stages of pillar formation could also be affected. In particular, I focused my attention on markers of the ECM, as they have been extensively described to play a crucial role in pillar development and have been defined as "propellant" for the development of inner ear projections (Haddon and Lewis, 1991; Geng *et al.*, 2013). *vcanb* was chosen as a representative marker of the ECM in the ventral projection and bulge due to its expression being previously described in detail (Geng *et al.*, 2013). This analysis was carried out on embryos at 60 hpf due to *vcanb* being highly expressed ahead of fusion of all projections, while around 72 hpf, its expression is completely lost in the pillars (Geng *et al.*, 2013).

At 60 hpf, the expression of *vcanb* was clearly visible in the lateral and ventral projection of the wild-type siblings. As expected, the mutants did not develop a ventral projection and, therefore, *vcanb* expression was only detectable in the lateral projection (Figure 4.4 G-H).

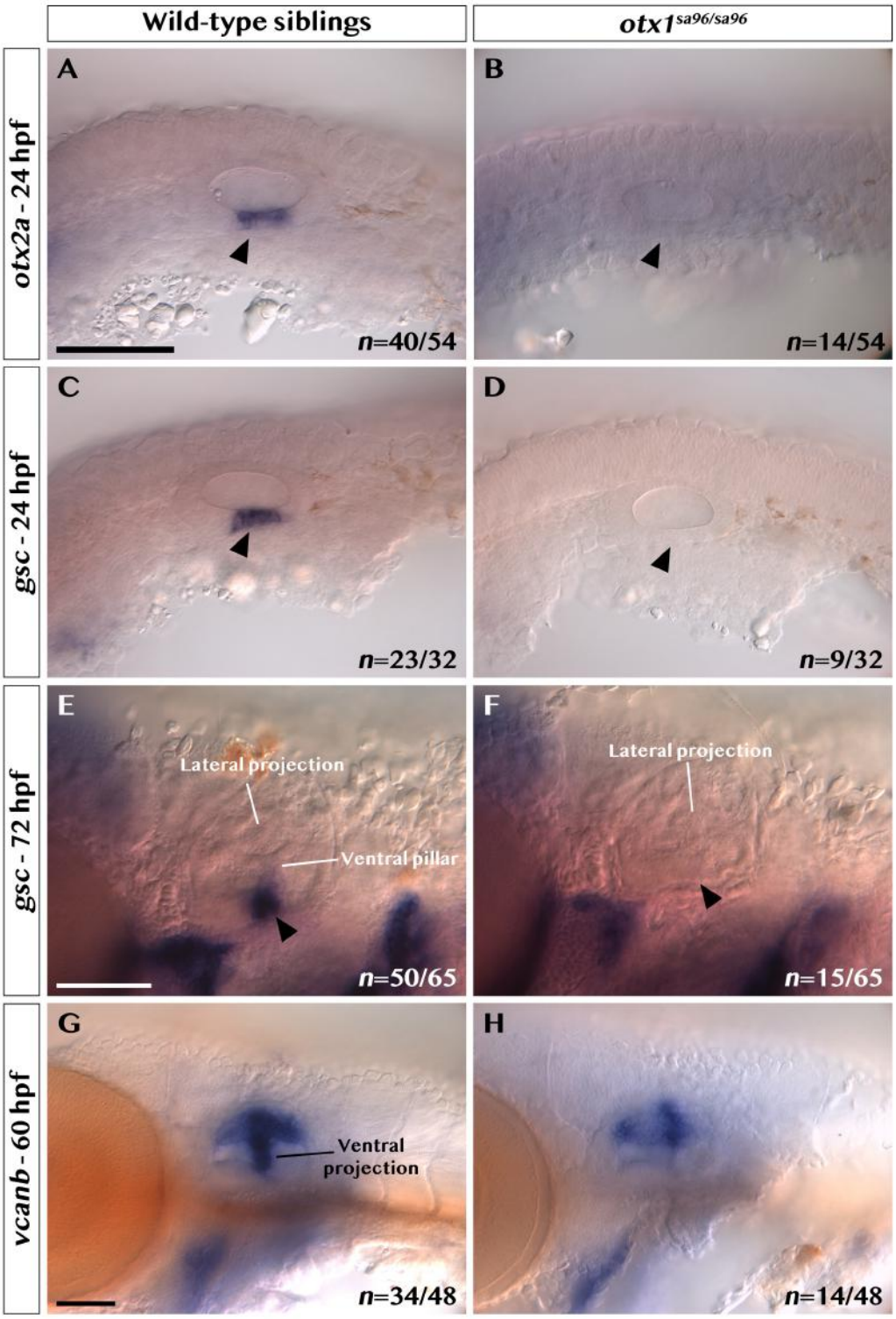

Figure 4.4. Whole mount *in situ* hybridisation panel of the *otx1*^{sa96} line. All pictures are lateral views, with anterior to the left. (A to D) 26 hpf wild-type sibling and *otx1*$^{sa96/sa96}$ embryos stained for *otx2a* (A and B) and *gsc* (C and D) expression, which is completely lost in the ventral otic epithelium of the mutants. Scale bar, 100 μm. (E and F) At 72 hpf, the loss of *gsc* is specifically restricted to the ventral domain of the ear. Scale bar, 50 μm. (G and H) Wild-type sibling and *otx1* mutant stained for *vcanb* expression at 60 hpf, which is completely lost in the ventral otic domain of the mutant. Scale bar, 100 μm (A and E) and 50 μm (G).

4.4.3. The expression of *ngn1* and *neurod1* are not affected by *otx1* mutation

The results of the phenotypical and gene expression analysis described in the previous sections suggest that the loss of *otx1* could lead the cells of the ventral otic epithelium to lose their commitment to become part of the ventral projection. This raised the question as to whether these cells simply lose their commitment or undergo a fate-switch that causes them to become part of a different structure. In this respect, previous unpublished work from our laboratory showed that the morpholino-mediated knockdown of *otx1* results in the expansion of *neurod1* expression along the anteroposterior axis of the otic vesicle (Giuliani, G. unpublished results). For all these reasons, I decided to test whether the loss of *otx1* was causing the cells that should become part of the ventral projection to switch towards a neural fate.

To this purpose, I repeated the gene expression analysis using a *neurod1* antisense probe to confirm the abovementioned results on the *otx1* mutants. The experiment was performed on embryos, at 26 hpf, derived from the incross between two heterozygous fish. Since the *otx1* mutants are not distinguishable from their siblings at 26 hpf, I evaluated whether a quarter of the population exhibited any difference in *neurod1* expression.

In contrast to what was previously observed in the morphants, out of 53 embryos tested (from two separate experiments on *n*=29 and *n*=24 embryos), I did not detect any embryo exhibiting a difference in the expression of *neurod1*. This suggests that the expanded expression observed in the morphants could be a result of morpholino injection.

To further confirm this, I crossed the *otx1*^{sa96} mutants with a Tg(*neurod1::EGFP*) line, which expressed *EGFP* in the delaminating neuronal progenitors and anterior and posterior lateral line ganglia (Obholzer *et al.*, 2008; Dyballa *et al.*, 2017), and imaged three homozygous mutants and three wild-type siblings (both ears for each embryo), at 72 hpf, using the light-sheet microscope. These embryos were also injected, at one cell stage, with lyn-tdTomato mRNA to allow for the visualisation of cell membranes (Zecca *et al.*, 2015). The use of this transgenic line confirmed the observations described above regarding the lack of significant differences, when it comes to *neurod1* expression in the inner ear (Figure 4.5). The only detectable difference was the lack of *neurod1* expression in the region of the ventral otic epithelium where the ventral crista fails to develop in the mutants (Figure 4.5).

Finally, I also tested the expression of *ngn1* in the *otx1* mutant due to this being also involved in the specification of neural cell fate in the otic vesicle (Hoijman *et al.*, 2017). As previously observed with *neurod1*, the mutants did

not show any difference in the expression of *ngn1* and were undistinguishable from the siblings. This experiment was performed on 29 embryos (from a single experiment) at 26 hpf. While these data suggest that the loss of *otx1* function does not interfere with the expression of *neurod1* and *ngn1* in the otic vesicle, they do not provide definitive evidence that the cells of the ventral otic epithelium do not undergo a switch from non-neural to neural fate. To further test this hypothesis, the expression pattern of *fgf3*, *fgf8a* and *fgf10a* was also analysed due to their involvement in neural specification.

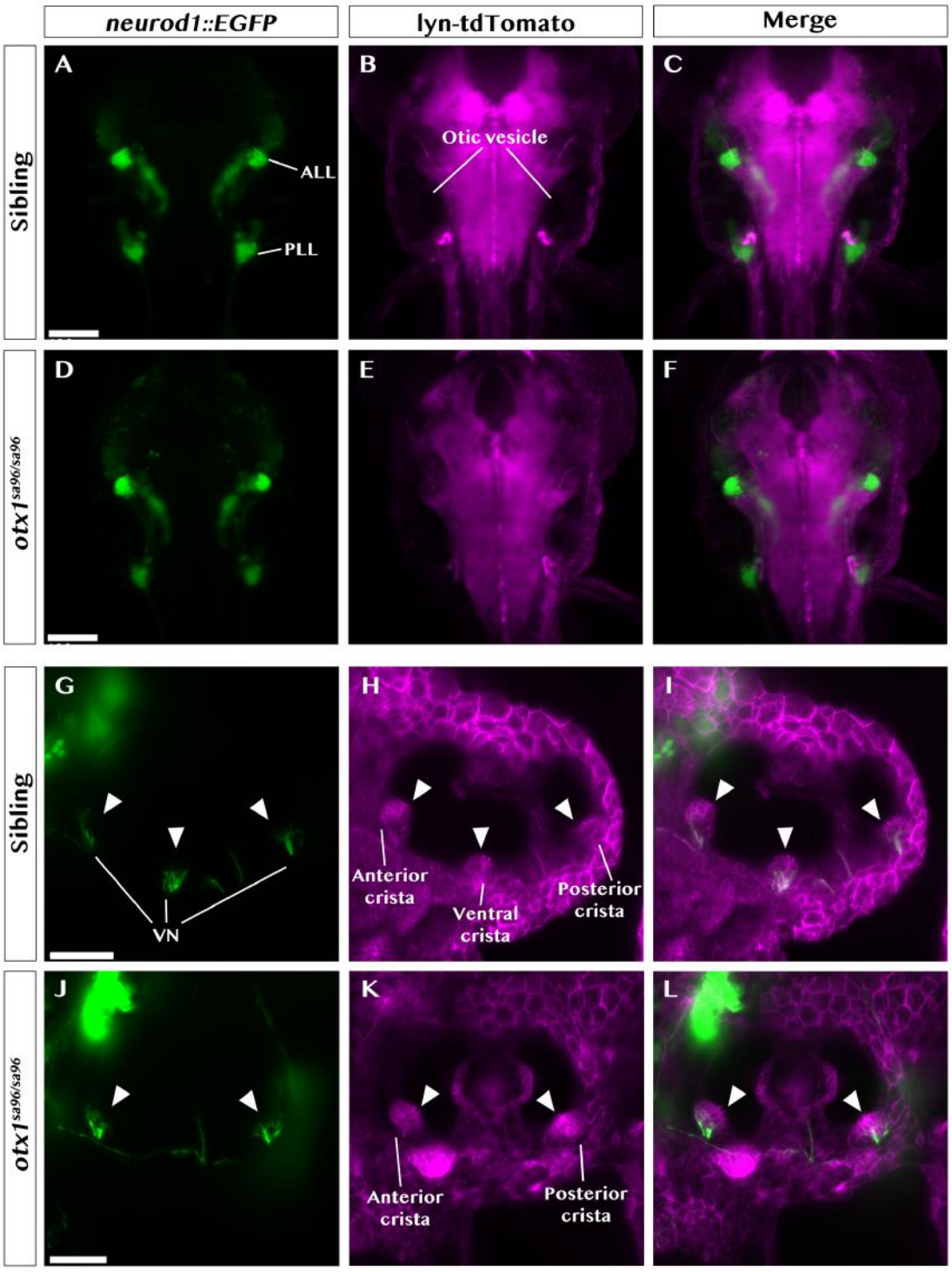

Figure 4.5. Light-sheet imaging showing the *neurod1::EGFP* expression in an *otx1* sibling and mutant at 72 hpf. Embryos were injected with lyn-tdTomato mRNA at one cell stage to visualise cell membranes. Figures A to F are dorsal views of both otic vesicles with anterior to the top. G to L are side views of one otic vesicle for each embryo with anterior to the left. No difference was detected between siblings and mutants, a part from the lack of nerve fibres in the region of the ventral otic epithelium where the ventral crista is lost in the mutants. Arrowheads highlight *neurod1::GFP* expression in the anterior, posterior and ventral cristae in figures G to I and the anterior and posterior cristae in figures J to L. Scale bar, 100 μm (A and D) and 50 μm (G and J). ALL = anterior lateral line ganglion; PLL = posterior lateral line ganglion; VN = vestibular nerves.

4.4.4. The mutation of *otx1* does not influence the expression of *fgf* genes in the otic vesicle

In sections 1.4.1 and 1.7, the importance of FGF signalling during otic development was highlighted. In particular, it is required to provide the cells with specific molecular cues which make them committed to become part of the otic placode both in the mouse and zebrafish and drives delamination of neural cells from the otic vesicle by modulating the activity of *ngn1* and *neurod1* (Léger and Brand, 2002; M. N. McCarroll *et al.*, 2012; Hoijman *et al.*, 2017). Therefore, to further test whether the mutation of *otx1* could cause the cells of the ventral otic epithelium to switch from non-neural to neural fate, I decided to analyse the expression of *fgf* genes in the otic vesicle of these mutants.

The otic expression pattern of *fgf3, 8a* and *10a* was assessed to look for any difference between *otx1*$^{sa96/sa96}$ and wild-type siblings. At 26 hpf, none of the three genes is affected by the mutation of *otx1* as I could not distinguish the mutants from the siblings based on the staining. For these experiments, 59 embryos were tested for *fgf3* (experiment was repeated twice on *n*=29 and *n*=30 embryos), 62 for *fgf8a* (from two separate experiments on *n*=29 and *n*=33 embryos) and 29 for *fgf10a* (from a single experiment).

4.5. Phenotypical analysis of *otx2a* morphants

In zebrafish, *otx2a* is expressed in the forebrain and a very restricted domain of the ventral otic vesicle, where also *otx1* is expressed. As demonstrated in section 4.4.1, the mutation of *otx1* results in the loss of *otx2a* expression in the otic vesicle, which raised the question as to whether the knockdown of *otx2a* could lead to the same phenotype as the *otx1* mutants. To test this, I injected an antisense morpholino designed to knockdown the expression of this gene (Foucher *et al.*, 2006) (see section 2.3). Various doses have been injected to find the smallest amount of morpholino that would give a specific effect. At first, each embryo was injected with 1 nl of injection mix containing 1.2 ng of *otx1a* morpholino, as this was the same concentration injected in the literature (Foucher *et al.*, 2006). The development of the injected embryos was followed over the course of three days to look for any disruption in ventral pillar formation. In accordance to what was previously described, this dose did not have any effect and the injected embryos (n=180) were phenotypically indistinguishable from the uninjected controls (n=60).

The dose of morpholino injected was subsequently raised to 1.8, 2.4 and 3 ng. For each concentration, a total of 120 embryos were injected with the

morpholino and 60 uninjected embryos were kept as controls. During the first 24 hours of development, 31 out of 120 embryos died in the 1.8 ng injected plates, 26 out of 120 embryos died in the 2.4 ng injected plates and 34 out of 120 embryos died in the 3 ng injected plates. Between 24 and 72 hpf, the injected embryos survived and developed just like the uninjected: no defects were detectable with respect to the forebrain or the inner ear. By 72 hpf, the anterior, posterior and ventral pillars developed normally and the otoliths appeared normal and in the correct position.

For this reason, the dose of morpholino to be injected was raised to 6 and 9 ng. At the dose of 6 ng, injected embryos (n=60) developed and survived as the uninjected (*n*=60) for the first 24 hours; only 4 embryos died in both the injected and uninjected plates. After 48 hpf, out of 56 injected embryos, 42 showed a severely swollen brain ventricle and no anterior or posterior projections (Figure 4.6 A to C) and 13 had slightly swollen brain ventricle and the inner ear is developing as in the uninjected embryos (Figure 4.6 D to F); only one embryo showed almost no blood flow and died before 72 hpf. After 72 hpf, the brain ventricle defect resolved in all the embryos, but in 32 out of 55 none of the three pillar projections developed, the otic vesicle was significantly smaller, the heart was swollen and the yolk extension was almost completely

absent compared to their uninjected siblings (Figure 4.6 J to M). The remaining 23 embryos had a smaller otic vesicle and with no pillars but a small residue of the anterior projection was still detectable. These embryos also exhibited a swollen heart and the yolk extension defect was less pronounced (Figure 4.6 N to Q). All the injected embryos had a severely smaller head (Figure 4.6).

At the dose of 9 ng, the injected embryos developed severe phenotypes as soon as 24 hpf. Out of 120 embryos, only 60 survived; of these, 6 exhibited severely smaller head and tail and the otic vesicle was hardly distinguishable (Figure 4.7 A to C), 31 had a small head and a smaller and more rounded otic vesicle with much smaller otoliths (Figure 4.7 D) and 23 had a less severe ear phenotype but the head was smaller (Figure 4.7 E) than the uninjected siblings (Figure 4.7 F). By 48 hpf, all embryos developed defects consisting of heart oedema, very slow blood flow, small head, otic vesicles not forming any projection or bulges and small otoliths. In addition, the injected embryos were less pigmented than the uninjected siblings. While defects on the head and ear could be expected, due to the expression pattern of *otx2a* (see at the beginning of this section), the heart, blood flow and tail defects do not fit with *otx2a* expression. Therefore, these defects were considered aspecific effects derived from the morpholino injection. These embryos did not survive until 72 hpf.

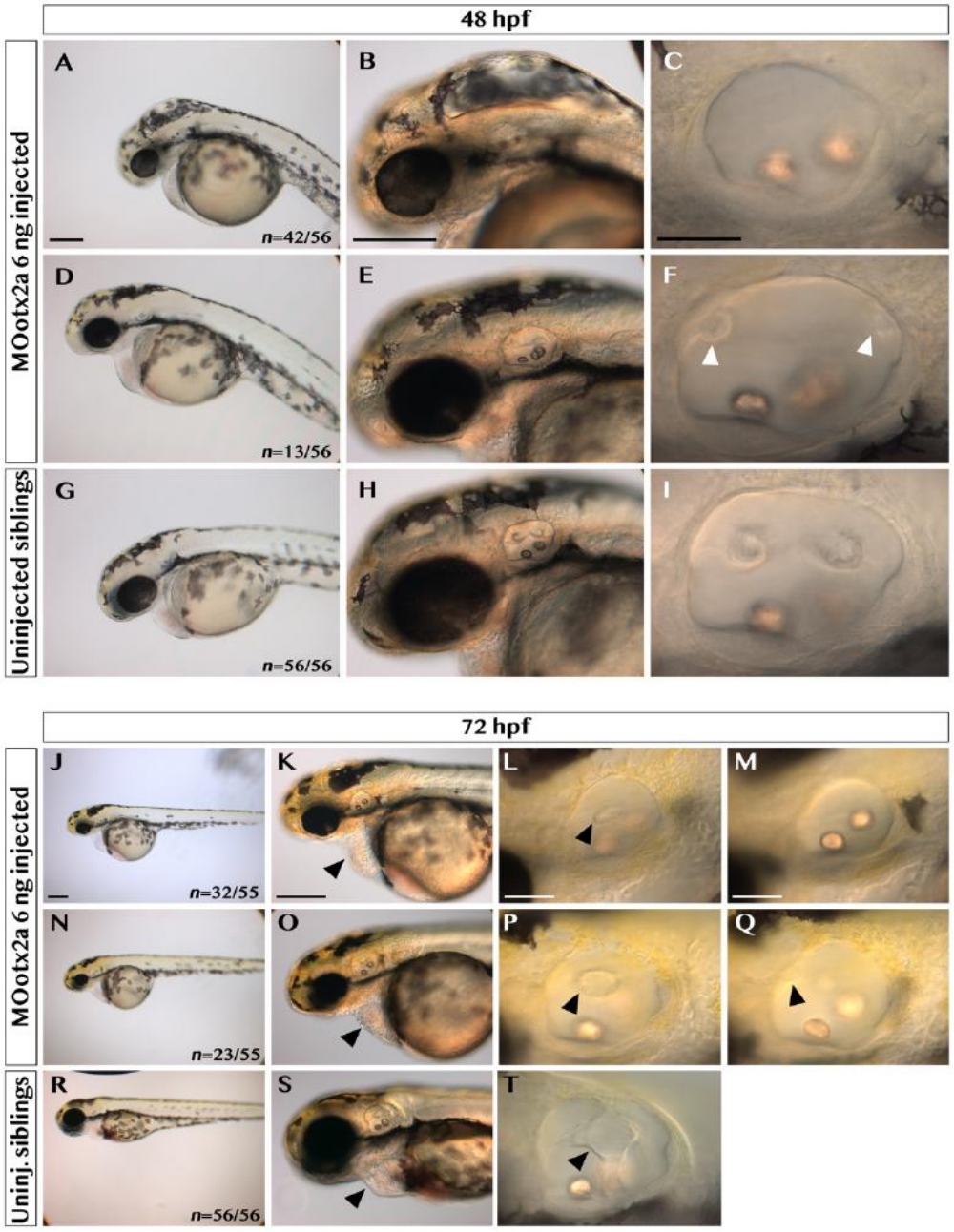

Figure 4.6. Live imaging of embryos injected with 6 ng of MOotx2a. All pictures are lateral views, with anterior to the left. (A and B) 48 hpf embryo exhibiting severely swollen brain ventricle and (C) lack of lateral, anterior and posterior projections. The overall vesicle is also smaller and more rounded compared to that of uninjected siblings (I). (D to F) A lower percentage of embryos exhibited a less severe phenotype with truncated anterior and posterior projections (white arrowheads in F). Only one embryo showed an almost complete lack of blood flow. (G to I) Uninjected siblings developed normally. Scale bar, 100 μm (A and B) and 50 μm (C). (J and N) Embryos showing no yolk extension, defective pericardial sac (arrowhead in K and O) and severely smaller head compared to uninjected siblings at 72 hpf. (L and M) Otic vesicle showing a complete lack of anterior, posterior or lateral projections (M) and extremely under-developed lateral projection (arrowhead in L). (P and Q) Less severe otic phenotype showing a slightly bigger lateral projection (arrowhead in P), truncated anterior projection (arrowhead in Q) but no posterior or lateral projection. (R to T) Uninjected siblings developed normally. Scale bar, 200 μm (J and K) and 50 μm (L).

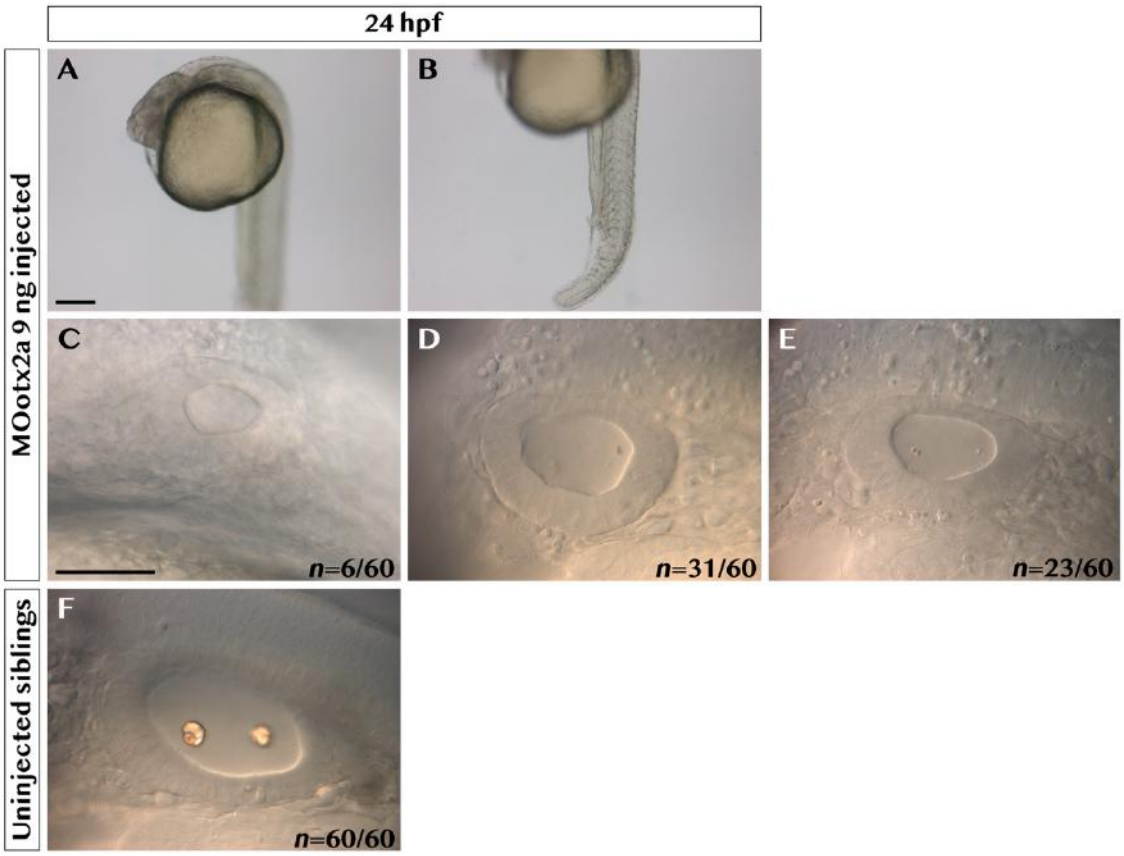

Figure 4.7. Live imaging of embryos injected with 9 ng of MOotx2a. All pictures are lateral views, with anterior to the left. (A and B) Overview of a 24 hpf representative embryo with focus on the head (A) and tail (B). These embryos exhibited necrosis in all their body, which is detectable due to the head, trunk and tail tissues being opaque compared to the uninjected siblings. 6 out of 60 injected embryos exhibited a more severe otic phenotype (C) comprising a very small otic vesicle and no otoliths. (D and E) Less severe phenotypes characterised by a smaller vesicle and otoliths. In 31 embryos the vesicle is also more rounded (D) than that of uninjected siblings (F). Scale bar, 200 μm (A) and 50 μm (C).

Due to the fact that the injection of 3 ng of *otx1a* morpholino did not give any effect and 6 ng had some aspecific effects, I decided to test the effects of the injection of 5 ng of morpholino. At this dose, 12 embryos out of 120 died within the first 24 hpf but the ones that survived did not develop any defect. After 48 hpf, 37 embryos exhibited a more rounded otic vesicle with no projections or bulges and a swollen brain ventricle (Figure 4.8 A and B) and 65 were morphologically indistinguishable from the uninjected (Figure 4.8 C and D). The brain ventricle phenotype disappeared after 72 hpf but 13 embryos, out of 37 that showed a phenotype at 48 hpf, had very small head and eyes, the ear was more rounded and had very small or no projections, while the remaining 24 had no defect (Figure 4.8 G and H). The embryos that did not have a phenotype at 48 hpf (n=65) developed normally and did not exhibit any defect on the ventral pillar at 72 hpf.

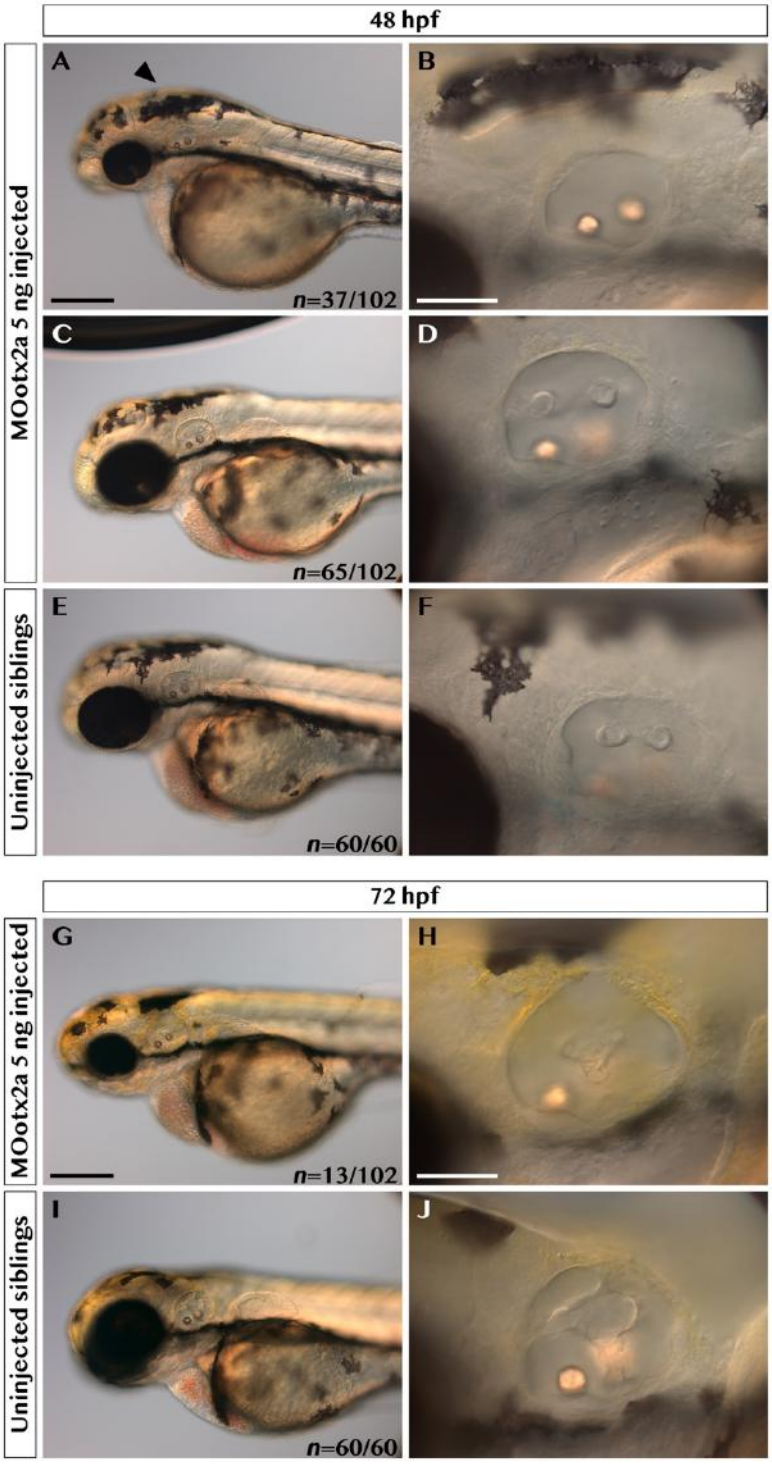

Figure 4.8. Live imaging of embryos injected with 5 ng of MOotx2a. All pictures are lateral views, with anterior to the left. (A) Embryo showing slightly swollen brain ventricle (arrowhead) and overall smaller head compared to uninjected siblings (E and F). The otic vesicle of these embryos did not develop a lateral, anterior and posterior projections. (C and D) Injected embryo showing no defect compared to the uninjected siblings. (G and H) At 72hpf, only 13 embryos exhibited severely smaller had (G) and did not develop an anterior, posterior or ventral pillar (H). Scale bar, 200 μm (A and G) and 50 μm (B and H).

4.6. Analysis of CRISPR-injected embryos

Due to the *otx2a* morpholino giving apparently aspecific effects, the CRISPR-Cas9 mutagenesis method was used to make an attempt at creating a new *otx2a* mutant line. Two out of three gRNAs injected (targeted to disrupt MwoI and MslI restriction sites, see Chapter 2.4) gave no morphological defects within the first 24 hpf. The DNA was, then, extracted from 9 out of 130 MwoI gRNA-injected embryos and 10 out of 100 MslI gRNA-injected embryos, amplified and digested with the respective restriction enzymes. Upon electrophoresis, it was possible to observe that neither of the two gRNAs induced a mutation in any of the embryos tested (Figure 4.9). The DNA of the injected embryos, indeed, got digested as efficiently as that from an uninjected control (Figure 4.9). Finally, the injection of the BslI gRNA caused all the embryos to die within the first 24 hours of development (n=120). To further confirm whether this gRNA was lethal, I made a second attempt at injecting it (n=120). In this experiment, a second gRNA, targeted against an MwoI restriction site in the *rad52* gene, was also injected as a control (n=120) (*rad52* gRNA obtained from Freek van Eeden laboratory). The *rad52* gRNA has previously proved to be efficient in creating a mutant line in the van Eeden lab (Freek van Eeden, unpublished data). After 24 hpf, all the embryos injected

with the gRNA against the BslI restriction site of *otx2a* died, while all the embryos injected with the *rad52* control gRNA, as expected, did not develop any morphological defects. This is due to the fact that the embryos injected with the CRISPR will have a spectrum of mosaic mutations, some of which might cause a phenotype, some of which might not (Hruscha *et al.*, 2013). With respect to this gRNA, this was previously tested and shown not to give any morphological defects within the first 24 hours after the injection. Upon, DNA extraction, amplification and digestion, all the embryos injected with the *rad52* gRNA were found to be mutated (Figure 4.9).

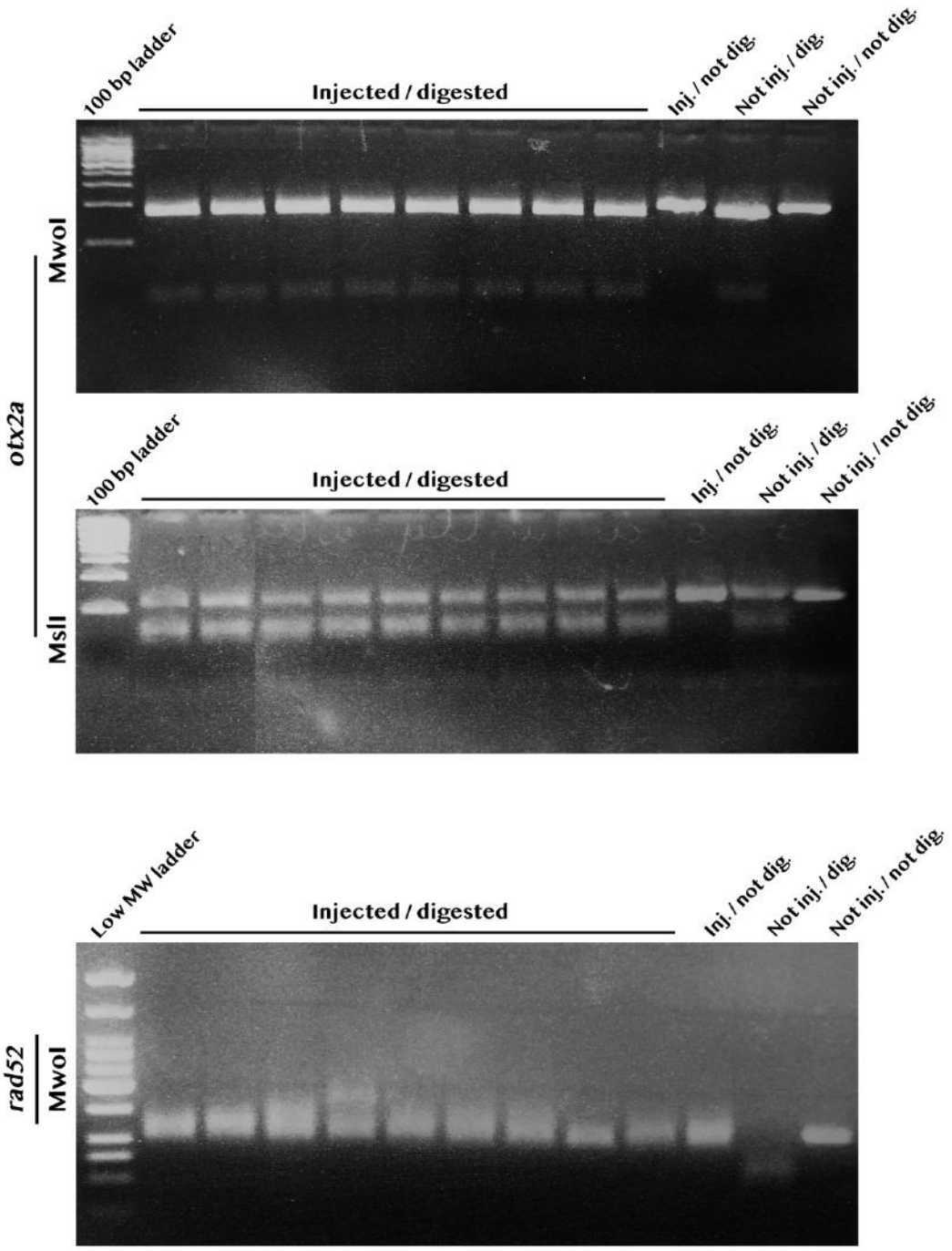

Figure 4.9. Results of the CRISPR injection against *otx2a* and *rad52*. The CRISPR designed against the MwoI and MslI restriction sites of *otx2a* did not induce any mutation. The samples injected with the CRISPR and digested with the corresponding enzyme (lines 1 to 8 for MwoI and 1 to 9 for MslI) got cut in the same fashion as the uninjected and digested controls (line 10 for MwoI and line 11 for MslI). Conversely, the injection of a control gRNA against the MwoI restriction site of *rad52* induced a mosaic of mutations, which can be observed in lines 1 to 9 of the corresponding agarose gel. In the injected samples, the restriction site has been mutated and, therefore, they are not cut by MwoI as the uninjected samples. As further control, the undigested DNA for one injected and one uninjected sample has been run alongside the others (for *otx2a* CRISPR: line 9 and 11 for MwoI and 10 and 12 for MslI; for *rad52* CRISPR: line 10 and 12).

4.7. Discussion

In this chapter, various aspects of the role of *otx1* in ventral pillar development have been discussed. Above all, it is important to notice that, for this study, I took advantage of the *otx1*^{sa96} mutant line to corroborate previous results derived from *otx1* morphants (Hammond and Whitfield, 2006). The results described in section 4.2 further strengthen our knowledge regarding the highly specific ventral pillar phenotype previously observed in the zebrafish morphants and in the mouse (Acampora *et al.*, 1996; Acampora and Simeone, 1999; Mazan *et al.*, 2000; Hammond and Whitfield, 2006). In addition to that, light-sheet imaging of the Tg(*otx1*^{sa96}*;mir137::EGFP;xEF1a::H2B-RFP*) line shows that, in the mutants, the cells forming the ventral pillar are not detectable at 48 hpf. This is important because in the wild-type siblings the GFP-positive cells forming the ventral projection start to be distinguishable at this stage (see sections 3.3 and 4.3).

While these data suggest that ventral projection cells are completely lost in the *otx1*^{sa96} mutants, they do not provide information as to whether these cells die or are simply not committed to become ventral pillar cells. In this respect, the movies show that there are no cell death events occurring between 48 and 72 hpf in the ventral otic epithelium. Therefore, it can be assumed that the loss

of *otx1* causes cells not to become committed to form the ventral projection and, subsequently, the pillar. However, it cannot be completely ruled out that cell death occurs at earlier stages.

The mutation of *otx1* also has repercussions on the development of the ventral bulge, which does not fully develop, between 48 and 72 hpf, in the mutants. Since the Tg(*mir137::EGFP*) line shows that the projection and the bulge are formed of two very distinct population of cells (see section 3.3) and knowing that *otx1* is never expressed in the ventral bulge, we can infer that the effects of the mutation of *otx1* on this structure are indirect. It is intriguing to think that the development of the ventral projection might serve as cue for the outpocketing of cells from the lateral projection to form the bulge. However, more experiments will be needed to test this hypothesis.

The gene expression analysis, described in section 4.4, confirms previous unpublished observations on morphants indicating that the lack of ventral projection in the *otx1* mutants correlates with the loss in the expression of a specific set of genes (*otx2a*, *gsc* and *vcanb*) (Giuliani, G. unpublished results). With respect to *otx2a* and *gsc*, the data presented in this chapter suggest that their activity inside the otic vesicle depend on the presence of *otx1* but it has not been possible to establish whether they are epistatic to *otx1* or not.

Another important aspect to consider is the loss of *vcanb*, which could be due to the fact that the loss of *otx1* causes the lack of cell commitment to become ventral pillar and therefore no ECM components are produced leading to the projection not being able to grow. Further studies on mutants for *gsc* or *otx2a* and for both *gsc* and *otx1* will be required to provide definitive evidence regarding the hierarchy between *otx1*, *otx2a* and *gsc*.

The observations derived from the *otx1* morphants regarding a possible expansion of the *neurod1* expression domain (Giuliani, G. unpublished data), together with the assumption that cells lack their commitment to become part of the pillar in the *otx1* mutants, led the Whitfield lab to hypothesise that the cells of the ventral otic epithelium could be undergoing a change in cell fate (semicircular canal to neural) in the absence of *otx1* function. However, this does not seem to be the case as the data presented in sections 4.4.3 show that the mutants stained for both *ngn1* and *neurod1* are undistinguishable from the siblings at 26 hpf. The only visible difference, observed using the Tg(*otx1*^{sa96}*;neurod1::EGFP*), line was the lack of ventral crista innervation in the mutants, at 72 hpf, which was predictable due to the absence of the ventral crista in the *otx1* mutants (see section 4.2).

I also found no changes in the expression of *fgf3*, *8a* and *10a*, which have been described to control the activity of *ngn1* and *neurod1* during otic

neurogenesis (Hoijman *et al.*, 2017). Taken together, all these data suggest that the results obtained in the *otx1* morphants regarding the expansion of *neurod1* could be a consequence of the morpholino injection rather than the knockdown of *otx1*. Therefore, it is reasonable to believe that the lack of cell commitment to become part of the pillar does not depend on these cells switching towards a neural fate. Nonetheless, it would be interesting to repeat the injection of the *otx1* morpholino and, as a control, inject a standard or mismatched morpholino. These embryos could be processed by WISH together with the mutants to provide definitive proof as to whether the expansion in *neurod1* expression is an effect of morpholino injection.

As far as *otx2a* is concerned, the morpholino injections (described in section 4.5) did not produce a specific effect on the ear. I observed a number of defects raging from heart oedema, to swollen brain ventricle, to the loss of all three pillars of the inner ear. Most of these defects (heart oedema and lack of pillars) do not correlate with the expression pattern of *otx2a* (see section 4.4) and were, therefore, considered as aspecific effects caused by morpholino injection.

As for the ear defects, it is unlikely that *otx2a* knockdown could lead to a defective or missing anterior or posterior pillar because it is only expressed in

the ventral otic epithelium and, most importantly, because the *otx1* mutants effectively exhibit the phenotype of double *otx1*;*otx2a* mutants in the ear. On the other hand, the effects of the morpholino injection on the development of the head could be the result of the knockdown of *otx2a*, as it is known that the activity of OTX family genes is pivotal for the development of the forebrain (Acampora and Simeone, 1999; Cecchi, Mallamaci and Boncinelli, 2000). However, also in this case, the morpholino injection led to a severely smaller head than that of *otx1* mutants. It is difficult to establish if an efficient knockdown was achieved at the lower doses and this did not cause any defect; more experiments using different controls would be required (for instance, a mismatched morpholino would provide a more stringent control). It is also important to notice that this morpholino was obtained from the laboratory of Corinne Houart (King's College, London), who published a study in 2006 showing that, when injected alone, this morpholino did not give rise to any defect during early developmental stages (up to 24 hpf) (Foucher *et al.*, 2006). For all these reasons, it will be important to create a new mutant line for *otx2a* and provide both phenotypical and gene expression analyses.

5. THE ROLE OF *eya1* IN FORMATION OF THE LATERAL SEMICIRCULAR CANAL

5.1. Introduction

In chapter 4, the strong correlation between the expression of *otx1* and the development of a ventral pillar has been discussed. To obtain a more complete overview of the gene network that is involved in this process, the *eya1* mutants have also been analysed. This line was chosen due to the fact that previous unpublished work from our laboratory suggested that the expression of *otx1* was expanded in these mutants (Blanco-Sánchez B., PhD thesis) but, so far, there are no indications as to what ventral pillar phenotype is elicited by this expansion.

The importance of *eya1* in the development of the inner ear has been extensively reported in amniotes and anamniotes (Bonini, Leiserson and Senzer, 1993; Abdelhak *et al.*, 1997; Kozlowski *et al.*, 2005; Xu and Xu, 2015). In zebrafish, the *eya1* mutation has been linked to a severe inner ear phenotype that is characterised by malformation of all three semicircular canals and an overall smaller otic vesicle, as well as increased apoptosis. In addition, *eya1*

mutants do not form any of the three cristae (Whitfield *et al.*, 1996; Kozlowski *et al.*, 2005), which have been proposed to be the source of signalling information required to form the non-sensory pillar structure (Chang, 2004; Bok, Chang and Wu, 2007). When combined, this knowledge regarding the *eya1* phenotype and the fact that the mutants show an expanded expression of *otx1*, raises several questions:

- Is enhanced apoptosis causing the cells to die ahead of ventral pillar formation?
- If a ventral pillar develops, in the *eya1* mutants, how does its phenotype correlate with the expression of *otx1*?
- Are there other genetic repercussions of *eya1* mutation that can affect ventral pillar development?

This chapter is intended to provide further understanding of the phenotypical and genetic outcomes of this mutation, with particular emphasis on the ventral pillar development. This was achieved by imaging *eya1*^{to15b} mutants in a Tg(*mir137::EGFP;xEF1a::H2B-RFP*) background, which allowed the visualisation of the ventral pillar phenotype, and by WISH to assess the consequences of *eya1* mutation on gene expression in the otic vesicle.

5.2. *eya1* mutants develop a misshapen ventral pillar

The first question I decided to address when I started analysing the *eya1* mutants was related to the phenotype elicited by this mutation. It is important to remember that these mutants show enhanced apoptosis in the otic vesicle (Kozlowski et al. 2005), which could prevent the development of the ventral pillar.

I analysed the phenotype arisen by the *eya1* mutation by crossing the *eya1*^{to15b} heterozygous with the Tg(*mir137::EGFP;xEF1a::H2B-RFP*) line. The reason for choosing this allele lies in the fact that, at that time, the fish carrying the *eya1*^{tm90b} or the *eya1*^{tp85b} mutations were not providing a viable progeny and no difference was observed between these three alleles in terms of phenotype arisen (Whitfield *et al.*, 1996; Kozlowski *et al.*, 2005). However, since the *eya1*^{tm90b} mutants have the advantage that they can be screened for the mutation using a PCR and digestion assay (see section 2.2.2), I also crossed this allele with the Tg(*mir137::EGFP;xEF1a::H2B-RFP*) line and compared their phenotype with that of the *eya1*^{to15b} allele.

As the *eya1* mutants are not adult viable (Whitfield *et al.*, 1996; Kozlowski *et al.*, 2005), the mutant phenotype was evaluated in the fraction (25%) resulting from incrossing two heterozygous fish. Fluorescent imaging revealed that, at

72 hpf, the *eya1*$^{to15b/to15b}$ mutants develop an inner ear phenotype consisting of a misshapen ventral pillar (Figure 5.1, 5.2 and Figure S1-S2). In terms of shape of the pillar, this is variable among mutants derived from the same parents, though they all share some important characteristics. The GFP-positive cells, forming the projection first and then the pillar, are not highly organised as in the wild type (see sections 3.3), but are more dispersed on the anteroposterior and mediolateral axis of the pillar (Figure 5.1, 5.2 and Figure S1-S2).

Another important characteristic of these mutants is that they have been described not to develop any of the cristae (Whitfield *et al.*, 1996). In section 3.2, it has been shown that the Tg(*mir137::EGFP;xEF1a::H2B-RFP*) line exhibit green fluorescent also in the three cristae. In the *eya1* mutants, it is interesting to notice that GFP-positive cells that contribute to the formation of the pillar can also be found in a very posterior region of the otic vesicle, which is close to the domain where the posterior crista should be (Figure 5.1). These characteristics are common to both the *eya1*$^{to15b/to15b}$ and the *eya1*$^{tm90b/tm90b}$ mutants. For these experiments, three *eya1*$^{to15b/to15b}$ and three *eya1*$^{tm90b/tm90b}$ (one otic vesicle for each embryo) have been imaged using light-sheet microscopy.

5.3. *eya1* siblings are morphologically indistinguishable from wild types

Previous publications have shown that the *eya1* siblings are morphologically indistinguishable from wild-type embryos (Whitfield *et al.*, 1996; Kozlowski *et al.*, 2005). This was tested in greater detail using the Tg(*mir137::EGFP;xEF1a::H2B-RFP*). In accordance with previous observations, I could not distinguish wild-type and heterozygous siblings, based on the general ventral pillar morphology. To further confirm this and provide a control for the imaging of the *eya1* mutant phenotype (see section 5.2), three *eya1* siblings (one otic vesicle for each embryo) were imaged between 48 and 72 hpf.

These embryos did not exhibit substantial differences compared to the wild-type embryos (described in section 3.3). The ventral projection forms from a more medial domain of the otic vesicle, while the bulge is more lateral (Figure 5.3 A-B and Figure S1-S2). Upon fusion, the ventral projection lines up with the bulge and forms a pillar made up by only GFP-positive cells (Figure 5.3 A-B and Figure S1-S2). Interestingly, in one out of three embryos, a very peculiar cell behaviour was observed. During the fusion event, starting around 58.5 hpf, a single GFP-positive cell detached from the rest of the its population

and invaded the GFP-negative domain, where it remained for almost 4 hours before dying (Figure 5.4). As the embryo was not genotyped, I am unable to tell whether this behaviour was observed in a wild-type or a heterozygous sibling. Therefore, it would be interesting to image a higher number of *eya1* siblings, genotype them afterwards and investigate whether this cell behaviour correlates with a specific genotype.

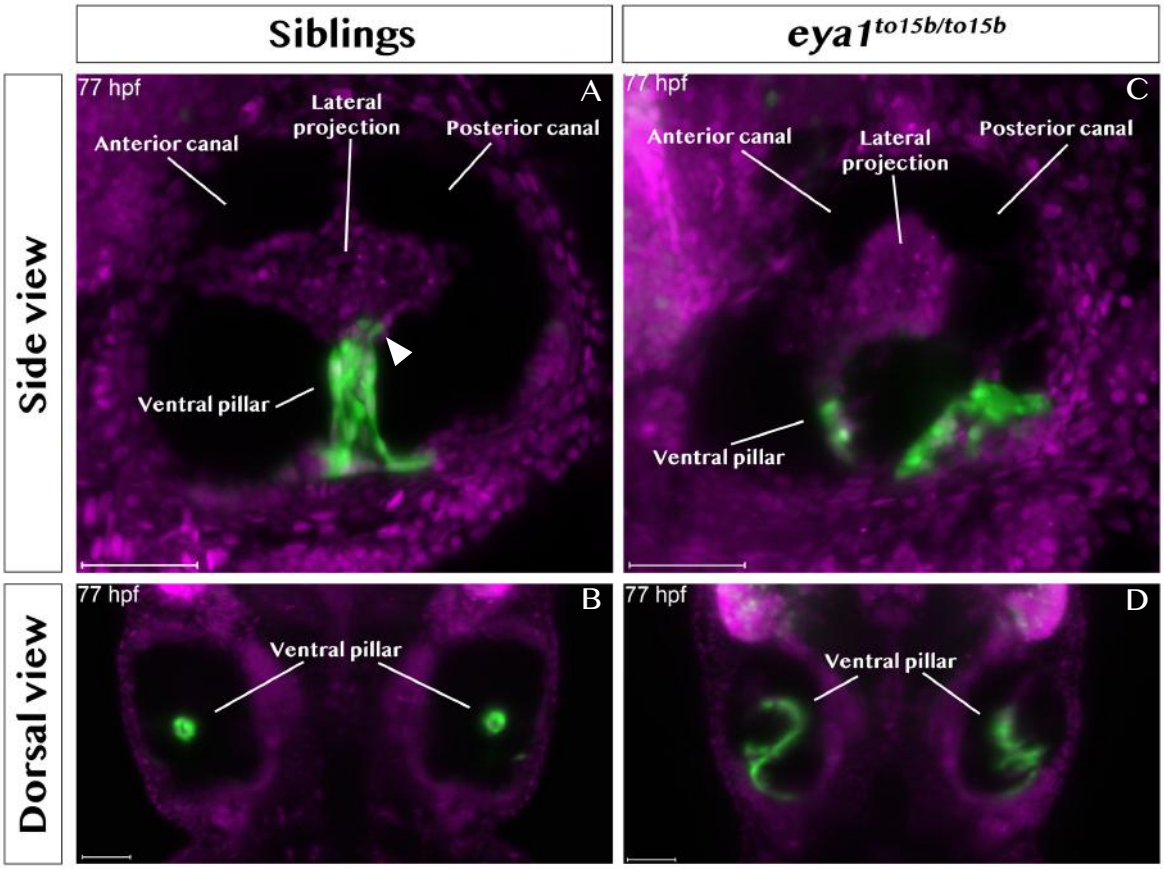

Figure 5.1. Pictures showing an *eya1* mutant and sibling at 77 hpf. All images are maximum intensity projections focused on the ventral pillar. (A-C) In the *eya1* siblings the pillar shows its typical cylindrical shape. Figure A also shows two GFP-positive cells (arrowheads) mixing with the GFP-negative cells. (B-D) The *eya1* mutant develop a misshapen pillar that extends towards a more medial domain of the otic vesicle. Scale bar for side views, 50 μm. Scale bar for dorsal views, 20 μm.

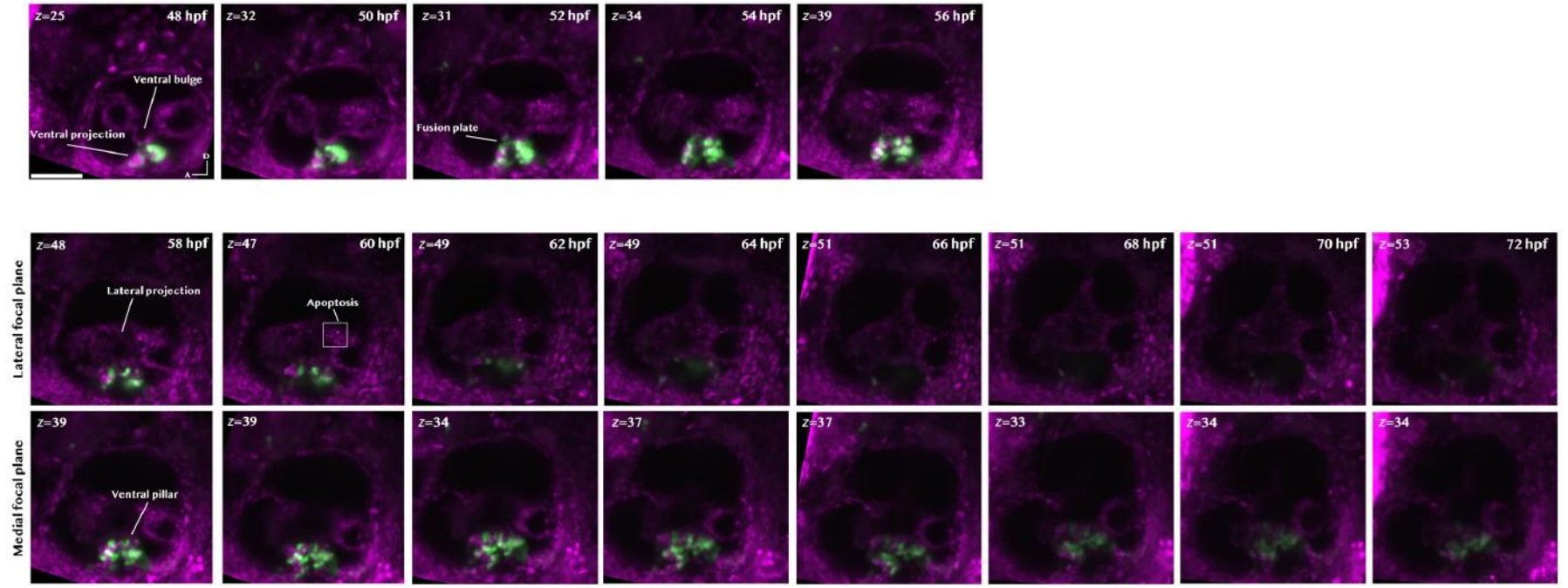

Figure 5.2 (A). Time-lapse imaging of the ventral pillar development of an *eya1*$^{to15b/to15b}$ mutant. Each frame is a maximum intensity projection of 2 to 5 *z*-stacks around the stack indicated in the figures. Between 48 and 56 hpf the projection and bulge lie on the same plane, due to the mutant ear being smaller on the lateromedial plane. Between 58 and 72 hpf, the projections cells (highlighted in the bottom row) remain more medial than the bulge cells (highlighted in the top row). During all the time-lapse, the ventral projection is composed by a mix of GFP-positive and negative cells. Brightness and contrast have been kept constant throughout the movie and the dimming in the intensity of the red and green fluorescence is most likely due to the enhanced apoptosis in the otic vesicle and the thickening of the skin caused by the development of the embryo. Scale bar, 50 μm.

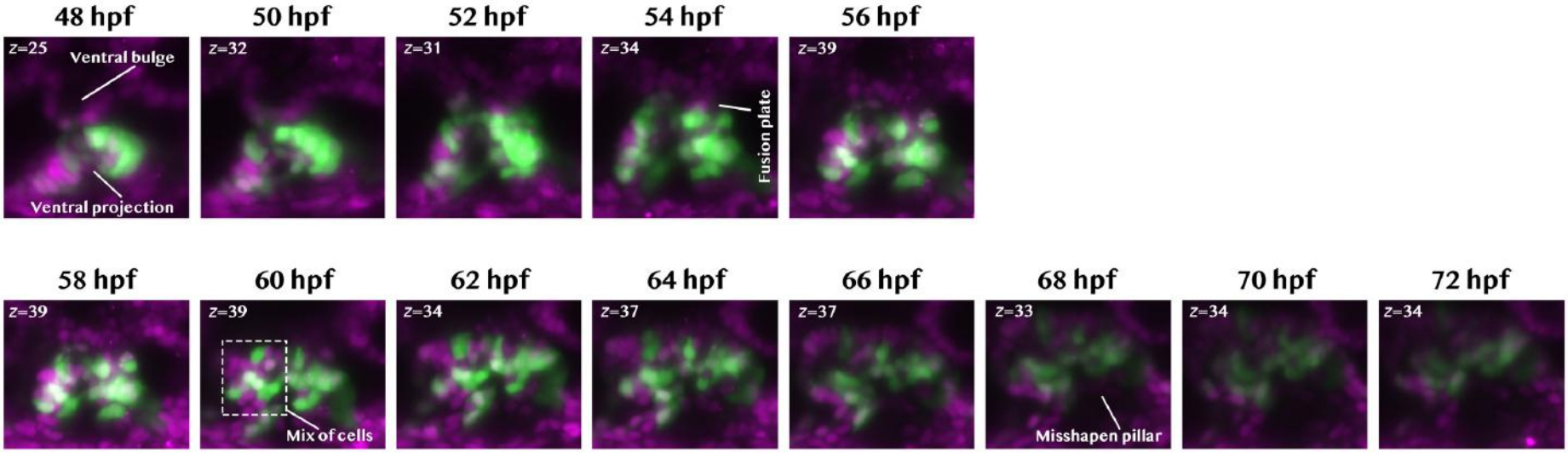

Figure 5.2 (B). Magnification of ventral pillar and bulge development in the *eya1* mutant from Figure 5.2 (A). The magnification focuses on the ventral bulge and projection development, which are visible on the same focal plane. The dashed square at 60 hpf highlights the fact that the ventral pillar is composed by a mix of GFP-positive and negative cells.

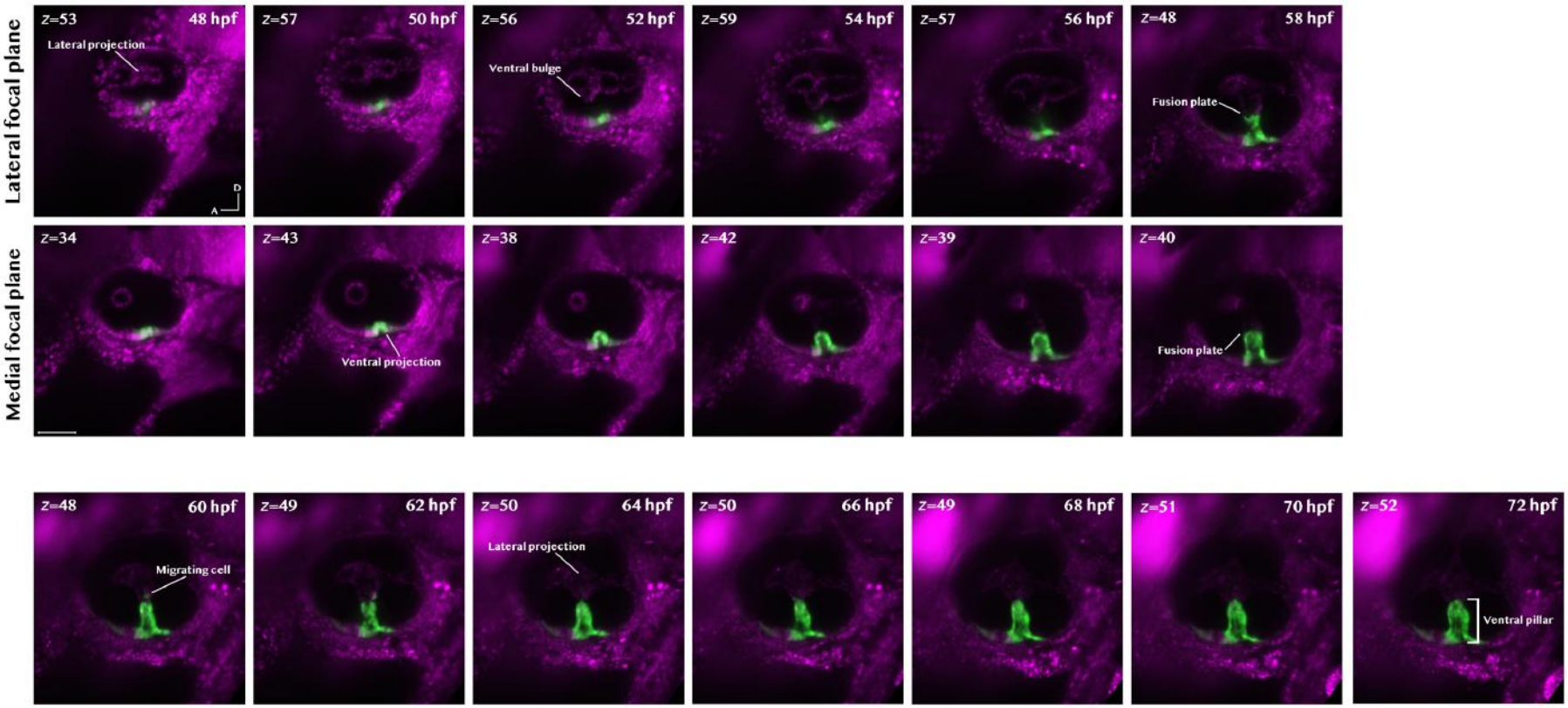

Figure 5.3 (A). Time-lapse of the ventral pillar development in an *eya1* sibling. Each frame is a maximum intensity projection of 2 to 5 *z*-stacks around the stack indicated in the picture. Between 48 and 58 hpf, the ventral bulge (top row) lies in a more lateral domain of the otic vesicle, while the ventral projection (bottom row) is more medial. From 60 hpf to 72 hpf, the ventral projection lines up with the bulge and the focal plane becomes the same. At these stages, the focus of the pictures was kept to the ventral pillar. The cells populating the ventral projection are GPF-positive and no GFP-negative cell was detected. A single GFP-positive cell detaching from the ventral projection can be observed in the 60 and 62 hpf frames. This behaviour will be described in greater detail in Figure 5.4. Scale bar 50 μm.

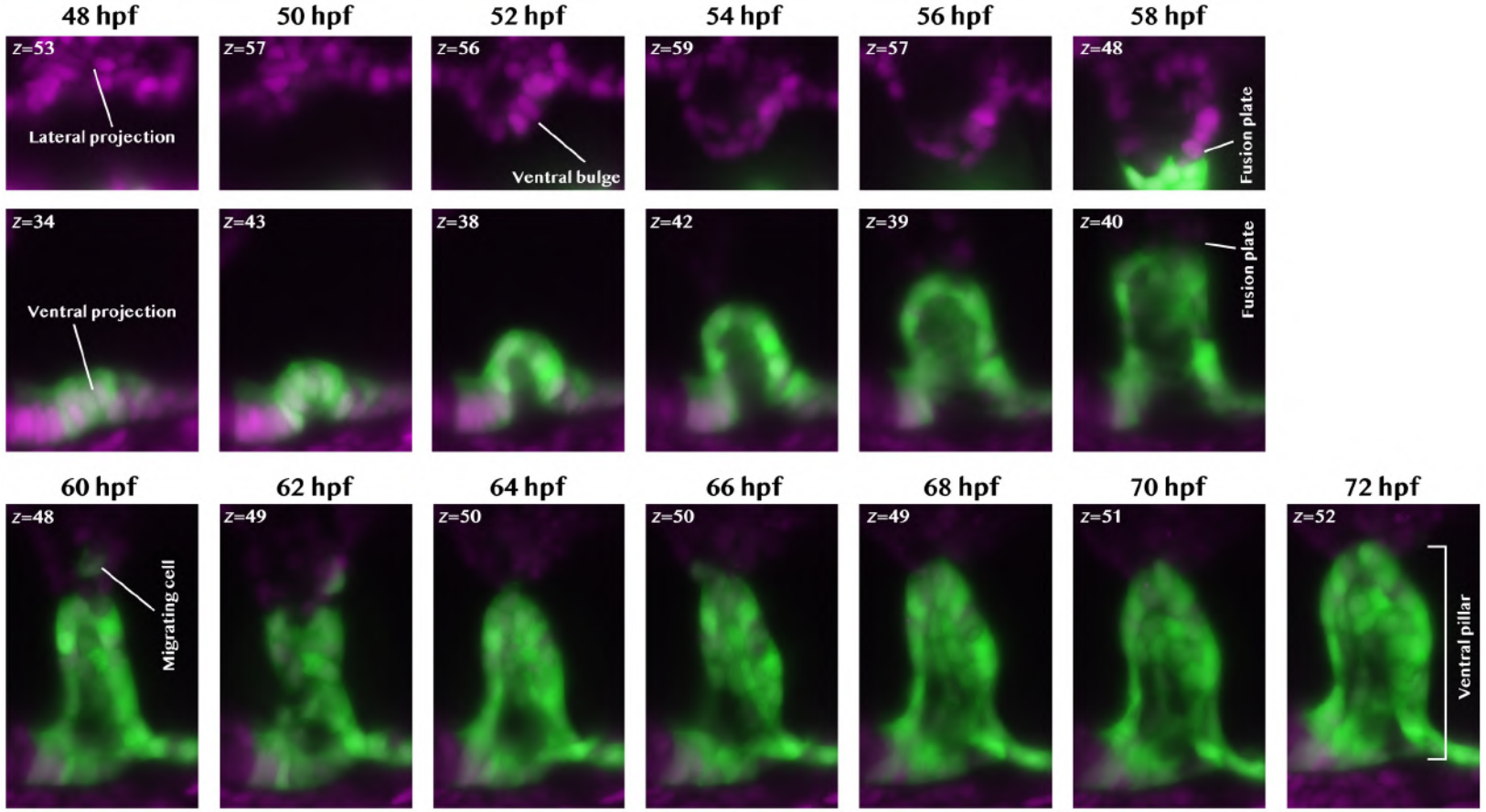

Figure 5.3 (B). Magnification of ventral pillar and bulge development in the *eya1* sibling from Figure 5.3 (A). The magnification focuses on the ventral bulge (top row) and projection (bottom row) development. The single migrating cell highlighted in the 60 hpf time-point is the same cell whose complete movement is shown in Figure 5.4.

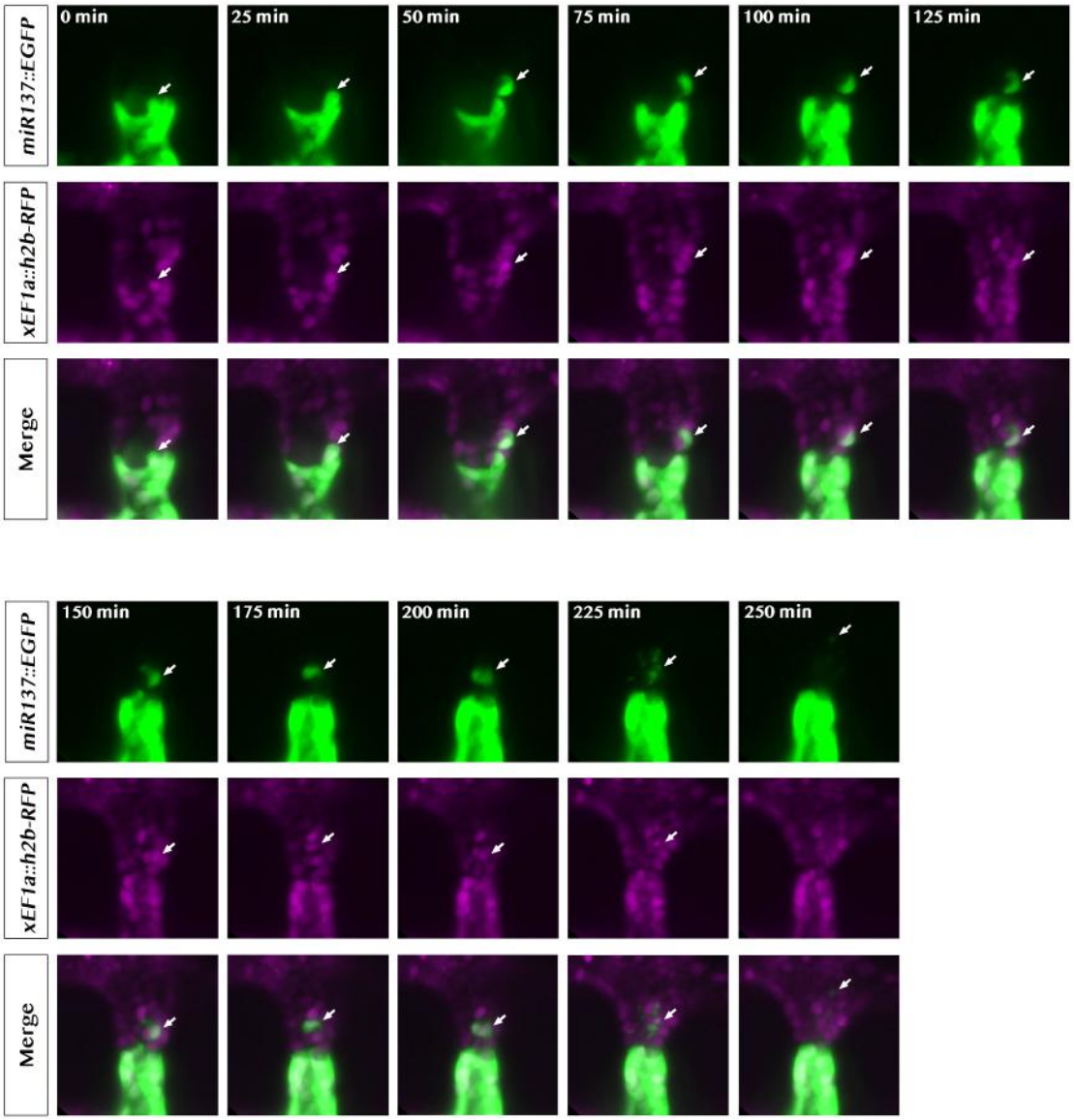

Figure 5.4. Time-lapse showing a single GFP-positive cell (arrow) detaching from its population and invading the GFP-negative domain before dying. The cell death event can be observed thanks to the presence of GFP-positive and negative particles, which become detectable 225 minutes after the start of the migratory behaviour. These particles are, then, cleared out within the following 25 minutes. This behaviour was observed in one time-lapse recording of an *eya1* sibling. The first time-point (0 min) corresponds to 58.5 hpf.

5.4. The ventral pillar of the *eya1* mutants is composed by a mix of cells

In section 3.2, it has been shown that the ventral pillar of wild-type embryos is made up by only GFP-positive cells and that the ventral projection starts to emerge around 52 hpf from a very restricted region of the ventral otic epithelium. In the *eya1* mutants, the ventral pillar is composed of a mix of GFP-positive and GFP-negative cells (Figure 5.2 A-B). This raised the question as to whether this was due to the ventral bulge and projection cells improperly mixing after fusion or if a mix of cells was already present, before the fusion event, in the bulge or projection. To test these hypotheses, I imaged the ventral pillar development in the *eya1* mutants between 48 and 72 hpf. This highlighted that, at 48 hpf, these embryos showed signs of early outgrowth of the projection and that this is already made up by a mix of GFP-positive and GFP-negative cells (Figure 5.2 A-B).

As for the ventral bulge, it is only made up by GFP-negative cells, as in the wild-type siblings. The fusion between the ventral projection and bulge happens earlier than in the sibling (around 54 hpf; Figure 5.2 A-B), but it has to be considered that the overall otic vesicle is smaller in the mutants and,

therefore, the projection and bulge cells travel a shorter distance before they can meet, which could account for the early fusion event.

5.4.1. Disadvantages of light-sheet microscopy for cell counting

The fact that the mutant ventral projection presents both GFP-positive and GFP-negative cells does not indicate whether there are more cells contributing to pillar formation, compared to the siblings. Thus, an attempt was made to count the number of GFP-positive and negative cells in both mutants and siblings using Arivis Vision4D. However, this proved to be challenging for several reasons: a) the images produced by the light-sheet microscope have a resolution which is too low to distinguish between neighbouring cells (see section 2.7.2.2); b) the ventral projection and bulge are structures where the cells are very dense, which makes it even more difficult for the software to distinguish them; c) the mutation of *eya1* is characterised by enhanced cell death (Whitfield *et al.*, 1996; Kozlowski *et al.*, 2005), which causes the production of debris that is often counted as a cell from the software, even if the diameter is smaller.

The approach adopted was to instruct Arivis Vision4D to count the number of RFP-positive nuclei (which includes both GFP-positive and negative cells), the number of GFP-positive cells and, finally, check in how many cases the RFP

colocalised with the GFP. To count one RFP-positive nucleus, the software selects the brightest RFP-positive pixel and then considers the other surrounding RFP-positive pixels as part of the same structure until it encounters a black pixel, which is considered the end of the nucleus. In the case of light-sheet images, the nuclei are not completely separated one from the other from a black background and, as a result, several nuclei are counted as one. In some cases, the intensity of the RFP signal is too low, resulting in many nuclei not being counted. As for the cytoplasmic GFP signal, the boundaries between each cell are not visible and neighbour cells are counted as one.

To overcome these problems, I took advantage of an Airyscan light-sheet microscope (see section 2.7.3) to obtain a high-resolution picture of the inner ear of an *eya1* mutant at 48 hpf (Figure 5.5). However, the resolution of this microscope proved to be too high for Arivis Vision4D to provide an accurate cell count. In this case, the problem resides in the fact that the resolution in so high that the nuclear RFP signal exhibits dark spots due to the presence of DNA. Therefore, when the software selects the brightest RFP-positive pixel and seeks for the surrounding RFP-positive pixels, it encounters black pixels, which are considered as background, resulting in one nucleus possibly being

counted as two. With respect to the GFP signal, the problems encountered were the same described above in this section for light-sheet images.

Finally, in the *eya1* mutants, the enhanced cell death results in the presence of debris, which appear as bright RFP or GFP-positive spots in the image (Figure 5.5). These are considered by the software as pixels to be counted as part of a nucleus (RFP-positive pixels) or cell (GFP-positive pixels). An attempt was made to set a limit for the diameter of the structure to be considered as a nucleus or cell, so that everything that had a diameter lower than 6 μm was discarded. However, in the case of the Airyscan image, this caused the software to also discard nuclei that were considered smaller than 6 μm in diameter due to the presence of black pixels inside the nuclei. For all these reasons, more experiments are required to provide an accurate count of the cells involved in pillar formation in the *eya1* mutants.

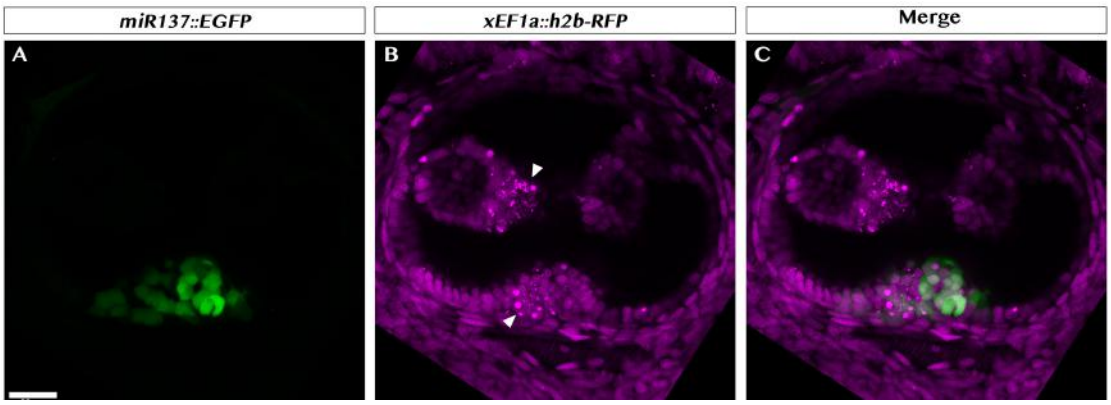

Figure 5.5. Airyscan image of an *eya1*$^{tm90b/tm90b}$ mutant. The picture is presented as a maximum intensity projection focused on the ventral projection, which comprised both GFP-positive and negative cells. Arrowheads in figure B indicate the bright RFP-positive spots caused by the enhanced cell death characterising this phenotype. Scale bar, 20 μm.

5.5. Gene expression analysis of *eya1* mutants

5.5.1. *otx1* and *gsc* are significantly expanded in the *eya1* mutants

The results of the phenotypical analysis of the *eya1* mutants raised many questions regarding gene expression modifications, resulting from this mutation, that could be linked to the misshapen ventral pillar phenotype.

In light of the fact that the mutation of *otx1* causes the complete loss of the ventral pillar (see section 4.1 and 4.2) and the mutation of *eya1* results in a misshapen pillar (see section 5.2), I tested whether there could be a correlation between the expression pattern of *otx1* and the *eya1*$^{tm90b/tm90b}$ phenotype. Previous unpublished work from our laboratory suggested that the expression of *otx1,* as well as other markers of the ventral otic epithelium, was expanded in the *eya1* mutants (Giuliani, G. and Blanco-Sánchez, B. unpublished data). I repeated these experiments and calculated the entity of this extension as further confirmation. For these experiments, embryos at 24 hpf were screened for the mutant phenotype ahead of WISH (Figure 5.6).

I was able to confirm that *otx1* expression is expanded in a more anterior domain in the *eya1* mutant vesicle (Figure 5.6 A and B). As for *gsc*, its expression is also expanded in the *eya1* mutants but it is difficult to establish whether it expands towards the anterior or posterior domain (Figure 5.6 E and F).

Moreover, since *otx2a* is expressed in a region of the ventral otic epithelium that overlaps with *otx1* and its expression is completely lost in the *otx1* mutants, I tested the repercussions of *eya1* mutation also on *otx2a* expression. Interestingly, also *otx2a* expression was significantly expanded in the *eya1* mutants (Figure 5.6 C and D). This is in line with previous unpublished work showing that both *otx1* and *otx2a* are expanded in the ventral otic epithelium of the *eya1* mutants (Giuliani, G., PhD thesis). To further confirm these data, I measured the entity of the expansion in both the siblings and mutants (Figure 5.6 I).

Due to the fact that the shape and size of the otic vesicle could be affected by fixation and staining protocols, the measurements were normalised to the size of the ear and represented as the percentage of the vesicle occupied by the staining (see section 2.8.1). This was achieved by imaging both the left and right ear of 14 mutants and 14 siblings each stained for *otx1* and *gsc* and 10 mutants and 10 siblings stained for *otx2a*. The results show that the expansion of *otx1*, *otx2a* and *gsc* in the *eya1* mutants is statistically significant when compared to the siblings (Figure 5.6 I). However, the staining for *otx2a* will need to be repeated for further confirmation and to increase the sample size.

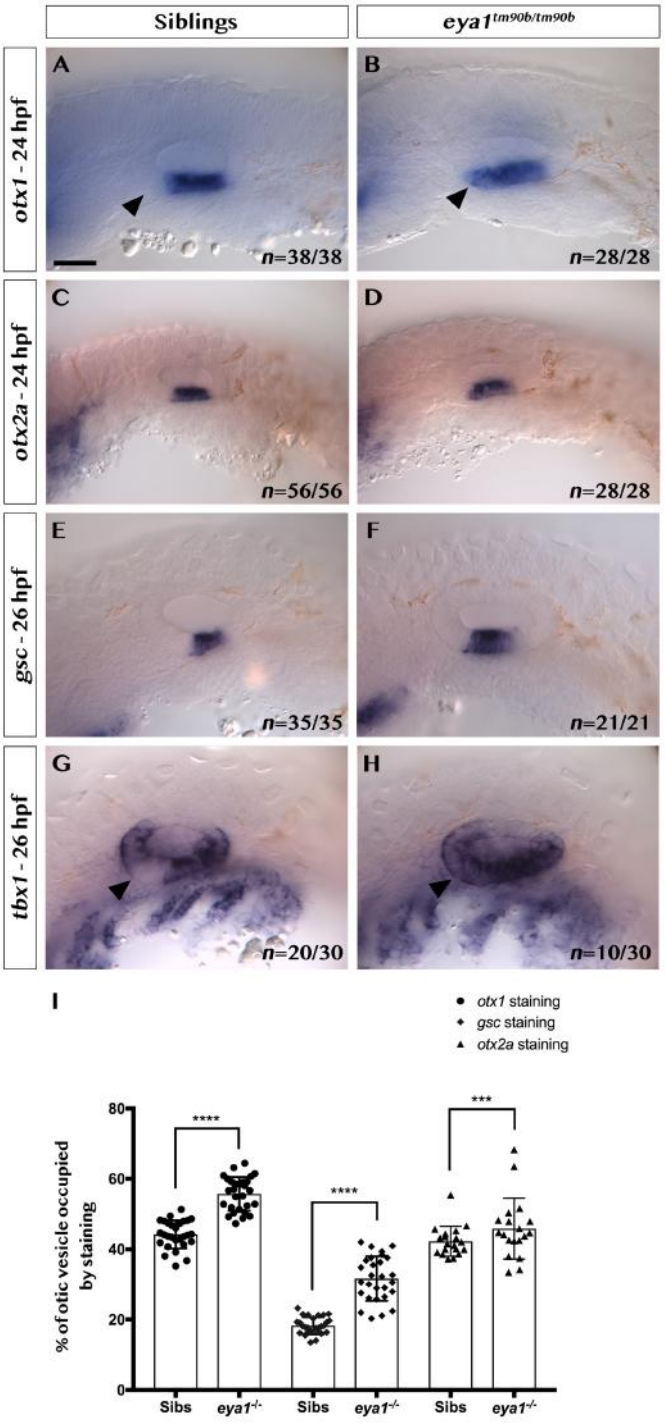

Figure 5.6. Whole mount *in situ* hybridisation panel of *eya1*^{tm90b} line showing a lateral view of each embryo, with anterior to the left. Wild-type sibling (A) and *eya1*$^{tm90b/tm90b}$ mutant (B) stained for *otx1* expression, which is expanded in the mutants (arrowhead). (C-D) Embryos stained for *otx2a* expression. The picture shows one representative embryo that appears much smaller compared to the other samples in the panel, even though it was imaged at the same magnification as the others (40x water immersion objective). The reason is due to the fact that these embryos were part of a batch of smaller embryos. This experiment will need retesting to further confirm the result. (E-F) Staining for *gsc*, which is expanded along the otic anteroposterior axis in the *eya1*$^{tm90b/tm90b}$ embryos. (G-H) *tbx1* staining on *eya1* mutants and siblings. Black arrowheads indicate the anteroventral region of the otic vesicle, corresponding to the prospective anterior macula, where *tbx1* is misexpressed in the mutants. These embryos were not screened for the mutation ahead of WISH. (I) D'Agostino and Pearson normality test was used on all populations. Student's *t*-test was performed on a total of 56 ears stained for *otx1* and *gsc* expression (right and left ear of 14 siblings and 14 mutants); for *otx2a*, a Kruskal-Wallis test was used, due to the population not having a normal distribution, and measurements were taken from a total of 38 ears (9 right ears and 10 left ears of 10 sibling and 10 mutants; one right ear for each population was discarded due to being damaged in the process). ****$p < 0.0001$; ***$p = 0.0004$. Error bars indicate SD. Scale bar, 50 μm.

5.5.2. The *eya1* mutation causes *tbx1* to be misexpressed in the prospective anterior macula

The correlation between the formation of a misshapen ventral pillar and the expansion of *otx1*, raised the question as to whether also *tbx1* expression could be affected in the *eya1* mutants. The mutation of *tbx1* has, indeed, been described to result in the formation of an otic vesicle lacking all three pillars (Piotrowski *et al.*, 2003). In line with this hypothesis, previous unpublished work suggested that the mutation of *eya1* results in the expansion of *tbx1* in the otic vesicle (Giuliani, G. and Blanco-Sánchez Bernardo, unpublished data). I confirmed these findings on 10 *eya1* mutants and 20 siblings, which, at 26 hpf, show an expansion of *tbx1* expression that extends to the anteroventral region of the otic vesicle (the prospective anterior macula) (Figure 5.6 G and H).

The fact that *tbx1* becomes expressed also in the anterior macula, coupled with the light-sheet data indicating that the ventral pillar is composed by a mix of GFP-positive and negative cells, could be an indication that, in the *eya1* mutants, more cells are becoming committed to become part of the ventral pillar. To further test this hypothesis, I analysed the expression of *vcanb*, a marker of the ECM expressed before the fusion between the projections and bulges of all three pillars (Geng *et al.*, 2013).

5.5.3. *vcanb* staining shows an expanded expression in *eya1* mutant ears

In section 4.4.2, it has been shown that, in the *otx1* mutants, *vcanb* is never expressed in the ventral otic epithelium. This, in addition to the other gene expression analyses carried out in these mutants, led me to hypothesise that, in these mutants, the cells of the ventral otic epithelium lose their commitment to become part of the ventral projection. Since in the *eya1* mutants, I observed opposite effects in terms of gene expression patterns and pillar phenotype, I decided to test whether also the expression of *vcanb* is affected by this mutation. To test this, WISH was performed at 60 hpf, due to this being a stage when the projection and bulge have developed but are not fused yet (Geng et al. 2013 and section 3.3).

At this stage, I observed that the expression of *vcanb* is expanded in the mutants, compared to that of wild-type siblings, and is expressed throughout the larger ventral projection (Figure 5.7). This result further supports the hypothesis that, in these mutants, more cells become improperly committed to give rise to the ventral pillar, leading to a misshapen structure composed by a mix of different cell populations.

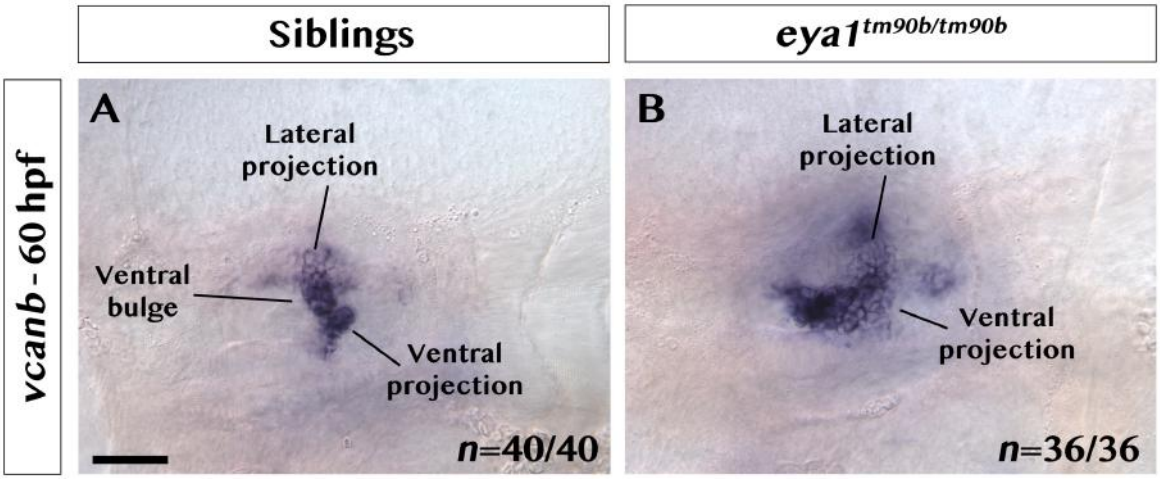

Figure 5.7. Analysis of *vcanb* expression, in *eya1* mutants and siblings, before the fusion between the ventral projection and bulge. In the mutants (B), the staining is expanded compared to the siblings (A). Scale bar, 50 μm.

5.5.4. *eya1* mutation causes the down regulation of *ngn1* and *neurod1* in the otic vesicle

In the sections above, it has been highlighted that the mutation of *eya1* results in the formation of a misshapen ventral pillar composed by a mix of cells and that this correlates with the expansion of *otx1*, *gsc*, *tbx1* and *vcanb* (sections 5.2 to 5.4.3). Previous work from our lab also suggested that, in the *eya1* mutants, the expression of *ngn1* and *neurod1* (formerly *neurod*) was downregulated (Blanco-Sánchez, B. unpublished data). These experiments were repeated to test the hypothesis that the expansion of markers of the ventral otic epithelium was affecting the expression of neural markers.

The expression of both *ngn1* and *neurod1* was tested at 26 hpf because, at this stage, they are found in precursor cells delaminating from the otic vesicle and forming the statoacoustic (VIII) ganglion (SAG), which will innervate the three cristae as well as the anterior and posterior maculae (Andermann, Ungos and Raible, 2002; Alsina and Whitfield, 2017; Hoijman *et al.*, 2017).

In line with previous observations, *eya1* mutants exhibit a strong downregulation of both *ngn1* and *neurod1* in the anteroventral domain of the otic vesicle, which has been described as the region from where precursor cells delaminate (Hoijman *et al.*, 2017) (Figure 5.8). The delamination of these cells and the expression of *ngn1* has been proposed to be controlled by FGF signalling (section 1.7, Hoijman et al. 2017), therefore, I decided to test whether the expression of *fgf* genes was also disrupted in the *eya1* mutants.

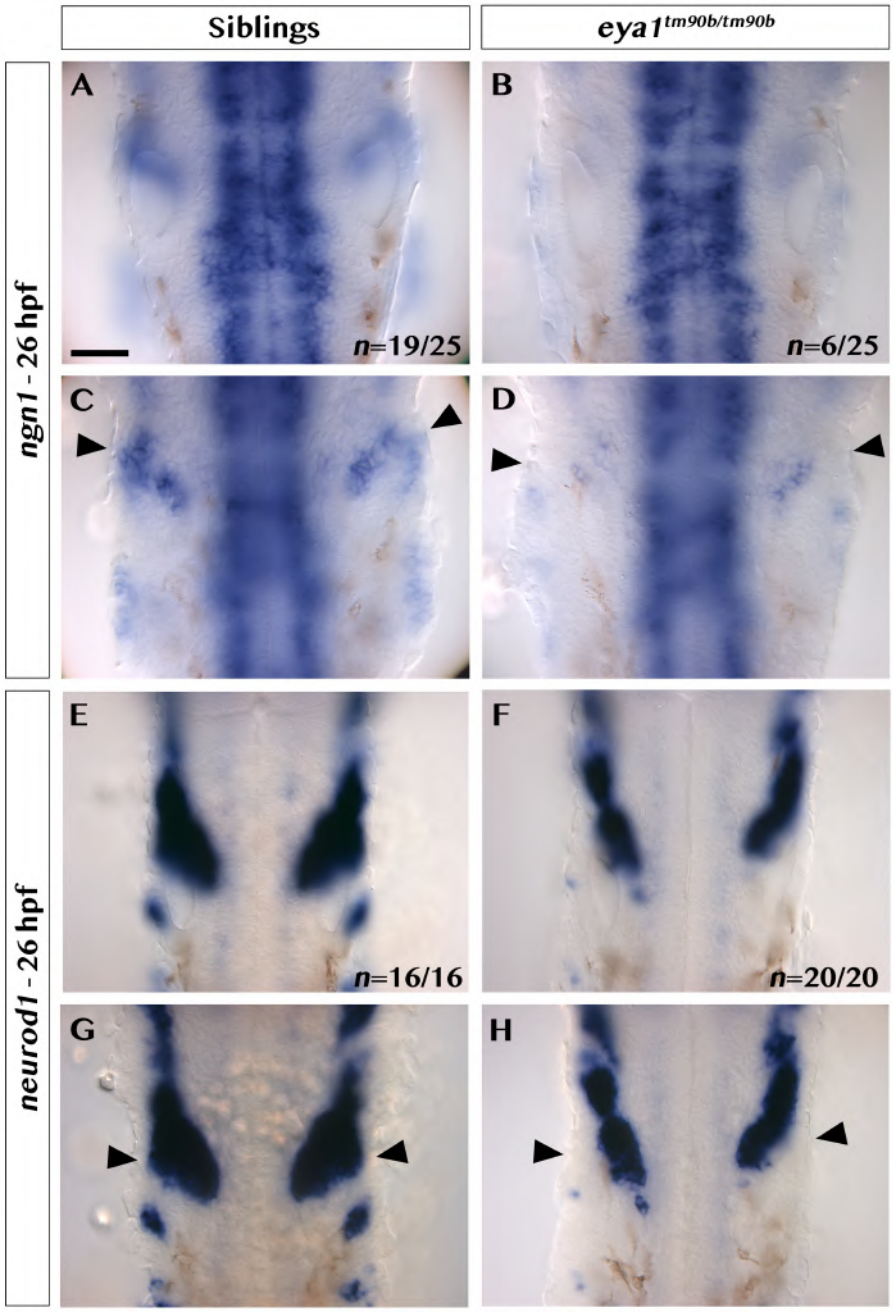

Figure 5.8. Analysis of *ngn1* and *neurod1* expression, in *eya1* mutants and siblings. A-B and E-F are dorsal views focusing on the outline of the otic vesicle. C-D and G-H are dorsal views of the same embryos focusing on a more ventral plane to highlight the expression patter respectively of *ngn1* and *neurod1*. (C-D) The expression of *ngn1* in the ventral floor of the otic vesicle (arrowheads) is almost completely lost in the mutants. For this experiment embryos were not screened for the mutation ahead of WISH. (G-H) In the mutants, *neurod1* expression (arrowheads) ablated in the ventrolateral otic vesicle. Scale bar, 50 μm.

5.5.5. *eya1* mutation causes *fgf3*, *8a* and *10a* expression to be downregulated in the otic vesicle

In sections 1.4.1 and 1.7, the FGF signalling has been described as a key player during placode induction and initiation of neurogenesis in the otic vesicle by controlling the expression of specific genes, such as *ngn1* and *eya1* (Léger and Brand, 2002; M. N. McCarroll *et al.*, 2012; Hoijman *et al.*, 2017). In light of the fact that *ngn1* and *neurod1* are downregulated in the *eya1* mutants, I tested whether this correlated with the disruption of expression of *fgf* genes. To test this, I analysed the expression of *fgf3*, *fgf8a* and *fgf10a*. The first two are known regulators of placode induction (see section 1.4.1), while *fgf10a* has been proposed to be required for the survival of cells forming the posterior crista (Ma and Zhang, 2015).

fgf3 expression in the anteroventral region of the vesicle is downregulated, but still detectable, in 18 out of 58 embryos tested (Figure 5.9 A to D). In a similar, but more severe, fashion, *fgf8a* expression is completely missing in the otic vesicle of 14 out of 60 embryos tested (Figure 5.9 E to H). Lastly, *fgf10a* expression is strongly reduced in the vesicle of 14 out of 55 embryos stained, to the point where it becomes barely detectable (Figure 5.9 I to L). All the WISH using *fgf3*, *8a* and *10a* probes were repeated twice and the numbers shown reflect the total of embryos tested in both experiments. For these assays,

embryos were obtained from a cross between heterozygous fish and not screened for the mutant phenotype ahead of staining.

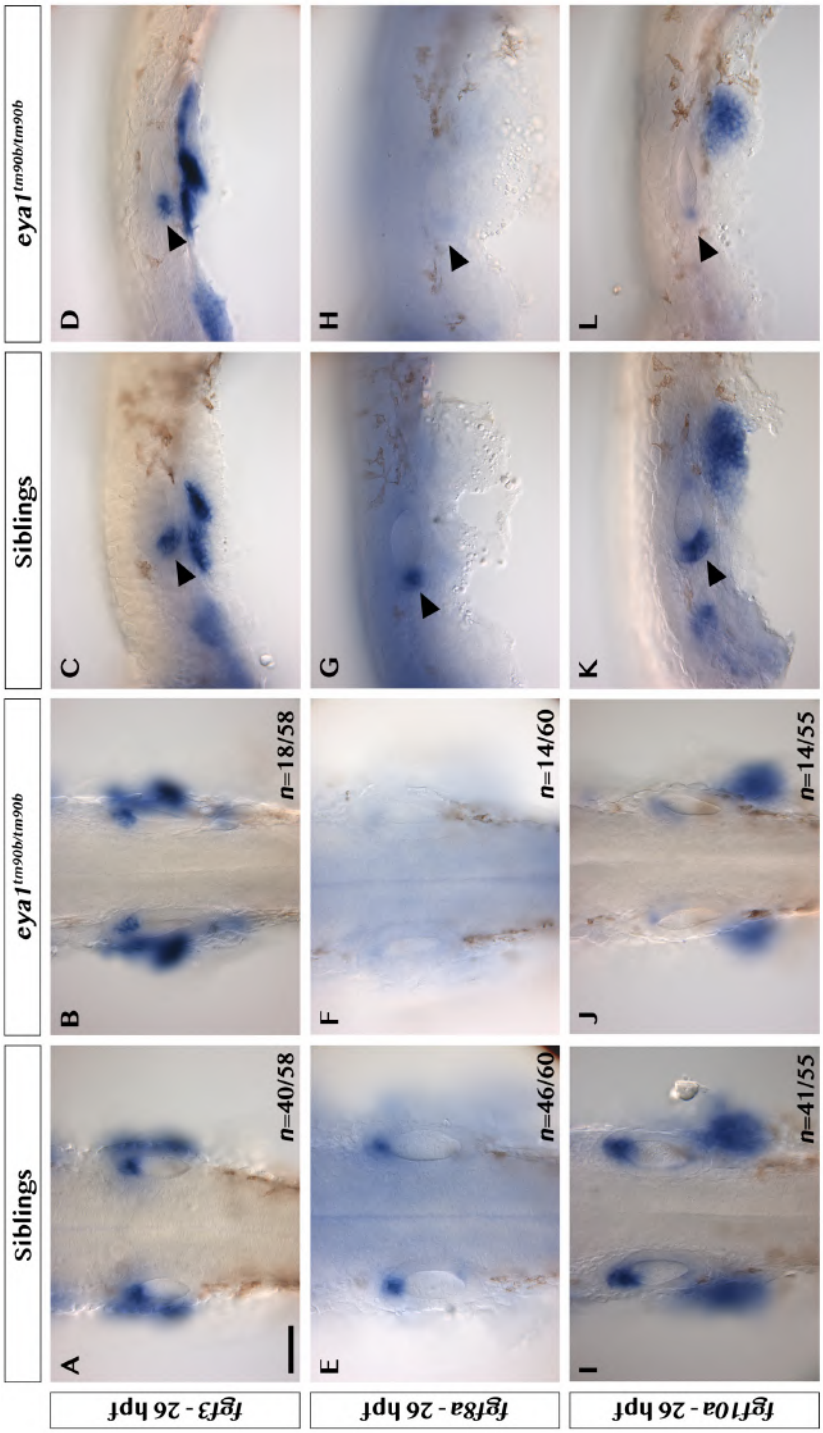

Figure 5.9. Expression analysis of *fgf3*, *8a* and *10a* in *eya1* mutants and siblings. In A-B, E-F and I-J are shown dorsal views highlighting the shape of the otic vesicle. C-D, G-H and K-L are side views of the same embryos (anterior to the left). For these experiments, embryos were not screened for the *eya1* phenotype ahead of WISH. Arrowheads highlight the expression of all genes in the otic vesicle of the siblings and the reduced, or missing, expression in the mutants. (A to D) *fgf3* expression is downregulated in the mutants compared to the siblings. (E to H) The expression of *fgf8a* is completely lost in the anterior otic vesicle. (I to L) *fgf10a* is strongly downregulated in the *eya1* mutants. Scale bar, 50 μm.

5.6. Discussion

This chapter is intended to provide more insights regarding the role of *eya1* in ventral pillar formation and its interaction with various genes involved in otic development. Since the mutation of *eya1* was described for the first time, the question about what was the ventral pillar phenotype has remained unanswered (Whitfield *et al.*, 1996; Kozlowski *et al.*, 2005). Here, I show that the projection and bulge cells contributing to pillar formation (Waterman & Bell 1984; Haddon & Lewis 1991 and sections 3.2 and 3.3) are still present in the *eya1* mutants, though they are misplaced and, therefore, do not give rise to the ordered structure seen in the wild-type siblings.

This is interesting if it is considered that this mutation has been associated with enhanced apoptosis both in mice and the zebrafish otic vesicle (Xu et al. 1999; Kozlowski et al. 2005; Xu & Xu 2015). Therefore, it would be reasonable to expect that these mutants could lack some structures in this region. Not only this is not the case for the ventral pillar, but the fact that the mutants exhibit a pillar made up by a mix of GFP-positive and negative cells suggests that possibly more cells than normal could be contributing to its development.

To this respect, the data shown in this chapter highlight that the mutation of *eya1* correlates with the expansion of *otx1* and the strong downregulation of

ngn1 and *neurod1*. This makes the *eya1* phenotype reciprocal to the *otx1* phenotype, where no ventral pillar can be observed by 72 hpf (Hammond & Whitfield 2006 and sections 4.2 and 4.3). As for *ngn1* and *neurod1*, they have been described to be key players in the delamination of neural precursor from the otic vesicle and it has also been shown that, in the mouse, their expression is controlled by the activity of *Tbx1* (Andermann, Ungos and Raible, 2002; Freyer and Morrow, 2010; Kantarci, Gerberding and Riley, 2016; Hoijman *et al.*, 2017). In the *eya1* mutants, *tbx1* becomes ectopically expressed in the prospective anterior macula, which is close to the domain where *ngn1* and *neurod1* are downregulated. Understanding whether the domain where *tbx1* is expanded overlaps with that where *ngn1* and *neurod1* are downregulated will need further testing. This will help to test whether the expansion of *tbx1* has a repercussion on the delamination of cells to form the statoacoustic ganglion, while inducing the expansion of *otx1*, therefore promoting a non-sensory cell fate at the expenses of a sensory fate. If this was true, it would mean that cells of the ventral otic epithelium become improperly committed to be part the ventral projection, also explaining the presence of a mix of GFP-positive and negative cells in this structure, that has not been observed in the siblings.

Nonetheless, it cannot be excluded that the loss of *ngn1* and *neurod1*, in these mutants, is a result of the enhanced apoptosis (Kozlowski *et al.*, 2005). If

this was the case, it would be reasonable to think that the expansion of *otx1*, promoted by the misexpression of *tbx1*, causes more cells to be committed to become part of the ventral pillar, regardless of the downregulation of *ngn1* and *neurod1*. This would explain the fact that, in the *eya1* mutants, the expansion of *gsc* expression correlates with the downregulation of these neural markers. In fact, it has been shown that the overexpression of *gsc* results in an increased amount of *ngn1*-expressing cells delaminating from the otic vesicle (Kantarci *et al.*, 2005). For all these reasons, more experiments will be required to test these hypotheses in greater detail and establish whether the pillar phenotype in the *eya1* mutants is a consequence of a change in cell fate or if it is independent from the loss of *ngn1* and *neurod1*.

In addition to that, it has to be considered the fact that the otic expression of *fgf* genes is also affected by the mutation of *eya1*. As previously mentioned, FGF signalling controls otic neurogenesis (Léger and Brand, 2002; M. N. McCarroll *et al.*, 2012; Hoijman *et al.*, 2017) and its depletion in the mutant otic vesicle, together with the expansion of *tbx1*, could account for the downregulation of *ngn1* and *neurod1*. However, more tests are required to establish the relation between *eya1* and the FGF pathway, as it has been described that the FGF signalling deriving from rhombomere 4 is responsible for maintaining the expression of *eya1* in the otic vesicle (Léger and Brand,

2002). Therefore, it will be interesting to establish whether there is a feedback loop between *eya1* and the members of FGF family that helps to maintain the expression of *fgf3*, *8a* and *10a* in the inner ear and whether, the downregulation of *ngn1* and *neurod1* is a direct consequence of the depletion of the FGF signalling in the otic vesicle.

Finally, in section 5.4.3, it has been shown that the expression *vcanb* is expanded, in the *eya1* mutants, as it is expressed throughout the bigger ventral projection compared to the siblings. It is well-established that the development of the projections is driven by the expression of proteoglycans and ECM components (Haddon and Lewis, 1991, 1996; Geng *et al.*, 2013). Therefore, it will be interesting to test at what stage the production of ECM components starts in these mutants, since it has been previously described that, in wild-type embryos, the development of the ventral projection starts around 52 hpf (Waterman and Bell, 1984; Haddon and Lewis, 1991), but I observed that the *eya1* mutants already exhibit cells protruding from the ventral otic epithelium at 48 hpf.

6. GENERAL DISCUSSION AND FUTURE WORKS

The development of the semicircular canals in the zebrafish inner ear is a remarkably complex process that involves a number of morphogenetic processes. These include the folding and fusion of epithelial projections to develop three pillars, which become the hub of the anterior, posterior and lateral semicircular canals within the first 72 hours of development (Waterman and Bell, 1984; Haddon and Lewis, 1996; Alsina and Whitfield, 2017).

The mechanisms underlying the epithelial folding and fusion have been subject to many studies in different model organisms. An example is the dorsal closure in the *Drosophila* embryo, where two sheets of epithelium need to meet and fuse to allow for the closure of the dorsal side of the developing embryo (Reed, Wilk and Lipshitz, 2001; Shen *et al.*, 2013). Similarly, palatal development has been described to require the formation and fusion of two opposing sheets of epithelium. In humans, a failure in this process results in the onset of cleft palate (Schutte and Murray, 1999; Li *et al.*, 2018). The advent of modern technology, such as light-sheet microscopy, has granted the scientific community with the possibility to study these processes in details

and further increase our knowledge regarding the mechanisms that regulate them.

In this respect, while several aspects of the pillar development in the zebrafish inner ear have been described, many questions remain unanswered. This study builds on previous knowledge regarding pillar formation and provides more insights regarding the cellular and genetic dynamics required to form the ventral pillar. There are two main reasons for choosing to study the ventral pillar development: a) it is thought to be the last to have evolved; b) it has been shown to be the most commonly affected by malformations of the inner ear (Sando, Takahara and Ogawa, 1984; Alsina and Whitfield, 2017).

In zebrafish, the formation of the ventral pillar is known to require the epithelial fusion between a ventral bulge and a ventral projection and the fusion has been proposed not to require cell death events unlike amniotes (Waterman and Bell, 1984; Martin and Swanson, 1993; Haddon and Lewis, 1996; Fekete *et al.*, 1997; Bever and Fekete, 1999). The data presented in this thesis confirm that few apoptotic events can be detected during the fusion event (see section 3.7), however, upon fusion, further steps take place. The cells of the ventral projection are, in fact, the only ones populating the pillar at 72 hpf and the lack of ventral bulge cells, at this stage, is not due to the cell death

events (Figure 6.1 A). Rather, this is due to the bulge cells retracting back into the lateral projection (see sections 3.3 and 3.4 and Figure 6.1 A).

This is interesting as it differentiates the pillar development form other models of epithelial fusion, such as the abovementioned dorsal closure in *Drosophila* and palate fusion in mouse, where the process resolves with the fusion of two epithelial sheets around a midline, without any of the two original cell population being the only one present in the dorsal region of the *Drosophila* embryo or in the palate afterwards (Shen *et al.*, 2013; Li *et al.*, 2018). At present, there are no indications as to whether this is the case also for the anterior and posterior pillars but, if that was confirmed, it would indicate that the purpose of the lateral projection is to provide the projections with an anchor point and the bulges are merely extensions needed to allow all three projections to align and fuse with the lateral projection.

Another important aspect to consider is the dynamism of these cells, which does not correlate with an epithelial state. These cells have, in fact, always been considered epithelial cells (Waterman and Bell, 1984), but their movements during pillar formation have never been investigated in detail. Here, I show that these cells exhibit specific movements consisting of cells exchanging neighbours by migrating towards the opposite population, and subsequently retracting back (see section 3.5). Epithelial cells were never

shown to exhibit these kinds of movement, which are more characteristic of a mesenchymal state (Revenu and Gilmour, 2009; Campbell and Casanova, 2016). It will be interesting to test whether this correlates with a change in the apico-basal polarity of these cells, as this would further confirm this hypothesis. An attempt to analyse the presence of cell-cell adhesion proteins has been made (Waterman and Bell, 1984), but a more in-depth study will be required to understand whether and how the position of junctional complexes changes between the extension, fusion and elongation phases.

This will be important to test also in the *eya1* and *otx1* siblings. The fact that, in one *eya1* sibling, a single cell was observed to detach from the GFP-positive population and migrate in the GFP-negative domain before dying (see section 5.3) could be an indication that, upon fusion, these cells gain a "more mesenchymal" state than the wild-type cells. Recently, in fact, the EMT has been described as a gradual process depending on various factors, including the relationship between cells and the ECM (Tseng *et al.*, 2012; Araya, Carmona-Fontaine and Clarke, 2016; Campbell and Casanova, 2016). It has, in fact, been described that ECM components can account for the positioning of junctional complexes between cells and that the formation of new cell-cell junctions can result in the production of a tensional force that could cause a cell to detach from the ECM (Tseng *et al.*, 2012). Conversely, the depletion of

the ECM components causes cells to migrate less and more slowly, both during inner ear and neural tube formation, but does not seem to impact cell polarity (Neuhauss *et al.*, 1996; Walsh and Stainier, 2001; Araya, Carmona-Fontaine and Clarke, 2016).

In the *eya1* mutants, the expression of *vcanb* is expanded and it correlates with the expanded expression of *tbx1*, *otx1*, *otx2a* and *gsc* (see section 5.5 and Figure 6.1 B and C). This might suggest that more cells than normal become committed to become part of the ventral projection and this results in more cells of the ventral otic epithelium producing ECM components, causing the formation of a misshapen pillar. More analysis will be needed to test whether these cells move faster or migrate for longer distances as this could be masked by the fact that the *eya1* mutants have been associated with enhanced cell death (Kozlowski *et al.*, 2005). However, the migration event observed in one of the siblings, might suggest that *eya1* heterozygous embryos could exhibit a mild abnormal phenotype consisting of cells with higher motility (possibly due to a higher production of ECM components) forming a morphologically wild-type ventral pillar. More experiments in a larger number of genotyped embryos will be required to test this hypothesis.

This notion regarding the fact that a misshapen pillar might form due to a larger number of cells of the ventral otic epithelium producing ECM

components is further strengthened by the fact that in the *otx1* mutants no *vcanb* expression was detectable in the ventral projection (see section 4.4 and Figure 6.1 C).

This suggests that the loss of *otx1* causes a lack of commitment, in the cells of the ventral otic epithelium, to give rise to a projection. At the same time, the *otx1* mutation does not affect the expression of both *eya1* and *tbx1* (see section 4.4), indicating that these could be involved in a network where *eya1* regulates *tbx1*, which promotes the expression of *otx1* (Figure 6.1 C). In this respect, more tests on double mutants will provide more details as to whether the activity of *otx1* is epistatic to that of *eya1* and *tbx1*, though it is important to consider that also the *tbx1* mutants (*van gogh*, *vgo*) lack the ventral pillar and crista while the *eya1* mutants exhibit a misshapen projection but no ventral crista. However, these mutations are not as specific to the ventral pillar as the *otx1* mutation, consistently with the expression pattern of these genes (Figure 6.1 B) (Whitfield *et al.*, 1996; Piotrowski *et al.*, 2003; Kozlowski *et al.*, 2005; Hammond and Whitfield, 2006). With respect to the activity of *otx2a* and *gsc* in the ventral pillar development, more tests will be required to test whether the *otx2a* and *gsc* mutations alone result in the loss of the pillar. Though, transcriptional analyses revealed both genes are lost on both the *otx1* morphants (Giuliani G., unpublished data) and mutants (see section 4.4).

The reason for hypothesising that the that the loss of the ventral pillar in the *otx1* mutant is due to the cells losing their commitment to become part of the projection resides in the fact that, in the light-sheet movies, no cell death events are detectable between 48 and 72 hpf (see section 4.3). However, it cannot be ruled out that this happens between 24 and 48 hpf. Conversely, in the *eya1* mutants, the question still remains as to whether the number of cells contributing to pillar formation is higher than in the siblings (see section 5.4). If there were more cells contributing to the ventral pillar development, it will be interesting to understand where are they located before the projection starts to form.

It is, indeed, important to consider that, in the *eya1* mutants, the pillar phenotype correlates with the expansion of *tbx1* and *otx1*, but also with the downregulation of *fgf3*, *8a* and *10a* and of the neural markers *ngn1* and *neurod1* (see section 5.5). The FGF pathway is a known regulator of neurogenesis through *ngn1* and *neurod1* (Andermann, Ungos and Raible, 2002; Freyer and Morrow, 2010; Kantarci, Gerberding and Riley, 2016; Hoijman *et al.*, 2017). This raises the question as to whether the *eya1* mutation could cause a fate switch, resulting in the cells of the ventral otic epithelium switching from a sensory to a non-sensory fate. The other possibility is that the lack of *ngn1* and *neurod1* expressing cells is caused by the enhanced apoptosis that characterises these

mutants (Kozlowski *et al.*, 2005). This would make the process of pillar formation independent from the neural specification linking *eya1* to two separate pathways: one that regulates *tbx1* and *otx1* for the formation of the pillar and the other that maintains the expression of *fgf3*, *8a* and *10a* in the otic vesicle to allow for neural specification.

Finally, more experiments will be required to provide clear evidence regarding the insertion of the *EGFP* enhancer trap construct, of the Tg(*mir137::EGFP*) line, upstream to the 5'UTR of *dpm3* (see section 3.8). A more in-depth analysis of the expression pattern of *dpm3* will help to understand whether it regulated the *EGFP* expression or if other regulatory elements are involved in the process. It is definitely interesting that the candidate insertion site is near to a gene coding for a mannosyltransferase, due to the importance of polysaccharides in the zebrafish inner ear formation as part of the ECM (Haddon and Lewis, 1991).

In conclusion, this study elucidates many aspects of the ventral pillar development and provides new insights with respect to the cell behaviour and genetics required for its formation. A better understanding of how such a complex process takes place will help to unravel the mechanisms underlying the epithelial fusion in other structures and organisms and better understand the genetic disorders resulting in diseases of the inner ear.

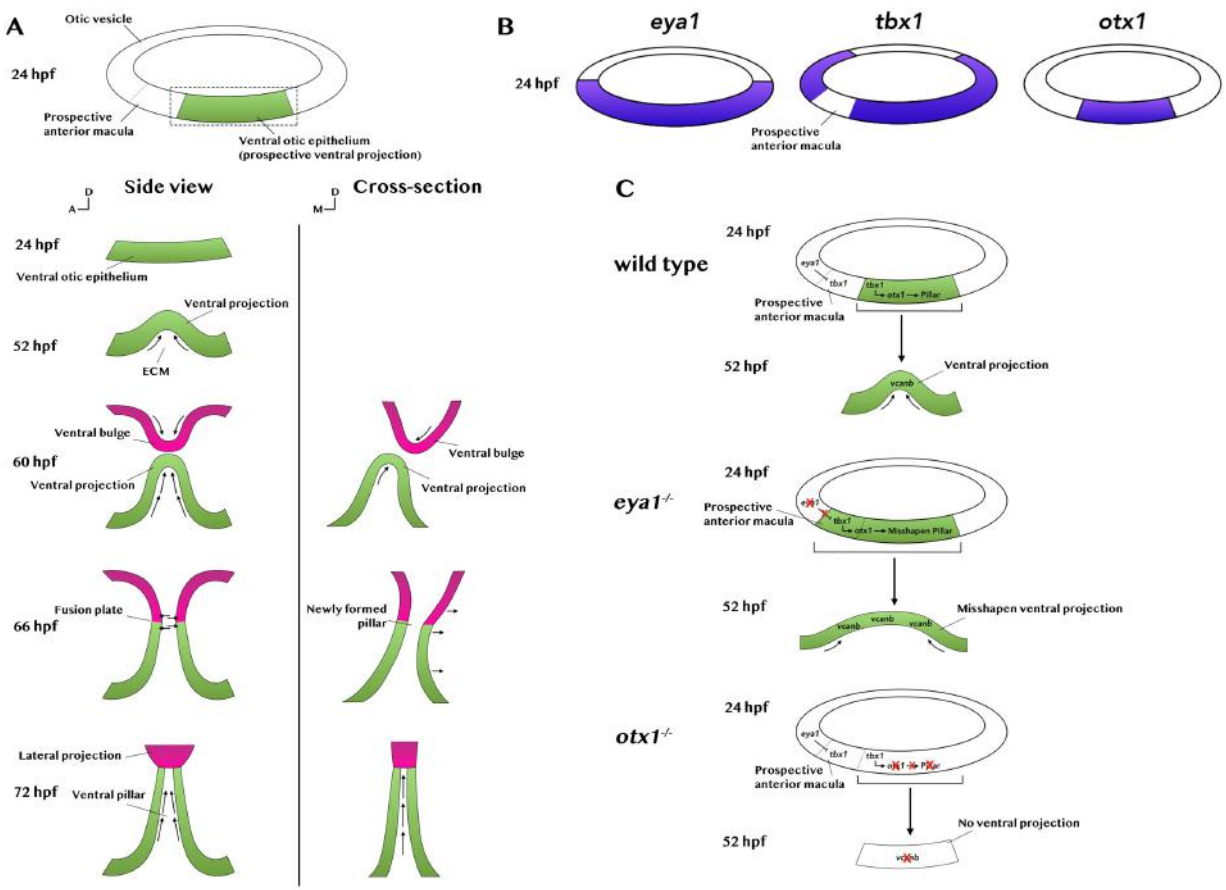

Figure 6.1. (A) Schematic representation of ventral pillar development between 48 and 72 hpf. Ventral projection and bulge are shown with a side view (anterior to the left) and as a cross section (medial to the left). The cross-section shows that the bulge sits on a more lateral focal plane compared to the projection and that the fusion happens at an angle. Arrows in (A) indicate the cell movement involved in pillar formation. (B) Otic expression of *eya1*, *tbx1* and *otx1* at 24 hpf. The expression of all three genes overlaps with the region of the ventral otic epithelium from which the ventral projection arises. (C) Hypothetical gene network regulating the correct development of the ventral pillar. *eya1* is required to inhibit the expression of *tbx1* in the anterior macula. When *eya1* is mutated, *tbx1* can promote the expression of *otx1* also in the prospective anterior macula, resulting in the development of a misshapen pillar. Conversely, when *otx1* is mutated the cells of the ventral otic epithelium lose their commitment to give rise to the ventral projection and do not express *vcanb*, resulting in the lack of ventral pillar.

7. SUPPLEMENTARY DATA

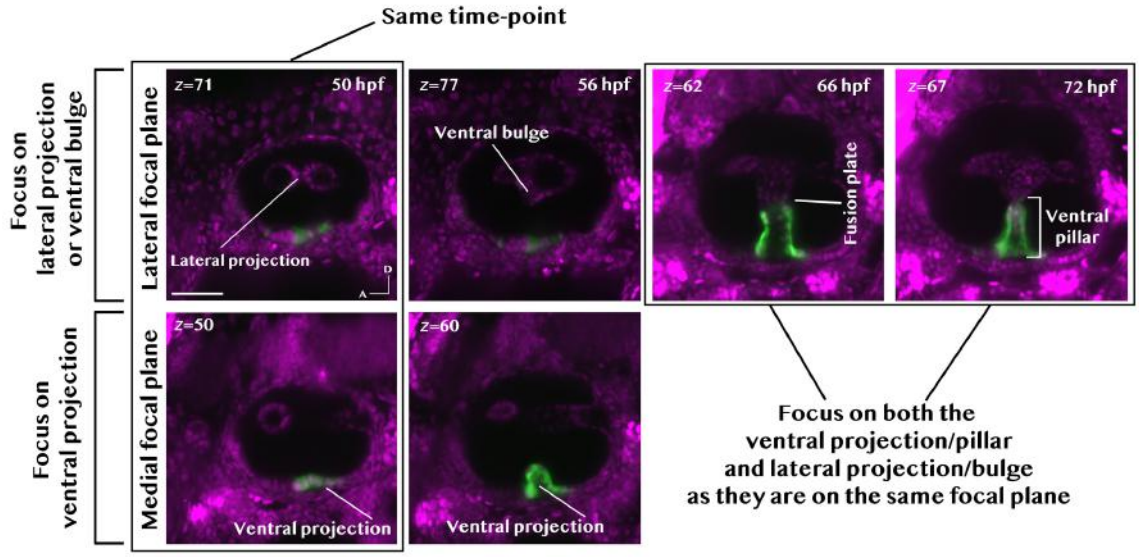

Supplementary Figure S1. Schematics showing how to read figures 3.2 (A), 4.2 (A), 4.3 (A), 5.2 (A) and 5.3 (A). To show both the ventral bulge and ventral projection development, the early stages of pillar formation have been divided into two focal planes: one more lateral (focused on the ventral bulge – top row) and one more medial (focused on the ventral projection – bottom row). In this figure the 50 and 56 hpf time-points are shown as an example. The later stages of pillar development show a single focal plane due to the fact that upon fusion, the newly formed ventral pillar and the ventral bulge are visible on the same focal plane (66 and 72 hpf are shown as an example).

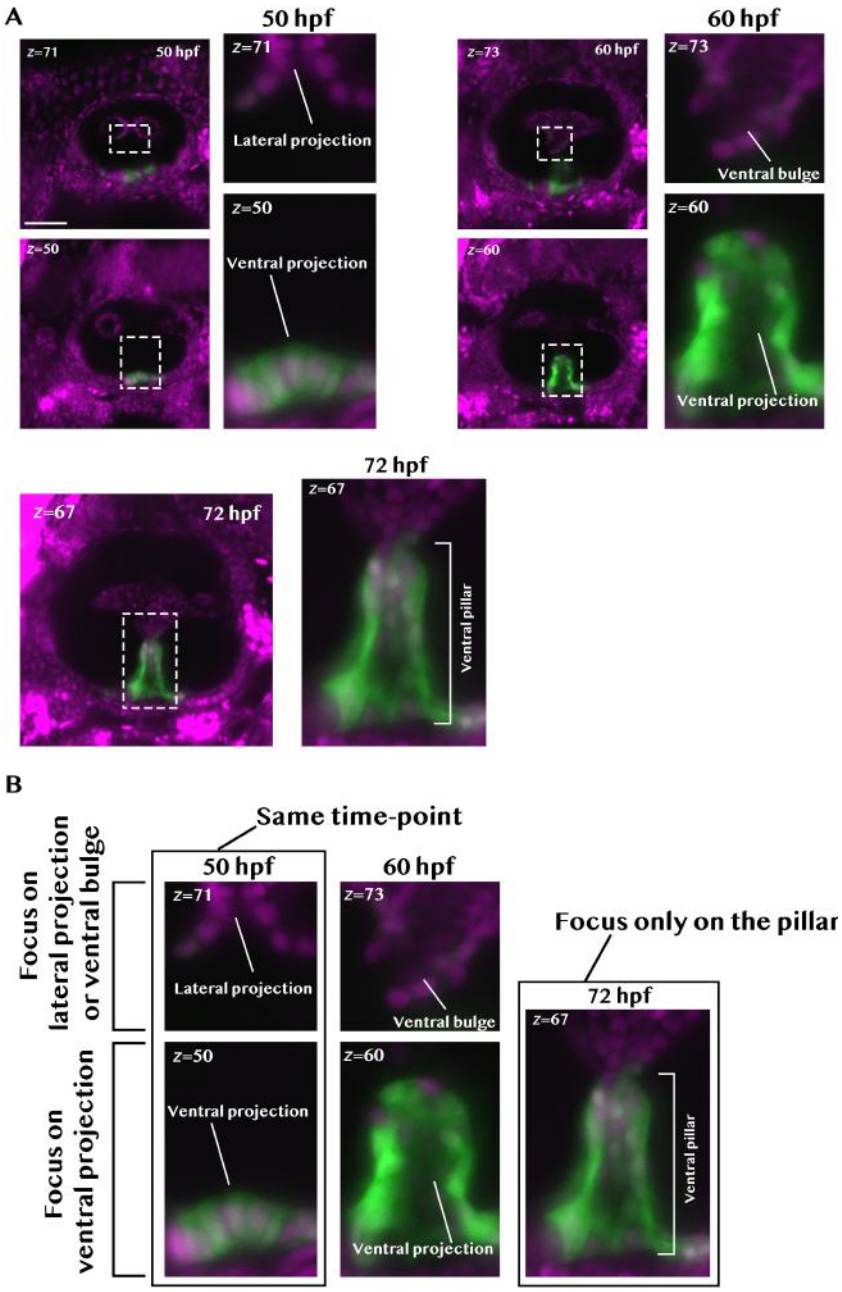

Supplementary Figure S2. Schematics showing how to read figures 3.2 (B), 4.2 (B), 4.3 (B), 5.2 (B) and 5.3 (B). Magnifications for each time-point were obtained by focusing on the region surrounding the lateral projection/ventral bulge and the ventral projection and cropping the image as indicated by the dashed square in (A). Time-points 50, 60 and 72 hpf are shown as an example. For early stages of pillar formation two separate focal planes were selected to highlight the ventral bulge (top row) and ventral projection (bottom row) development (B, 50 and 60 hpf). As for late stages of pillar development, a single focal plane that highlights both the pillar and lateral projection is shown due to them being detectable on the same plane (B, 72 hpf).

8. REFERENCES

- Abdelhak, S., Kalatzis, V., Heilig, R., Compain, S., Samson, D., Vincent, C., Weil, D., Cruaud, C., Sahly, I., Leibovici, M., Bitner-Glindzicz, M., Francis, M., Lacombe, D., Vigneron, J., Charachon, R., Boven, K., Bedbeder, P., Van Regemorter, N., Weissenbach, J. and Petit, C. (1997) 'A human homologue of the Drosophila eyes absent gene underlies branchio-oto-renal (BOR) syndrome and identifies a novel gene family.', *Nature Genetics*, 15(2), pp. 157–164.
- Acampora, D., Avantaggiato, V., Tuorto, F., Barone, P., Reichert, H., Finkelstein, R. and Simeone, A. (1998) 'Murine Otx1 and Drosophila otd genes share conserved genetic functions required in invertebrate and vertebrate brain development.', *Development*, 125(9), pp. 1691–1702.
- Acampora, D., Mazan, S., Avantaggiato, V., Barone, P., Tuorto, F., Lallemand, Y., Brûlet, P. and Simeone, A. (1996) 'Epilepsy and brain abnormalities in mice lacking the Otx1 gene.', *Nature Genetics*, 14(2), pp. 218–222.
- Acampora, D. and Simeone, A. (1999) 'Understanding the roles of Otx1 and Otx2 in the control of brain morphogenesis', *Trends in Neurosciences*, 22(3), pp. 116–122.

- Alsina, B. and Whitfield, T. T. (2017) 'Sculpting the labyrinth: Morphogenesis of the developing inner ear', *Seminars in Cell and Developmental Biology*. Elsevier Ltd, 65, pp. 47–59.
- Amores, A., Catchen, J., Ferrara, A., Fontenot, Q. and Postlethwait, J. H. (2011) 'Genome evolution and meiotic maps by massively parallel DNA sequencing: Spotted gar, an outgroup for the teleost genome duplication', *Genetics*, 188(4), pp. 799–808.
- Andermann, P., Ungos, J. and Raible, D. W. (2002) 'Neurogenin1 defines zebrafish cranial sensory ganglia precursors', *Developmental Biology*, 251(1), pp. 45–58.
- Araya, C., Carmona-Fontaine, C. and Clarke, J. D. W. (2016) 'Extracellular matrix couples the convergence movements of mesoderm and neural plate during the early stages of neurulation', *Developmental Dynamics*, 245(5), pp. 580–589.
- Bahri, S., Wang, S., Conder, R., Choy, J., Vlachos, S., Dong, K., Merino, C., Sigrist, S., Molnar, C., Yang, X., Manser, E. and Harden, N. (2010) 'The leading edge during dorsal closure as a model for epithelial plasticity: Pak is required for recruitment of the Scribble complex and septate junction formation', *Development*, 137, pp. 2023–2032.
- Bally-Cuif, L., Gulisano, M., Broccoli, V. and Boncinelli, E. (1995) 'C-Otx2 Is

Expressed in Two Different Phases of Gastrulation and Is Sensitive To Retinoic Acid Treatment in Chick Embryo', *Mechanisms of Development*, 49(1–2), pp. 49–63.

- Bellipanni, G., Murakami, T. and Weinberg, E. S. (2010) 'Molecular dissection of Otx1 functional domains in the zebrafish embryo', *Journal of Cellular Physiology*, 222(2), pp. 286–293.
- Bever, M. M. and Fekete, D. M. (1999) 'Ventromedial focus of cell death is absent during development of Xenopus and zebrafish inner ears.', *Journal of Neurocytology*. United States, 28(10–11), pp. 781–793.
- Bok, J., Chang, W. and Wu, D. K. (2007) 'Patterning and morphogenesis of the vertebrate inner ear', *International Journal of Developmental Biology*, pp. 521–533.
- Bonini, N. M., Leiserson, W. M. and Senzer, S. (1993) 'The eyes absent Gene : Genetic Control of Cell Survival and Differentiation in the Developping Drosophila Eye', *Cell*, 72, pp. 379–395.
- Borsani, G., DeGrandi, A., Ballabio, A., Bulfone, A., Bernard, L., Banfi, S., Gattuso, C., Mariani, M., Dixon, M., Donnai, D., Metcalfe, K., Winter, R., Robertson, M., Axton, R., Brown, A., van Heyningen, V. and Hanson, I. (1999) 'EYA4, a novel vertebrate gene related to Drosophila eyes absent.', *Human Molecular Genetics*. England, 8(1), pp. 11–23.

- Buller, C., Xu, X., Marquis, V., Schwanke, R. and Xu, P. X. (2001) 'Molecular effects of Eya1 domain mutations causing organ defects in BOR syndrome.', *Human Molecular Genetics*, 10(24), pp. 2775–2781.
- Campbell, K. and Casanova, J. (2015) 'A role for E-cadherin in ensuring cohesive migration of a heterogeneous population of non-epithelial cells', *Nature Communications*. Nature Publishing Group, 6, pp. 1–11.
- Campbell, K. and Casanova, J. (2016) 'A common framework for EMT and collective cell migration', *Development*, 143(23), pp. 4291–4300.
- Cecchi, C., Mallamaci, A. and Boncinelli, E. (2000) 'Otx and Emx homeobox genes in brain development.', *The International Journal of Developmental Biology*, 44, pp. 663–668.
- Chang, W. (2004) 'The development of semicircular canals in the inner ear: role of FGFs in sensory cristae', *Development*, 131(17), pp. 4201–4211.
- Chen, S., Wang, Q., Nie, Z., Sun, H., Lennon, G., Copeland, N. G., Gilbert, D. J., Jenkins, N. A. and Zack, D. J. (1997) 'Crx , a Novel Otx-like Paired-Homeodomain Protein , Binds to and Transactivates Photoreceptor Cell-Specific Genes', *Neuron*, 19, pp. 1017–1030.
- Cole, L. K. and Ross, L. S. (2001) 'Apoptosis in the developing zebrafish embryo', *Developmental Biology*, 240(1), pp. 123–142.
- Dyballa, S., Savy, T., Germann, P., Mikula, K., Remesikova, M., Spir, R., Zecca,

A., Peyrieras, N. and Pujades, C. (2017) 'Distribution of neurosensory progenitor pools during inner ear morphogenesis unveiled by cell lineage reconstruction', *eLife*, 6, pp. 1–22.

- Fekete, D. M., Homburger, S. a, Waring, M. T., Riedl, a E. and Garcia, L. F. (1997) 'Involvement of programmed cell death in morphogenesis of the vertebrate inner ear.', *Development*, 124(12), pp. 2451–61.
- Finkelstein, R. and Boncinelli, E. (1994) 'From fly head to mammalian forebrain: the story of otd and Otx', *Trends in Genetics*, 10(9), pp. 310–315.
- Foucher, I., Mione, M., Simeone, A., Acampora, D., Bally-Cuif, L. and Houart, C. (2006) 'Differentiation of cerebellar cell identities in absence of Fgf signalling in zebrafish Otx morphants.', *Development*, 133(10), pp. 1891–1900.
- Fraser, F. C., Sproule, J. R. and Halal, F. (1980) 'Frequency of the branchio-oto-renal (BOR) syndrome in children with profound hearing loss.', *American Journal of Medical Genetics*. United States, 7(3), pp. 341–349.
- Freyer, L. and Morrow, B. E. (2010) 'Canonical Wnt signaling modulates Tbx1, Eya1, and Six1 expression, restricting neurogenesis in the otic vesicle', *Developmental Dynamics*, 239(May), pp. 1708–1722.
- Friedl, P. and Gilmour, D. (2009) 'Collective cell migration in morphogenesis, regeneration and cancer', *Nature Reviews Molecular Cell*

Biology. Nature Publishing Group, 10(7), pp. 445–457. doi: 10.1038/nrm2720.

- Furukawa, T., Morrow, E. M. and Cepko, C. L. (1997) 'Crx, a novel otx-like homeobox gene, shows photoreceptor-specific expression and regulates photoreceptor differentiation.', *Cell*, 91(4), pp. 531–541.
- Galliot, B., De Vargas, C. and Miller, D. (1999) 'Evolution of homeobox genes: Q50 Paired-like genes founded the Paired class', *Development Genes and Evolution*, 209(3), pp. 186–197.
- Gehring, W. J., Müller, M., Affolter, M., Percival-Smith, A., Billeter, M., Qian, Y. Q., Otting, G. and Wüthrich, K. (1990) 'The structure of the homeodomain and its functional implications', *Trends in Genetics*, 6(C), pp. 325–328.
- Geng, F.-S., Abbas, L., Baxendale, S., Holdsworth, C. J., Swanson, A. G., Slanchev, K., Hammerschmidt, M., Topczewski, J. and Whitfield, T. T. (2013) 'Semicircular canal morphogenesis in the zebrafish inner ear requires the function of gpr126 (lauscher), an adhesion class G protein-coupled receptor gene', *Development*, 140(21), pp. 4362–4374.
- Germot, A., Lecointre, G., Plouhinec, J. L., Le Mentec, C., Girardot, F. and Mazan, S. (2001) 'Structural evolution of Otx genes in craniates', *Molecular Biology and Evolution*, 18(9), pp. 1668–1678.
- Gillespie, P. G. and Müller, U. (2009) 'Mechanotransduction by Hair Cells: Models, Molecules, and Mechanisms', *Cell*, 139(1), pp. 33–44.

- Haddon, C. and Lewis, J. (1991) 'Hyaluronan as a propellant for epithelial movement: the development of semicircular canals in the inner ear of *Xenopus*', *Development*, 112(2), pp. 541–550.
- Haddon, C. and Lewis, J. (1996) 'Early ear development in the embryo of the zebrafish, Danio rerio', *Journal of Comparative Neurology*, 365(1), pp. 113–128.
- Haffter, P., Granato, M., Brand, M., Mullins, M. C., Hammerschmidt, M., Kane, D. A., Odenthal, J., van Eeden, F. J., Jiang, Y. J., Heisenberg, C. P., Kelsh, R. N., Furutani-Seiki, M., Vogelsang, E., Beuchle, D., Schach, U., Fabian, C. and Nusslein-Volhard, C. (1996) 'The identification of genes with unique and essential functions in the development of the zebrafish, Danio rerio.', *Development*. England, 123, pp. 1–36.
- Hammond, K. L. and Whitfield, T. T. (2006) 'The developing lamprey ear closely resembles the zebrafish otic vesicle: otx1 expression can account for all major patterning differences.', *Development*, 133(7), pp. 1347–1357.
- Hava, D., Forster, U., Matsuda, M., Cui, S., Link, B. A., Eichhorst, J., Wiesner, B., Chitnis, A. and Abdelilah-Seyfried, S. (2009) 'Apical membrane maturation and cellular rosette formation during morphogenesis of the zebrafish lateral line', *Journal of Cell Science*, 122(5), pp. 687–695.
- Hay, E. D. (2005) 'The mesenchymal cell, its role in the embryo, and the

remarkable signaling mechanisms that create it', *Developmental Dynamics*, 233(3), pp. 706–720.

- Heddleston, J. M. and Chew, T. L. (2016) 'Light sheet microscopes: Novel imaging toolbox for visualizing life's processes', *International Journal of Biochemistry and Cell Biology*. Elsevier Ltd, 80, pp. 119–123.
- Hoijman, E., Fargas, L., Blader, P. and Alsina, B. (2017) 'Pioneer neurog1 expressing cells ingress into the otic epithelium and instruct neuronal specification', *eLife*, 6, pp. 1–25.
- Hoijman, E., Rubbini, D., Colombelli, J. and Alsina, B. (2015) 'Mitotic cell rounding and epithelial thinning regulate lumen growth and shape', *Nature Communications*. Nature Publishing Group, 6, pp. 1–13.
- Howe, K., Clark, M. D., Torroja, C. F., Torrance, J., Berthelot, C., Muffato, M., Collins, J. E., Humphray, S., McLaren, K., Matthews, L., McLaren, S., Sealy, I., Caccamo, M., Churcher, C., Scott, C., Barrett, J. C. and Koch, R. (2013) 'The zebrafish reference genome sequence and its relationship to the human genome', *Nature*, 496(7446), pp. 498–503.
- Hruscha, A., Krawitz, P., Rechenberg, A., Heinrich, V., Hecht, J., Haass, C. and Schmid, B. (2013) 'Efficient CRISPR/Cas9 genome editing with low off-target effects in zebrafish', *Development*, 140(24), pp. 4982–4987.
- Huff, J. (2015) 'The Airyscan detector from ZEISS: confocal imaging with

improved signal-to-noise ratio and super-resolution', *Nature Methods*. Nature Publishing Group, 12(12), pp. 1–2.

- Kalatzis, V., Sahly, I., El-Amraoui, A. and Petit, C. (1998) 'Eya1 expression in the developing ear and kidney: Towards the understanding of the pathogenesis of Branchio-Oto-Renal (BOR) syndrome', *Developmental Dynamics*, 213(4), pp. 486–499.
- Kantarci, H., Gerberding, A. and Riley, B. B. (2016) 'Spemann organizer gene *Goosecoid* promotes delamination of neuroblasts from the otic vesicle', *Proceedings of the National Academy of Sciences*, 113(44), pp. E6840–E6848.
- Kantarci, H., Gerberding, A., Riley, B. B., Hammond, K. L., Whitfield, T. T., Zecca, A., Dyballa, S., Voltes, A., Bradley, R., Pujades, C., Anwar, M., Tambalo, M., Ranganathan, R., Grocott, T., Streit, A., Howe, K., Clark, M. D., Torroja, C. F., Torrance, J., Berthelot, C., Muffato, M., Collins, J. E., Humphray, S., McLaren, K., Matthews, L., McLaren, S., Sealy, I., Caccamo, M., Churcher, C., Scott, C., Barrett, J. C., Koch, R., Schindelin, J., Arganda-Carreras, I., Frise, E., Kaynig, V., Longair, M., Pietzsch, T., Preibisch, S., Rueden, C., Saalfeld, S., Schmid, B., Tinevez, J.-Y., White, D. J., Hartenstein, V., Eliceiri, K., Tomancak, P., Cardona, A., Stower, M. J., Bertocchini, F., Solnica-Krezel, L., Turing, A. M., Santi, P. A., Zagato, E., Toon, B., De Smedt, S. C., Remaut, K., Neyts, K.,

Braeckmans, K., Fritzsch, B., Beisel, K. W., Jones, K., Farinas, I., Maklad, A., Lee, J., Reichardt, L. F., Rodríguez-Aznar, E., Barrallo-Gimeno, A., Nieto, M. A., Reginato, M. J., Mills, K. R., Paulus, J. K., Lynch, D. K., Sgroi, D. C., Debnath, J., Muthuswamy, S. K., Brugge, J. S., Frisch SM, F. H., Zartman, J. J., Shvartsman, S. Y., Pilot, F., Lecuit, T., Campbell, K., Casanova, J., Haddon, C., Lewis, J., Chang, W., Brigande, J. V, Fekete, D. M., Wu, D. K., Bok, J., Chang, W., Wu, D. K., Lin, Z., Kulessa, H., Hebert, J., Hogan, B. L. M., Wu, D. K., Hammond, K. L., Loynes, H. E., Mowbray, C., Runke, G., Mullins, M. C., Hildreth, V., Chaudhry, B. and Whitfield, T. T. (2005) 'Conserved patterns of cell movements during vertebrate gastrulation', *Wiley Interdisciplinary Reviews: Developmental Biology*. Nature Publishing Group, 6(2), pp. 213–228.

- Keller, R., Davidson, L. A. and Shook, D. R. (2003) 'How we are shaped: The biomechanics of gastrulation', *Differentiation*. International Society of Differentiation, 71(3), pp. 171–205.
- Khorevin, V. I. (2008) 'The lagena (the third otolith endorgan in vertebrates)', *Neurophysiology*, 40(2), pp. 142–159.
- Kobayashi, Y., Nakamura, H. and Funahashi, J. (2008) 'Epithelial-mesenchymal transition as a possible mechanism of semicircular canal morphogenesis in chick inner ear', *Tohoku Journal of Experimental*

Medicine, 215(1349–3329 (Electronic)), pp. 207–217.

- Kozlowski, D. J., Whitfield, T. T., Hukriede, N. a., Lam, W. K. and Weinberg, E. S. (2005) 'The zebrafish dog-eared mutation disrupts eya1, a gene required for cell survival and differentiation in the inner ear and lateral line', *Developmental Biology*, 277(1), pp. 27–41.
- Lane, B. M. and Lister, J. a (2012) 'Otx but not Mitf transcription factors are required for zebrafish retinal pigment epithelium development.', *PloS One*, 7(11), p. e49357.
- Léger, S. and Brand, M. (2002) 'Fgf8 and Fgf3 are required for zebrafish ear placode induction, maintenance and inner ear patterning', *Mechanisms of Development*, 119(1), pp. 91–108.
- Li, J., Yuan, Y., He, J., Feng, J., Han, X., Jing, J., Ho, T. V., Xu, J. and Chai, Y. (2018) 'Constitutive activation of hedgehog signaling adversely affects epithelial cell fate during palatal fusion', *Developmental Biology*. Elsevier Inc., 441(1), pp. 191–203.
- Li, Y., Allende, M. L., Finkelstein, R. and Weinberg, E. S. (1994) 'Expression of two zebrafish orthodenticle-related genes in the embryonic brain', *Mechanisms of Development*, 48(3), pp. 229–244.
- Liu, Y. G. and Whittier, R. F. (1995a) 'Thermal asymmetric interlaced PCR: automatable amplification and sequencing of insert end fragments from

P1 and YAC clones for chromosome walking', *Genomics*, 25(3), pp. 674–681.

- Liu, Y. G. and Whittier, R. F. (1995b) 'Thermal Asymmetric Interlaced PCR: automatable amplification and sequencing of insert end fragments from P1 and YAC clones for chromosome walking', *Genomics*, 25, p. 674-.
- Liu, Y., Shen, Y. C., Rest, J. S., Raymond, P. A. and Zack, D. J. (2001) 'Isolation and characterization of a zebrafish homologue of the cone rod homeobox gene', *Investigative Ophthalmology and Visual Science*, 42(2), pp. 481–487.
- Ma, W. R. and Zhang, J. (2015) 'Jag1b is essential for patterning inner ear sensory cristae by regulating anterior morphogenetic tissue separation and preventing posterior cell death', *Development*, 142(4), pp. 763–773.
- Marchese, M., Pappalardo, A., Baldacci, J., Verri, T., Doccini, S., Cassandrini, D., Bruno, C., Fiorillo, C., Garcia-Gil, M., Bertini, E., Pitto, L. and Santorelli, F. M. (2016) 'Dolichol-phosphate mannose synthase depletion in zebrafish leads to dystrophic muscle with hypoglycosylated α-dystroglycan', *Biochemical and Biophysical Research Communications*. Elsevier Ltd, 477(1), pp. 137–143.
- Martin, P. and Swanson, G. J. (1993) 'Descriptive and experimental analysis of the epithelial remodellings that control semicircular canal formation in the developing mouse inner ear', *Developmental Biology*, 159, pp. 549–558.
- Mazan, S., Jaillard, D., Baratte, B. and Janvier, P. (2000) 'Otx1 gene-

controlled morphogenesis of the horizontal semicircular canal and the origin of the gnathostome characteristics.', *Evolution & Development*, 2(4), pp. 186–93.

- McCarroll, M., Lewis, Z., Culbertson, M. D., Martin, B. L., Kimelman, D. and Nechiporuk, A. V. (2012) 'Graded levels of Pax2a and Pax8 regulate cell differentiation during sensory placode formation', *Development*, 2750, pp. 2740–2750.
- McCarroll, M. N., Lewis, Z. R., Culbertson, M. D., Martin, B. L., Kimelman, D. and Nechiporuk, a. V. (2012) 'Graded levels of Pax2a and Pax8 regulate cell differentiation during sensory placode formation', *Development*, 139(15), pp. 2740–2750.
- Meijering, E., Dzyubachyk, O. and Smal, I. (2012) 'Methods for cell and particle tracking', *Methods in Enzymology*, 504(9), pp. 183–200.
- Mercier, P., Simeone, A., Cotelli, F. and Boncinelli, E. (1995) 'Expression pattern of two otx genes suggests a role in specifying anterior body structures in zebrafish', *International Journal of Developmental Biology*, 39(4), pp. 559–573.
- Mori, H., Miyazaki, Y., Morita, T., Nitta, H. and Mishina, M. (1994) 'Different spatio-temporal expressions of three otx homeoprotein transcripts during zebrafish embryogenesis.', *Molecular Brain Research*, 27(2), pp.

221–31.

- Morsli, H., Choo, D., Ryan, A., Johnson, R. and Wu, D. K. (1998) 'Development of the mouse inner ear and origin of its sensory organs.', *The Journal of Neuroscience*, 18(9), pp. 3327–3335.
- Morsli, H., Tuorto, F., Choo, D., Postiglione, M. P., Simeone, A. and Wu, D. K. (1999) 'Otx1 and Otx2 activities are required for the normal development of the mouse inner ear.', *Development*, 126(11), pp. 2335–43.
- Musharraf, A., Kruspe, D., Tomasch, J., Besenbeck, B., Englert, C. and Landgraf, K. (2014) 'BOR-syndrome-associated Eya1 mutations lead to enhanced proteasomal degradation of Eya1 protein.', *PloS One*, 9(1), p. e87407/1-e87407/7.
- Neuhauss, S. C., Solnica-Krezel, L., Schier, a F., Zwartkruis, F., Stemple, D. L., Malicki, J., Abdelilah, S., Stainier, D. Y. and Driever, W. (1996) 'Mutations affecting craniofacial development in zebrafish.', *Development*, 123(Sp. Iss. SI), pp. 357–367.
- Obholzer, N., Wolfson, S., Trapani, J. G., Mo, W., Nechiporuk, A., Busch-Nentwich, E., Seiler, C., Sidi, S., Sollner, C., Duncan, R. N., Boehland, A. and Nicolson, T. (2008) 'Vesicular Glutamate Transporter 3 Is Required for Synaptic Transmission in Zebrafish Hair Cells', *Journal of Neuroscience*, 28(9), pp. 2110–2118.

- Ohto, H., Kamada, S., Tago, K., Tominaga, S. I., Ozaki, H., Sato, S. and Kawakami, K. (1999) 'Cooperation of six and eya in activation of their target genes through nuclear translocation of Eya.', *Molecular and Cellular Biology*, 19(10), pp. 6815–6824.
- Pannese, M., Polo, C., Andreazzoli, M., Vignali, R., Kablar, B., Barsacchi, G. and Boncinelli, E. (1995) 'The Xenopus homologue of Otx2 is a maternal homeobox gene that demarcates and specifies anterior body regions.', *Development*, 121(3), pp. 707–720.
- Piotrowski, T., Ahn, D., Schilling, T. F., Nair, S., Ruvinsky, I., Geisler, R., Rauch, G.-J., Haffter, P., Zon, L. I., Zhou, Y., Foott, H., Dawid, I. B. and Ho, R. K. (2003) 'The zebrafish van gogh mutation disrupts tbx1, which is involved in the DiGeorge deletion syndrome in humans.', *Development*, 130(20), pp. 5043–5052.
- Qiu, X. and Müller, U. (2018) 'Mechanically Gated Ion Channels in Mammalian Hair Cells', *Frontiers in Cellular Neuroscience*, 12(April), pp. 1–10.
- Reed, B. H., Wilk, R. and Lipshitz, H. D. (2001) 'Downregulation of Jun kinase signaling in the amnioserosa is essential for dorsal closure of the Drosophila embryo', *Current Biology*, 11(14), pp. 1098–1108.
- Reginato, M. J., Mills, K. R., Paulus, J. K., Lynch, D. K., Sgroi, D. C., Debnath, J.,

Muthuswamy, S. K. and Brugge, J. S. (2003) 'Integrins and EGFR coordinately regulate the pro-apoptotic protein Bim to prevent anoikis', *Nature Cell Biology*, 5(8), pp. 733–740.

- Revenu, C. and Gilmour, D. (2009) 'EMT 2.0: shaping epithelia through collective migration', *Current Opinion in Genetics and Development*, 19(4), pp. 338–342.
- Revenu, C., Streichan, S., Dona, E., Lecaudey, V., Hufnagel, L. and Gilmour, D. (2014) 'Quantitative cell polarity imaging defines leader-to-follower transitions during collective migration and the key role of microtubule-dependent adherens junction formation', *Development*, 141(6), pp. 1282–1291.
- Riley, B. B., Zhu, C., Janetopoulos, C. and Aufderheide, K. J. (1997) 'A critical period of ear development controlled by distinct populations of ciliated cells in the zebrafish.', *Developmental Biology*, 191(2), pp. 191–201.
- Rodríguez-Aznar, E., Barrallo-Gimeno, A. and Nieto, M. A. (2013) 'Scratch2 prevents cell cycle re-entry by repressing miR-25 in postmitotic primary neurons', *The Journal of Neuroscience*, 33(12), pp. 5095–5105.
- Salminen, M., Meyer, B. I., Bober, E. and Gruss, P. (2000) 'Netrin 1 is required for semicircular canal formation in the mouse inner ear.', *Development*, 127(1), pp. 13–22.

- Sando, I., Takahara, T. and Ogawa, A. (1984) 'Congenital anomalies of the inner ear', *The Annals of Otology, Rhinology & Laryngology*, 112, pp. 110–118.
- Santi, P. A. (2011) 'Light sheet fluorescence microscopy: A review', *Journal of Histochemistry and Cytochemistry*, 59(2), pp. 129–138.
- Schindelin, J., Arganda-Carreras, I., Frise, E., Kaynig, V., Longair, M., Pietzsch, T., Preibisch, S., Rueden, C., Saalfeld, S., Schmid, B., Tinevez, J.-Y., White, D. J., Hartenstein, V., Eliceiri, K., Tomancak, P. and Cardona, A. (2012) 'Fiji: an open-source platform for biological-image analysis', *Nature Methods*. Nature Publishing Group, 9(7), pp. 676–682.
- Schutte, B. C. and Murray, J. C. (1999) 'The many faces and factors of orofacial clefts', *Human Molecular Genetics*, 8(10), pp. 1853–1859.
- Shen, W., Chen, X., Cormier, O., Cheng, D. C., Reed, B. and Harden, N. (2013) 'Modulation of Morphogenesis by Egfr during Dorsal Closure in Drosophila', *PloS One*, 8(4), pp. 1–13.
- Simeone, A. (1998) 'Otx1 and Otx2 in the development and evolution of the mammalian brain', *The EMBO Journal*, 17(23), pp. 6790–6798.
- Simeone, A., Acampora, D., Mallamaci, A., Stornaiuolo, A., D'Apice, M. R., Nigro, V. and Boncinelli, E. (1993) 'A vertebrate gene related to orthodenticle contains a homeodomain of the bicoid class and

demarcates anterior neuroectoderm in the gastrulating mouse embryo.', *The EMBO Journal*, 12(7), pp. 2735–47.

- Stower, M. J. and Bertocchini, F. (2017) 'The evolution of amniote gastrulation: the blastopore-primitive streak transition', *Wiley Interdisciplinary Reviews: Developmental Biology*, 6(2), pp. 1–17.
- Streit, A. (2002) 'Extensive cell movements accompany formation of the otic placode', *Developmental Biology*, 249(2), pp. 237–254.
- Torres, M. and Giráldez, F. (1998) 'Development of the vertebrate inner ear.', *Mechanisms of Development*, (71), pp. 5–21.
- Tseng, Q., Duchemin-Pelletier, E., Deshiere, A., Balland, M., Guillou, H., Filhol, O. and Thery, M. (2012) 'Spatial organization of the extracellular matrix regulates cell-cell junction positioning', *Proceedings of the National Academy of Sciences*, 109(5), pp. 1506–1511.
- Turing, A. M. (1952) 'The chemical basis of morphogenesis', *Philosophical Transactions of the Royal Society of London, Series B, Biological Sciences*, 237(641), pp. 37–72.
- Walsh, E. C. and Stainier, D. Y. (2001) 'UDP-Glucose Dehydrogenase Required for Cardiac Valve Formation in Zebrafish', *Science*, 293(5535), pp. 1670–1673.
- Waterman, R. E. and Bell, D. H. (1984) 'Epithelial fusion during early

semicircular canal formation in the embryonic zebrafish, Brachydanio rerio', *Anatomical Record*, 210(1), pp. 101–114.

- Whitfield, T. T., Granato, M., Eeden, F. J. M. Van, Schach, U., Brand, M., Furutani-seiki, M., Haffter, P., Hammerschmidt, M., Heisenberg, C., Jiang, Y., Kane, D. A., Kelsh, R. N., Mullins, M. C., Odenthal, J. and Nusslein-Volhard, C. (1996) 'Mutations affecting development of the zebrafish inner ear and lateral line', *Development*, 123, pp. 241–254.
- Whitfield, T. T., Riley, B. B., Chiang, M.-Y. and Phillips, B. (2002) 'Development of the zebrafish inner ear', *Developmental Dynamics*, 223(4), pp. 427–458.
- Xu, J. and Xu, P. X. (2015) 'Eya-six are necessary for survival of nephrogenic cord progenitors and inducing nephric duct development before ureteric bud formation', *Developmental Dynamics*, 244(7), pp. 866–873.
- Xu, P.-X., Zheng, W., Huang, L., Maire, P., Laclef, C. and Silvius, D. (2003) 'Six1 is required for the early organogenesis of mammalian kidney', *Development*, 130, pp. 3085–3094.
- Xu, P. X., Adams, J., Peters, H., Brown, M. C., Heaney, S. and Maas, R. (1999) 'Eya1-deficient mice lack ears and kidneys and show abnormal apoptosis of organ primordia.', *Nature Genetics*, 23(1), pp. 113–117.
- Zagato, E., Toon, B., De Smedt, S. C., Remaut, K., Neyts, K. and Braeckmans, K. (2018) 'Technical implementations of light sheet microscopy',

Microscopy Research and Technique, (December 2017).

- Zecca, A., Dyballa, S., Voltes, A., Bradley, R. and Pujades, C. (2015) 'The Order and Place of Neuronal Differentiation Establish the Topography of Sensory Projections and the Entry Points within the Hindbrain.', *The Journal of neuroscience : the official journal of the Society for Neuroscience*, 35(19), pp. 7475–86.
- Zheng, W., Huang, L., Wei, Z.-B., Silvius, D., Tang, B. and Xu, P.-X. (2003) 'The role of Six1 in mammalian auditory system development.', *Development*, 130(17), pp. 3989–4000.

WEBSITES:

- https://blog.zeiss.com (date last accessed 24th November 2018).
- www.graphpad.com (date last accessed 24th November 2018).